A game of RF and gradient pulses: Obtaining an efficient homogeneous flip angle with strong inhomogeneous B_1 fields

Irene Maria Louise van Kalleveen

The research was supported by Stichting voor de technische wetenschappen (STW).
This thesis was financially sponsored by Philips Healthcare.

Published by: Uitgeverij Ridderprint B.V., Ridderkerk, The Netherlands.
ISBN: 978-94-6299-398-3

A game of RF and gradient pulses: Obtaining an efficient homogeneous flip angle with strong inhomogeneous B_1 fields

Een spel van RF en gradiënt pulsen: Het behalen van een efficiënte homogene flip hoek in combinatie met sterk inhomogene B_1 velden
(met een samenvatting in het Nederlands)

Proefschrift

ter verkrijging van de graad van doctor aan de Universiteit Utrecht op gezag van de rector magnificus, prof.dr. G.J. van der Zwaan, ingevolge het besluit van het college voor promoties in het openbaar te verdedigen op
dinsdag 6 september 2016 des middags te 12.45 uur

door

Irene Maria Louise van Kalleveen

geboren op 24 januari 1984 te Amersfoort

Promotor: Prof. dr. P.R. Luijten

Copromotor: Dr. ing. D.W.J. Klomp

Voor mijn moeder en vader
Dankzij jullie heb ik veel kunnen bereiken

Table of Contents

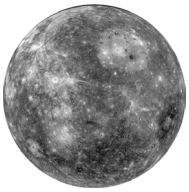

Chapter 1

General Introduction

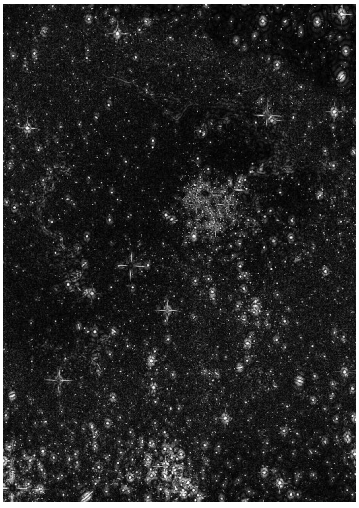

"The diversity of the phenomena of nature is so great, and the treasures hidden in the heavens so rich, precisely in order that the human mind shall never be lacking in fresh nourishment."

Johannes Kepler

1.1 Magnetic Resonance Imaging

Magnetic Resonance Imaging is an imaging method based on the utilization of three different magnetic fields. The first one is the static main magnetic field (B_0). This is the field strength which is mentioned often in combination with MRI (e.g. 3 tesla MRI or 7 tesla MRI). In isotopes with a nuclear spin, this spin precesses (rotation similar to a spinning-top) with a certain resonance frequency (Larmor frequency) which is directly proportional to the strength of the static magnetic field. At a given field strength each isotope has its own specific resonance frequency which is determined by its gyromagnetic ratio. Also, the signal strength scales with the gyromagnetic ratio. Clinical MRI uses the nuclear magnetic resonance signal of the hydrogen atom as this represents the most abundant molecule (water) in living tissue and at the same time has a relatively high gyromagnetic ratio. However, other isotopes can be used as well to generate clinical images.
The second field is created by (pulsed) gradients, which are e.g. responsible for localization of the signals from which the MR images are created. By applying a linear magnetic field in a volume, the spatial dependency of the signal can be extracted in order to creating an image.
And the last one is the local magnetic field (B_1^+ field), which is created by a Radio Frequency (RF) coil. By applying a current through the coil (RF pulse), a local magnetic field is created. When the frequency of the B_1^+ field matches the Larmor frequency, the resonance condition is fulfilled, resulting in small signals in an RF receive coil that subsequently can be digitized and send as data to the computer. The interplay between these three different magnetic fields makes MRI very versatile. At the same time, the magnetic resonance signal itself is weak which makes MRI a rather insensitive technique. As this sensitivity scales linear with the static magnetic field, interest rises for MRI at higher field strengths.

1.2 Ultra high Field MRI

Going to higher field strengths improves this sensitivity (Signal-to-Noise Ratio; SNR), but this comes at a price as other technical and instrumental challenges do appear.
One of them is the Specific Absorption Rate (SAR). When applying an RF magnetic field, the tissue is exposed to both the magnetic and the concomitant electrical field. This electric field distributes energy to the tissue on which the magnetic field is applied. For each body part a safety limit is set for the energy distribution in a certain time frame per unit mass (i.e. SAR). One of the challenges when going to higher field strengths is the increased electric field and therefore the SAR limitations are more challenging, resulting in longer scan times. This poses serious constraints on the scan times

and the shape and number of RF pulses that can be used to manipulate the magnetic spins.
Another challenge is imposed by the shortened wavelength. At 7 tesla the resonance frequency of hydrogen is increased to 300 MHz (compared to 128 MHz at 3T). Because of the increase in frequency, the wavelength will become shorter (about 11 cm in human tissue), resulting in visibility of the wave itself in the images due to the fact that these wavelengths become smaller than the object being scanned.

1.3 Radiofrequency pulses

Traditional RF pulses
A traditional RF pulse rotates the magnetization of the spins (M) into the transverse plane and how far the spins are being rotated depends on the power and duration of the RF pulse (B_1^+). Rotating the spins completely into the transverse plane (flip angle), maximizes the signal obtained by the coil. The maximum signal will be obtained at a flip angle of 90° (Fig. 1.1a). When increasing the duration of the pulse even more, the flip angle will start to decrease just like a sinusoidal function. To summon, the magnetization vector will continue to rotate around the B_1^+ field of the RF pulse until the RF pulse finishes. However, when a local surface coil is applied, the B_1^+ field changes over the spatial dimensions. Therefore only at a certain location a flip angle of 90° is obtained, while somewhat further away, where the B_1^+ field is lower, the flip angle is less than 90° (Fig. 1.1b).
These spatial dependencies give artifacts in the MR images and especially spin echo sequences are very sensitive for these flip angle inhomogeneities as multiple RF pulses constitute the image. To mitigate the non-uniformity, these traditional RF pulses can be replaced by other RF pulses like adiabatic RF pulses[1,2].

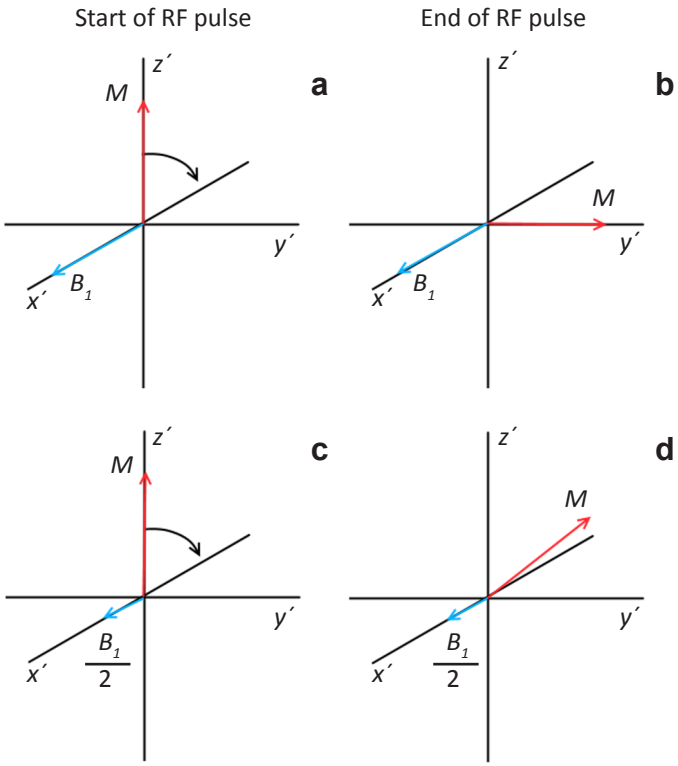

Fig. 1.1. a) At a certain distance from the surface coil an RF pulse will get the desired B_1^+ strength for its duration which will result in a 90° flip angle. **b**) Somewhat further away from the surface coil, the B_1^+ strength is halved, however the duration of the RF pulse is still the same, resulting in a flip angle which is not 90°.

Adiabatic RF pulses

The power of the RF pulse can be modulated during the pulse (amplitude modulation; AM). When the power of the RF pulse is higher at a certain time point, the magnetization vector will rotate faster around the axis of the B_1^+ field. However, during the RF pulse the resonance frequency of the pulse can also be set to a little bit off-resonance. Applying an extra offset to the resonance of the RF pulse is called a frequency modulation (FM). These two parts (AM and FM) of the RF pulse are played out synchronously.

Looking back at the traditional RF pulse, the frequency modulation of these pulses where constantly on resonance and therefore the frequency modulation during the pulses are set on zero.

Combining the AM and FM in an RF pulse gives an extra degree of freedom. As the AM part is merely present in the transverse plane, the FM part can be visualized as presence solemnly along the longitudinal axis. These two vectors can be combined as an effective field (ω_{eff}) which acts on the magnetization vector.

By aligning the start of the RF pulse along the magnetization vector, the magnetization vector starts to rotate around the effective field vector of the RF pulse. By slowly rotating the RF pulse, the magnetization vector keeps rotating around this effective field, which can be drawn to the transverse plane and finally ending up with a 90° flip angle (Fig. 1.2). Rotating the RF pulse is achieved by starting off-resonance and gradually going to on-resonance case (represented by the FM part of the RF pulse) while increasing the AM. For every time point during the RF pulse a new effective field vector is created.

One of the simplest flavors of the adiabatic RF pulses is the Adiabatic Half Passage pulse (AHP) (Fig. 1.2a,b). This pulse is often used as an excitation pulse. The AHP starts off-resonance (AM set to zero and FM set to minimum) along the magnetization vector (Fig. 1.2a). The magnetization vector will start to rotate around the ω_{eff} with a certain tilted angle which is determined by the initial angle between the AHP and the magnetization vector. When the AHP rotates towards the transverse plane, the magnetization vector is being pulled along the AHP, still rotating around ω_{eff} (Fig. 1.2b). Finally, the magnetization vector will end along ω_{eff} in the transverse plane.

When spins are off-resonance, ω_{eff} is somewhat larger or smaller and therefore ω_{eff} and the magnetization vector will not end perfectly in the transverse plane, but a bit tilted towards the longitudinal axis and therefore not creating a perfect 90° flip angle. As a consequence, the frequency profile of the AHP pulse is poor and therefore the AHP cannot be used as a slice selective RF pulse and can only be used as a 3D excitation pulse.

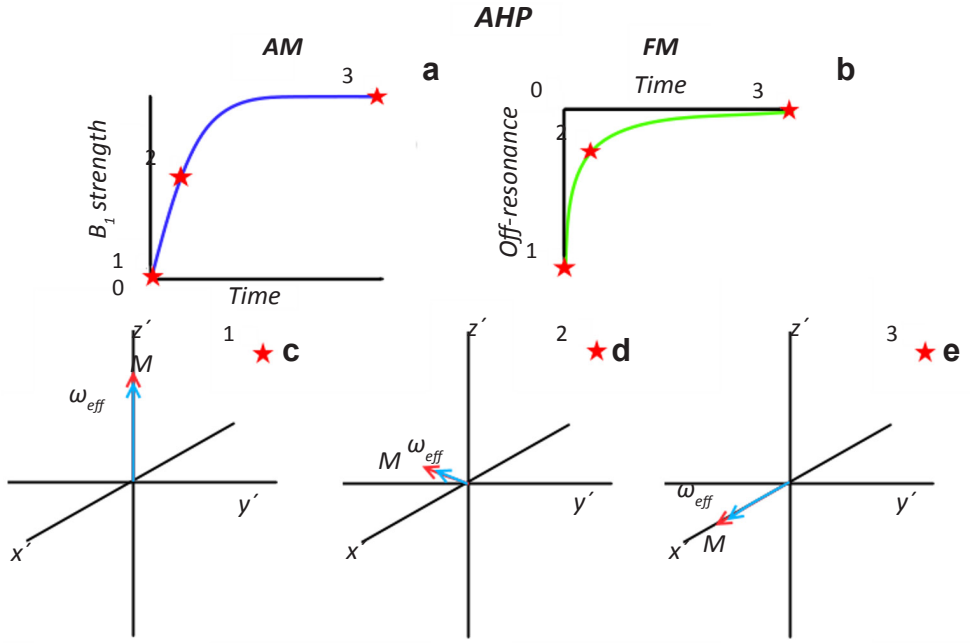

Fig. 1.2. a) The AM and **b**) FM of the AHP pulse. In **c-e** the effect of the AHP as an excitation pulse is shown, where the magnetization vector is located along the longitudinal axis. **c**) At the start of the AHP pulse (used as an excitation pulse), the magnetization vector and the ω_{eff} aligned with the longitudinal axis. **d**) The ω_{eff} starts to move slowly towards the transverse plane, hereby drawing the magnetization vector along with it. **e**) At the end of the AHP pulse, the ω_{eff} is located in the transverse plane along with the magnetization vector. The numbered stars in the AM and FM shapes (**a,b**), which represent time points, correspond to the numbered stars in **c-e**.

If ω_{eff} is rotating too fast, or the strength of ω_{eff} is too weak, the magnetization vector will have problems keeping up, and will deviate from ω_{eff}. This will result in a larger tilted angle between ω_{eff} and the magnetization vector. In this case the adiabaticity is lost and the adiabatic RF pulse might not act independent from the B_1^+ field in these regions. Because of the slow rotation of the effective field vector, the pulses are quite long and the power of these pulses is commonly high. Therefore, SAR issues arise that increase scan time, making these RF pulses challenging to work with.

There has been research about adiabaticity and superadiabaticity[3] that showed that while the traditional adiabatic condition is not fulfilled, the pulse might still act adiabatic. This is caused by the fact that the adiabatic condition is only looking at the simplest path of the adiabatic pulses, while in more complex paths, the adiabaticity might still be fulfilled. To summarize, the ratio between the angular speed and the strength of ω_{eff} (a new vector E) has to satisfy the adiabatic condition, however this can be extrapolated to the angular speed and strength of E and therefore an adiabatic RF pulse can still act adiabatic, while not fulfill the traditional adiabatic condition.

1.4 Adiabatic turbo spin echo

Using a combination of adiabatic RF pulses in a TSE sequence can improve image quality as explained in the upper section and shown in a rat brain[4]. The article from Deschamps et al.[3] about superadiabaticity can give us an extra margin to satisfy the SAR limitations and create shorter adiabatic pulses which fit in a TSE sequence at 7 T in human applications (chapter 2). Combining an adiabatic half passage (AHP) as an excitation pulse with an adiabatic full passage (AFP) as refocusing pulse and a B_1-insensitive rotations using 4 segments (BIR-4) as multi-echo pulses (refocusing pulses following the first refocusing pulse), results in a slice selective TSE sequence. The AFP is used as a pair to select a slice and the AHP and BIR-4 are used as less SAR intensive RF pulses. However, SAR limitations with the adiabatic TSE sequence is still a challenge.

1.5 One-dimensional RF pulses

To overcome SAR challenges at higher field strengths, use can be made of local surface coils[5,6] (e.g. breast surface coil[7]). These coils can create a stronger excitation near the coil and SAR issues are less of a problem. However due to the geometrical shape of these coils, the B_1 field will depend on the location in the tissue in comparison to the location of the coil. Therefore, the RF power in the tissue will be different at different depths. This creates inhomogeneous image contrast. However surface coils often have one dominant direction in which the B_1^+ field drops off. In this case these coils can be combined with slab selective RF pulses using a gradient (traditionally used only for region selection) to compensate for the dominant dimension (chapter 3). Knowing the dominant inhomogeneous B_1^+ field of an RF coil can be used to design an RF pulse which excites the spins inversely proportional. Because of the knowledge of the dominant inhomogeneous B_1^+ field of the coil, the RF pulse can be designed more efficient than when using adiabatic RF pulses. Using this combination the SAR can stay low, while restoring flip angle uniformity.

1.6 Two-dimensional RF pulses

The use of endorectal coils for improved signal to noise in e.g. prostate imaging can be of limited use to study rectal cancer. When using an endorectal coil, tumor structures that partially obstruct the rectum could be damaged. Therefore a monopole antenna[8] can be used for rectal cavities. We have designed an ultra-thin monopole antenna which fits an urinary catheter (< 6 mm diameter) and can be inserted endorectally. The antenna can be used as a transceiver and is a single channel coil.

However, when using an antenna as an RF coil, there is a severe inhomogeneous B_1^+ field present which drops off radially from the antenna and not a single, but multiple dominant dimensions of non-uniformities are present. One of the methods is to use two time varying gradients combined with an RF pulse[9,10] (chapter 4). Compensating for the inhomogeneous field of a surface coil, these gradients can be used to distribute energy (determined by the power of the RF pulse) at certain defined locations. However, the gradients have hardware limitations; i.e. maximum gradient strength of 40 mT/m and a maximum slew rate of 200 T/m at a clinical 7 T MR system. The slew rate describes how fast the gradient can switch between different values (basically the slope of a function). Therefore, modulating these gradients is most effective when using sinusoidal function, because the limiting factor in the whole RF pulse and gradient design will often be the slew rate of the gradients.

1.7 SNR gain and TSE imaging in the cervix

In cervical cancer patients clinical information about whether tumor tissue has invaded neighboring tissue (parametria) is very important. Further treatment planning is based on this information. Clinical MRI scans are now performed at 1.5T, so going to ultra-high field strength can increase the spatial and spectral resolution and contain beneficial information. Because of the location of the cervix near the rectum, we can use a setup where we can locally boost the SNR by inserting the antenna in the rectum for receive only and combine this with seven external fractionated dipole antennas on a multi-transmit platform. Using RF shimming[11], we are able to obtain uniform flip angles in the region of the cervix. Due to the monopole antenna, we are able to boost the SNR and therefore increase the single-shot T_2-weighted image resolution, which can be used as a guidance for clinical diagnostics. In chapter 5 the clinical value of the T_2-weighted imaging in 20 women with histology proven cervical cancer is discussed. In chapter 6 the potential gain in SNR when using the monopole antenna is investigated.

1.8 Thesis overview

MRI is a rather insensitive technique and becomes more sensitive going to higher field strengths. At 7 tesla the B_1^+ inhomogeneity is challenging and therefore traditional RF pulses are not working properly. To compensate for the inhomogeneous B_1^+ field multiple RF pulses are designed. One of the most common used RF pulses to improve flip angle uniformity are the adiabatic RF pulses. These RF pulses have a B_1^+ independent flip angle above a certain threshold. However, these pulses are quite SAR intensive. De Graaf et al.[4] already showed the applicability of creating a turbo spin echo sequence

in animal studies. However, the limitations due to the SAR are more strict when applying the sequence in humans. We designed the adiabatic turbo spin echo sequence in humans (chapter 2) and clarified the shorter RF pulses by using the superadiabaticity described by Deschamps et al.[3]

Local surface RF coils used for e.g. breast imaging[7] have been designed to overcome SAR constraints. However these coils have an even stronger inhomogeneous B_1^+ field which is dominant in one direction, resulting in inhomogeneous image contrast. To restore the image contrast and while preserving low SAR, an RF pulse can be designed and combined with a slab selective gradient which counteracts the B_1^+ field distribution. The slice selection gradient will translate the RF energy corresponding to the frequencies, to energy corresponding to the spatial dimension. We have shown these results in chapter 3 containing the Tilt Optimized Flip Uniformity (TOFU) RF pulse.

For rectal cancer patients the thickness of an endorectal coil is limited due to tumor growth inside the rectal cavity. Therefore a single channel ultra-thin monopole antenna used for transceive, which is less than 6 mm in diameter and fits a urinary catheter, could be an option for imaging the rectal wall. However, using a monopole antenna, the inhomogeneous B_1^+ field is not dominant in one dimension, but is inhomogeneous in a radial pattern from the antenna. Therefore we designed a 2D compensating RF pulse (2D RACE) pulse, as shown in chapter 4. This pulse contains an RF pulse and two gradients, where the two gradients are normally used for localization. In this case the gradients are used for compensating the extreme inhomogeneous B_1^+ of the monopole antenna. We have obtained high resolution T_2-weighted images in a feasibility study on 20 women with histology proven cervical cancer (chapter 5). Clinical information about whether or not the cervical tumor tissue grows in the tissue neighboring the cervix (parametria) are very important, because further treatment planning (surgery or radiotherapy) is based on these answers. Going to ultra-high field strength and increasing the resolution of these images can have beneficial information for the radiologist. Because the cervix lies near the rectum, the antenna is present near the cervix. Finally, we also showed that the monopole antenna only as a receiver is also beneficial to boost the SNR in the cervix (chapter 6). Combining these with seven fractionated dipole antennas which are driven with the multi-transmit platform, results in a homogeneous B_1^+ region in the cervix and boosted the SNR with the additional endorectally placed monopole antenna. This may be used in the future to determine treatment planning of cervix cancer patients.

1.9 References

1 **Garwood M, DeLaBarre L.** The return of the frequency sweep: Designing adiabatic pulses for contemporary NMR. J Magn Reson 2001;153:155-177.

2 **Tannus A, Garwood M.** Adiabatic pulses. NMR biomed 1997;10:423-434.

3 **Deschamps M, Kervern G, Massiot D, Pintacuda G, Emsley L, Grandinetti PJ.** Superadiabaticity in magnetic resonance. J Chem Phys 2008;129.

4 **De Graaf RA, Rothman DL, Behar KL.** Adiabatic RARE imaging. NMR biomed 2003;16:29-35.

5 **Arteaga de Castro CS, Van den Bergen B, Luijten PR, Van der Heide UA, Van Vulpen M, Klomp DWJ.** Improving SNR and B_1 transmit field for an endorectal coil in 7 T MRI and MRS of prostate cancer. Magn Reson Med 2012;68:311-318.

6 **Van den Bergen B, Klomp DWJ, Raaijmakers AJE, Arteaga de Castro CS, Boer VO, Kroeze H, Luijten PR, Lagendijk JJW, Van den Berg CAT.** Uniform prostate imaging and spectroscopy at 7 T: comparison between a microstrip array and an endorectal coil. NMR Biomed 2011;24:358-365.

7 **Van de Bank BL, Voogt IJ, Italiaander M, Stehouwer BL, Boer VO, Luijten PR, Klomp DWJ.** Ultra high spatial and temporal resolution breast imaging at 7T. NMR in Biomed 2012;26:367-375.

8 **Erturk MA, El-Sharkawy AM, Moore J, Bottomley PA.** Interventional loopless antenna at 7 T. Magn Reson Med 2012;68:980-988.

9 **Sbrizzi A, Hoogduin H, Lagendijk JJ, Luijten PR, Sleijpen GLG, Van den Berg CAT.** Time efficient design of multi dimensional RF pulses: application of a multi shift CGLS algorithm. Magn Reson Med 2011;66:879-885.

10 **Grissom WA, McKinnon GC, Vogel MW.** Nonuniform and multidimensional Shinnar-Le Roux RF pulse design method. Magn Reson Med 2012;68:690-702.

11 **Metzger GJ, Snyder C, Akgun C, Vaughan T, Ugurbil K, Van de Moortele PF.** Local B_1^+ shimming for prostate imaging with transceiver arrays at 7T based on subject-dependent transmit phase measurements. Magn Reson Med 2008;59:396-409.

Chapter 2

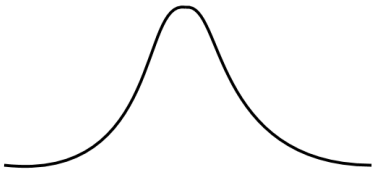

Adiabatic turbo spin echo in human applications at 7 Tesla

I.M.L. van Kalleveen[1], W. Koning[1], V.O. Boer[1], P.R. Luijten[1], J.J.M. Zwanenburg[1], D.W.J. Klomp[1]

[1]Department of Radiology, UMC Utrecht, the Netherlands

Published in 2012 in Magnetic Resonance in Medicine (68: 580-587)
DOI: 10.1002/mrm.23264

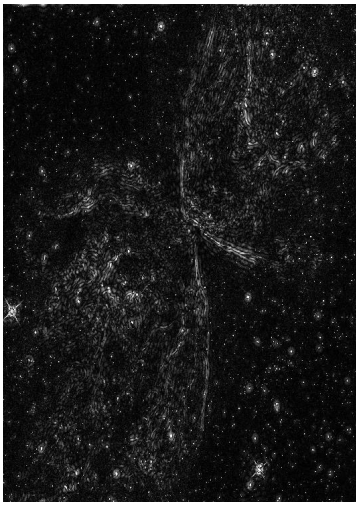

"Mathematicians may flatter themselves that they possess new ideas which mere human language is as yet unable to express."

James Clerck Maxwell

Abstract

Non-uniform B_1 fields in ultra-high field MR imaging cause severe image artifacts when conventional radiofrequency (RF) pulses are used. Particularly in MR sequences that encompass multiple RF pulses, e.g., turbo spin echo (TSE) sequences, complete signal loss may occur in certain areas. When using a surface coil for transmitting the RF pulses, these problems become even more challenging, as the spatial B_1 field variance is substantial. As an alternative to conventional TSE sequences, adiabatic TSE sequences can be applied, which have the benefit that these sequences are insensitive to B_1 non-uniformity. In this study we investigate the potential of using adiabatic TSE at 7 T with surface coil transceivers in human applications. The adiabatic RF pulses were tuned to deal with the constraints in B_1 strength and RF power deposition, but remained in the superadiabatic regime. As a consequence, the dynamic range in B_1 is compromised and signal modulation is obtained over the echo train. Multi-dimensional Bloch simulations over the echo train and phantom measurements were obtained to assess these limitations. Still, using proper k-space sampling, we demonstrate improved image quality of the adiabatic TSE versus conventional TSE in the brain, the neck (carotid artery) and in the pelvis (prostate) at 7 T.

2.1 Introduction

T_2-weighted MR images are used for detection and staging of multiple diseases (e.g., cancerous tissue, brain lesions[1-4]), due to the high contrast-to-noise ratio. Therefore, turbo spin echo sequences are of great importance for clinical applications. At ultra-high field MRI (≥7 Tesla), the signal-to-noise ratio is increased, however, the non-uniform B_1 fields have been shown to cause severe image artifacts when conventional radiofrequency (RF) pulses are used[5]. The B_1 non-uniformities are due to standing wave effects in the human body as a consequence of the shortened wavelength of the applied RF fields at 7 T. Also in human applications, the maximal B_1 strength is limited, which can be increased by applying a surface coil transceiver close to the object of interest. However, the surface coil produces a non-uniform B_1 field, which depends on the distance to the surface coil. Because the flip angle of a conventional pulse depends linear on the B_1 strength, this will result in a spatial dependent flip angle and signal attenuation. Particularly in MR sequences that encompass many RF pulses, e.g., turbo spin echo (TSE) sequences, complete signal loss may occur in certain areas[6].
A solution may be to use adiabatic pulses in TSE sequences, which are insensitive to B_1 non-uniformity, as was shown for the rat brain when using surface transceivers[7]. The adiabatic TSE sequence consists of adiabatic half passage (AHP)[8-10] pulses (excitation), adiabatic full passage (AFP)[9-11] pulses (slice selective refocusing) and B_1 -independent plane rotation pulses using four segments (BIR-4)[8-10, 2] (refocusing). However, for human applications, the available B_1 strength is much lower, which means that the conventional adiabatic condition ($Q_{\text{factor}} >> 1$) may be violated. Here,

$$Q_{factor} = \frac{\omega_{eff}}{d\alpha / dt} \quad , \qquad \textbf{[2.1]}$$

where

$$\omega_{eff}(t) = \omega_0(t) + \omega_1(t) = \omega_0(t) + \gamma B_1(t) = FM + AM. \qquad \textbf{[2.2]}$$

In words, ω_{eff} is the summation vector of the B_1 strength in the rotating frame multiplied by gyromagnetic ratio γ (amplitude modulation, AM) and the offset frequency of the pulse (frequency modulation, FM), and da/dt is the angular velocity of ω_{eff} in the rotating frame. Furthermore, compared with the rat applications, the RF power deposition in human applications increases dramatically when applying these pulses. This results in high Specific Absorption Rate (SAR) values that can exceed the safety guidelines. Recently, Deschamps et al.[13] have shown that adiabatic RF pulses can be designed to remain in a so-called superadiabatic regime which provides substantially less constraints to the B_1 and RF power deposition, as compared to the conventional adiabatic regime. Although the pulses behave adiabatic, when used in a TSE, artifacts

may still occur that originate from phase alterations, similar as demonstrated with the conventional pulses. However, when applied in an echo train, the even echoes refocus these alterations completely[14]. In this study, we demonstrate that the loss of phase coherence can be refocused during a train of BIR-4 pulses. Therefore, most of the transverse magnetization remains observable, while pulse durations and therefore echo trains can be short and SAR substantially reduced. As a consequence, adiabatic TSE becomes feasible for human applications at 7 T, as we have shown for human applications in head, neck and pelvis.

2.2 Theory

Adiabatic pulses consist of an amplitude modulation (AM) and a frequency modulation (FM), which result in an effective rotating magnetic field vector (B_{eff}; Fig. 2.1). As long as the precession of magnetization around B_{eff} is substantially faster than the rotation of B_{eff} itself in the rotating frame (adiabatic condition), the spins will remain locked to B_{eff}, hence providing an adiabatic spin perturbation. For human applications at high fields however, this conventional adiabatic condition may not be met. The B_1 field that can be obtained in the human body at 7 T is relatively low, causing a slow precession around the B_{eff}. To still fulfill the adiabatic condition, the adiabatic RF pulses must become longer, resulting in relatively high RF power deposition and hence can lead to violation of SAR guidelines.

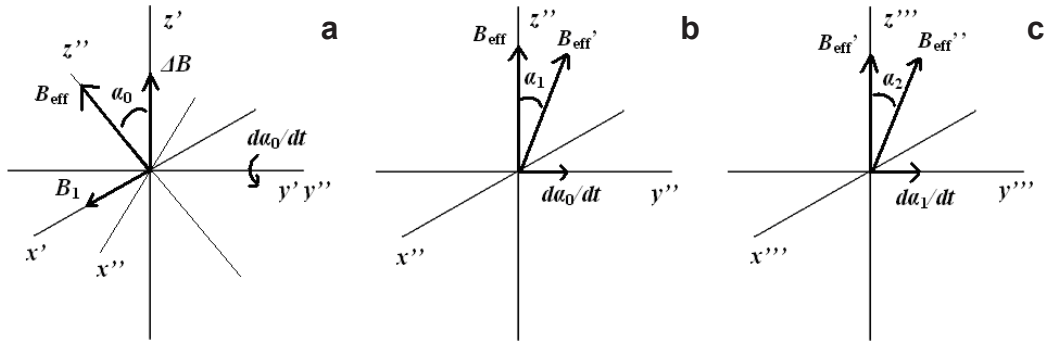

Fig. 2.1. Visualization of effective field over multiple rotating frames. The first frame, rotating at the Larmor frequency, where the amplitude (B_1) and frequency modulation (ΔB) create the effective field (B_{eff}; **a**). Also the second rotating frame is given, which is oriented along B_{eff}. The second rotating frame, also known as the first adiabatic frame, is shown in (**b**). Here the effective magnetic field vector B_{eff}, together with the angular velocity of B_{eff} (da_0/dt), result in a new effective field vector, B_{eff}' with a corresponding angular velocity da_1/dt. The third rotating frame (**c**), also known as the second adiabatic frame, is oriented along B_{eff}', resulting in a new effective vector (B_{eff}'') together with an angular velocity (da_2/dt).

Adiabatic RF pulses are being used at high fields in human applications with limited B_1 fields. Particularly, inversion pulses for inversion recovery sequences[15] and slice selective refocusing pulses in spectroscopy[16,17] seem to behave better than the conventional adiabatic condition would predict. In a recent article[13], Deschamps et al. have exploited the quantum mechanical principles of adiabaticity, where they show that the conventional adiabatic condition, as observed in a double rotating frame, is only the first-order term describing the perturbation of the system. However, higher order terms can also be calculated. When looking at higher order terms, adiabatic behavior of certain pulses can be explained, though these pulses should not behave adiabatic according to the conventional adiabatic condition. The adiabaticity can be evaluated by looking at a rotating frame along the B_{eff}, where the angular velocity of B_{eff} (da_0/dt) is located perpendicular to B_{eff} (i.e., double rotating frame). Take B_{eff}' as the summation vector of B_{eff} and da_0/dt and take da_1/dt as the angular velocity of B_{eff}'. Then, the second-order term can be visualized in a rotating frame along the summation vector of B_{eff}' and the perpendicular component is da_1/dt (i.e., third rotating frame, Fig. 2.1). In this manner, multiple frames can be created. In each frame, the error (the ratio of the angular velocity and the effective vector) will reach a maximum at a certain time point during the pulse. In one of these frames, the maximal error will have the lowest value. This frame will determine how well the adiabatic condition is fulfilled. If the adiabatic condition is fulfilled, the magnetization vector can be assessed. However, the trajectory the magnetization vector follows becomes more complex with increasing optimal frame number[13].

2.3 Methods

Adiabatic pulse shapes

The AHP is a non-selective excitation pulse, due to the behavior of its frequency profile. Therefore, the AFP pulse was applied as a refocusing pulse to obtain a slice, because of the well-determined frequency profile (in contrast to the AHP and BIR-4). The downside of using the AFP as a refocusing pulse is the fact that two AFPs are necessary for one echo, because the magnetization needs to be unwrapped. The multi-echoes are created by BIR-4 pulses, which demand less SAR (and time) in comparison with two AFP pulses.

Shapes of the AM and FM functions for the BIR-4 pulses were created from analytical functions (Matpulse[18]). For the excitation pulse, a standard AHP pulse was used based on a tanh/tan function:

$$AM = \omega_1 \tanh(a_1 t / T_p), \qquad \textbf{[2.3]}$$

$$FM = A\tan(a_2(t/T_p - 1)) \quad , \qquad \textbf{[2.4]}$$

where T_p is the pulse duration, $\omega_1 = \gamma B_1$, $a_1 = 5$, $a_2 = \text{atan}(18)$ and $A = 52$ kHz. AFP pulses were used for slice selective refocusing[19]:

$$AM = \omega_1 \tanh(a_1 t/T_p) \quad , \qquad \textbf{[2.3]}$$

$$FM = A\tan(a_2(t/T_p - 1)) \quad , \qquad \textbf{[2.4]}$$

$$AM = \omega_1 \sec h(b(2t/T_p - 1)) \quad , \qquad \textbf{[2.5]}$$

$$FM = A\tanh(1.3b(2t/T_p - 1)) \quad , \qquad \textbf{[2.6]}$$

where b = 5 and A = 612 Hz. The BIR-4 pulses were based on *tanh/tan* shapes:

$$AM = \omega_1 \tanh(a_1(4t/T_p - 1)) \quad , \qquad \textbf{[2.7]}$$

$$FM = A\tan(4a_2 t/T_p) \quad , \qquad \textbf{[2.8]}$$

where $a_1 = 10$, $a_2 = \text{atan}(18)$ and $A = 11005$ Hz. At a fixed TP of 6 ms, the refocusing performance of single BIR-4 pulses and a train of BIR-4 pulses were evaluated for different frequency sweeps (11-54 kHz). The frequency sweep is the maximal frequency offset given by the FM. The refocused component was calculated over the regime of B_0 ($\pm$1 kHz) and B_1 (0-40 μT) offsets that can be obtained in human applications at 7 T. In addition, the adiabatic condition was calculated up to the 10th frame in the superadiabatic regime, by simulating the higher order frames of the pulse. In this region (n = 1-10), the optimal frame for each B_1 strength was reached and therefore applying more frames was not needed[13]. For each B_1 strength, an optimal frequency sweep can be chosen, however for surface coils the B_1 strength varies strong over space. Therefore, the optimal frequency sweep was chosen for the B_1 region of interest which in this case is 11 kHz.

Adiabatic TSE sequence

An adiabatic TSE (Fig. 2.2) was implemented on a 7 T whole body MR system (Philips, Cleveland). The non-selective AHP pulse of 2 ms was used for excitation and a pair of slice selective AFP pulses of 10 ms each was used to obtain the first echo at a T_E of 30 ms. The following echoes were generated with the BIR-4 refocusing pulses of 6 ms each with an echo spacing (T_E') of 15 ms. A train of 15 echoes was used in all phantom measurements and for the *in vivo* measurements, 7 echoes were used. The turbo factor (number of echoes) was mostly determined by the SAR limits. Unfortu-

nately, this train of BIR-4 pulses contributes substantially to the RF power deposition and therefore needs to be addressed to remain within SAR limits. With a turbo factor of 7, the AHP contributes 2.7%, the AFP 16.5%, and the BIR-4 80.8% to the SAR. By reducing the frequency sweep for relative short BIR-4 pulses, the superadiabatic conditions can be fulfilled, which results in a reduction of the SAR. As a result, the bandwidth became smaller, but as the bandwidth of the pulse is still much larger than the offset frequencies, this is not a problem. As the adiabatic condition is fulfilled in a higher order frame, a signal modulation between even and odd echoes is expected that can lead to ghosting artifacts[14]. Therefore, the even echoes are ordered in the upper part of k-space and the odd echoes in the lower part[7]. In addition, to exclude a transition between the even and odd echoes in the center of k-space, an odd number of echoes is chosen. Different ways of ordering k-space have been chosen to demonstrate different T_2-weightings. Phantom measurements were obtained to demonstrate the optimized k-space sampling regarding the reduction of the ghosting artifact and to verify the dynamic range in B_1 for effective use of the adiabatic TSE.

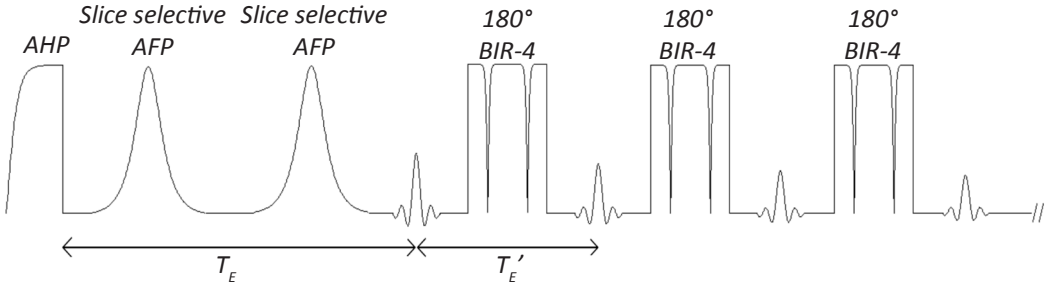

Fig. 2.2. The adiabatic turbo spin echo, starting with a non-selective AHP pulse, followed by a pair of AFP pulses. The remaining echoes are obtained by a train of non-selective B_1 -insensitive rotation pulses using four segments (BIR-4). All pulses are scaled to the same nominal B_1 strength.

In vivo experiments

With the volume head coil (quadrature transmit birdcage with 16 channel receivers, Nova medical), the adiabatic TSE sequence was applied on a healthy volunteer (voxel size of 0.55x0.56x2 mm^3, FOV = 220x220x2 mm^3, turbo factor = 7, T_R = 8685 ms, T_E = 30 ms, T_E' = 15 ms and acquisition time = 3.03 min) to show the feasibility of the adiabatic TSE at limited B_1 strength. The B_1 in the head ranged from 20 μT (center of the brain) to 10 μT (temporal lobes). To demonstrate the performance of the adiabatic TSE over a range of B_1 values, a transmit and receive surface coil (Machnet, Eelde, the Netherlands), with a B_1 range of 0-40 μT, was used for the head and neck, consisting of two inductively decoupled loops with a diameter of 5 cm each. TSE images of the primary visual cortex were obtained using the surface coil as a transceiver (voxel size of 0.5x0.5x2 mm^3, FOV = 110x110x2 mm^3, turbo factor = 7, T_R = 2000 ms, T_E = 30

ms, T_E' = 15 ms and acquisition time = 1.05 min). Adiabatic and conventional TSE images were obtained from the neck of a healthy volunteer to demonstrate the *in vivo* applicability of the method outside the human brain. For this region, a single slice image was obtained using both the adiabatic TSE and the conventional TSE (voxel size of 0.5x0.5x2 mm^3, FOV = 110x110x2 mm^3, turbo factor = 7, T_R = 2000 ms, T_E = 30 ms, T_E' = 15 ms, acquisition time = 1.05 min). Finally, an endorectal coil[19] , with a B_1 range of 0-50 μT, was used as a transceiver to illustrate the potential of uniform imaging with adiabatic TSE of the human prostate at 7 T. A comparison of adiabatic spin echo versus conventional spin echo was made with a single slice in the pelvis (voxel size of 0.5x0.5x2 mm^3. FOV = 120x120x2 mm^3, turbo factor = 7, T_R = 5000 ms, T_E = 30 ms, T_E' = 15 ms and acquisition time = 2.86 min). All *in vivo* experiments were obtained within SAR guidelines (< 10 W/kg local SAR)[19,20].

2.4 Results

For the 6 ms BIR-4 pulses, the $Q_{\text{factor}}\,\omega_{\text{eff}} / (da/dt)$ ranges between 0 and 7 over the relevant B_1 regime (13-50 μT). This value is not much larger than 1, and therefore the conventional adiabatic condition is not fulfilled. However, the superadiabaticity factor (Q_s) for this B_1 range varies from 31 to 170. As such, the superadiabatic condition ($Q_s = \omega_{\text{eff, n}} / (da_n/dt) >> 1$) is fulfilled, and the BIR-4 pulse in fact behaves adiabatically (Fig. 2.3). Decreasing the frequency sweep results in adiabatic behavior at lower B_1 levels (Fig. 2.4), thereby decreasing the SAR.

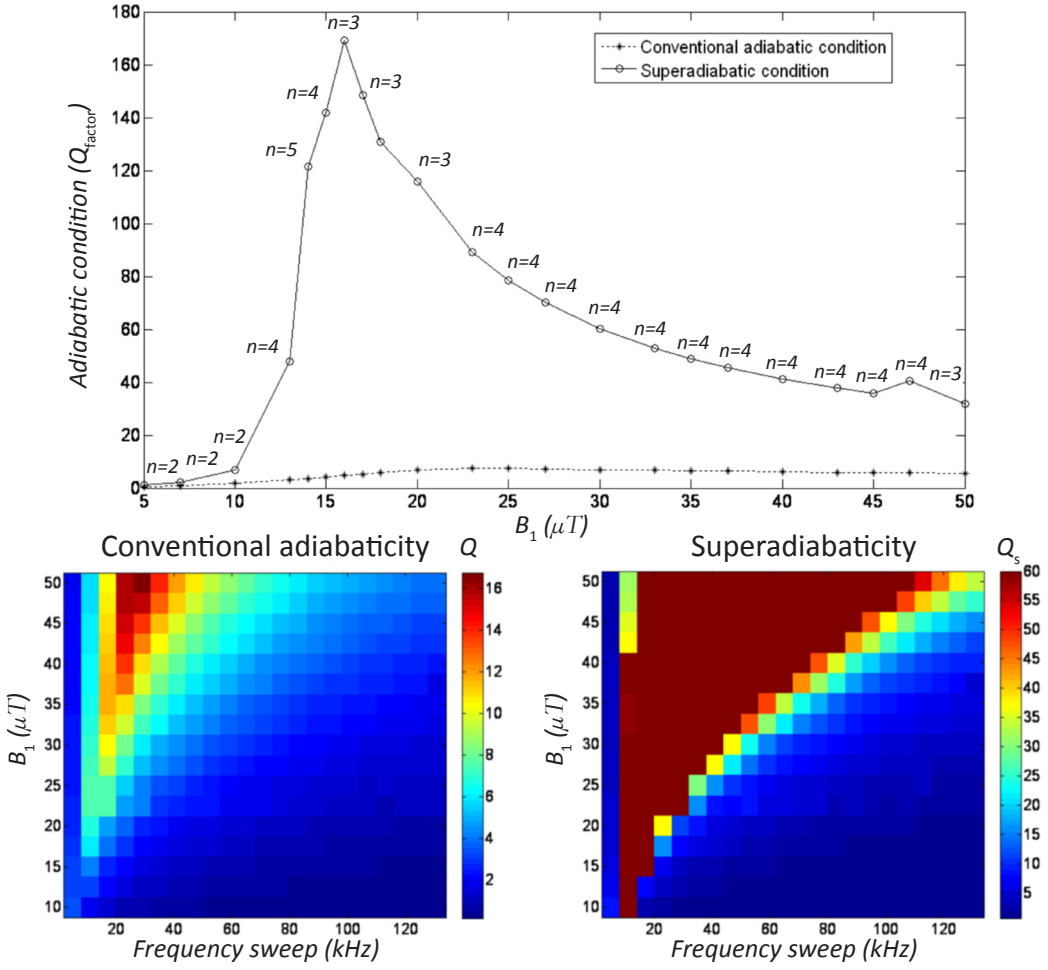

Fig. 2.3. The upper image shows the conventional adiabatic and the superadiabatic condition for multiple B_1 strengths of the BIR-4 pulse with a frequency sweep of 11 kHz. The lower images show the conventional adiabatic factors (left) and the superadiabatic factors (right) for multiple combinations of B_1 strengths and frequency sweeps. The superadiabatic factors are clipped to a Q_s of 60.

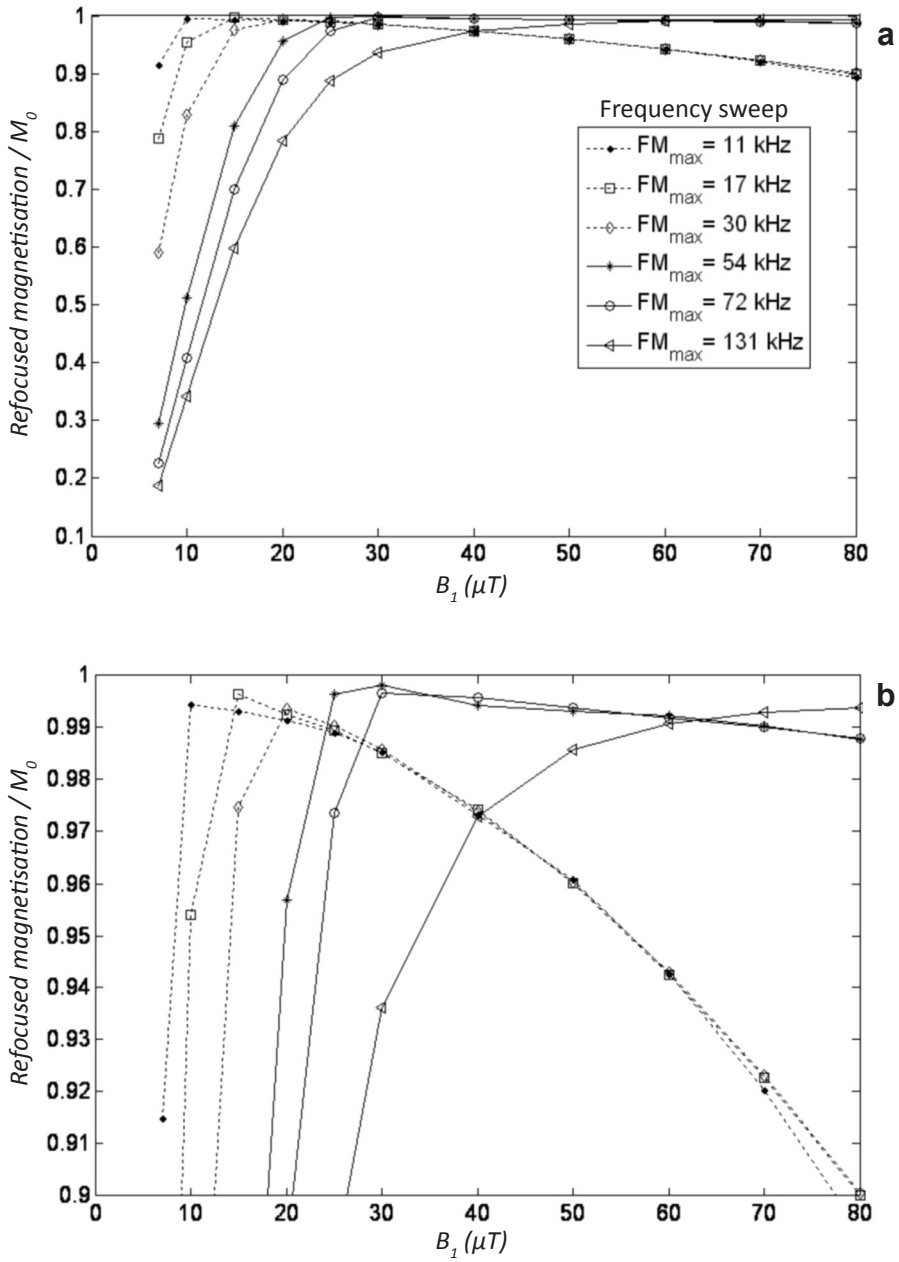

Fig. 2.4. The refocused magnetization after a BIR-4 pulse plotted for different FM values. A lower frequency sweep will result in a refocused magnetization at lower B_1 strengths, in comparison to pulses with a higher frequency sweep. However, for higher B_1 strengths, these pulses degrade in performance compared to pulses with a higher frequency sweep. A magnification of **a**) image is given in **b**).

The even and odd BIR-4 pulses result in phase alternations, as shown by Bloch sim-

ulations (Fig. 2.5). These phase alternations will result in a high frequency ghost. By splitting up the even and odd echoes in k-space, this ghost can be reduced to a shift of only one pixel. Also at much higher B_1 strengths artifacts are induced (Fig. 2.5).

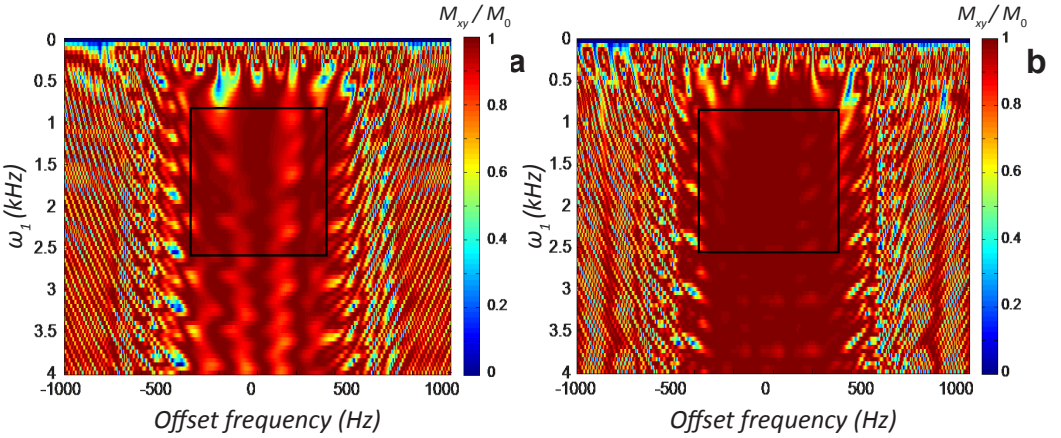

Fig. 2.5. Bloch simulations of adiabatic TSE pulses. The horizontal axis represents the offset frequency (Hz) and the vertical axis represents ω_1 value (kHz). **a**) The magnetization after 1 BIR-4 and **b**) after 2 BIR-4's. Note that the second BIR-4 pulse corrects most of the phase errors that show up after the first BIR-4. Also notice that the adiabatic regime is restricted, indicated by the square.

A prostate phantom (diameter of 4 cm, containing physiological salt) was used to show the signal loss of the conventional TSE (Fig. 2.6a), and the high frequency ghost (Fig. 2.6b) of the adiabatic TSE. Also the reduced ghost by splitting up the even and odd echoes in the adiabatic TSE is shown (Fig. 2.6c). If the strength of the transmit field is increased to twice the nominal value, artifacts are introduced in the image (Fig. 2.6d), however, these high B_1 strengths are not within the regime of interest for the applied surface coils. Compared with the conventional TSE (Fig. 2.6a), the adiabatic TSE (Fig. 2.6c) provides better image quality.

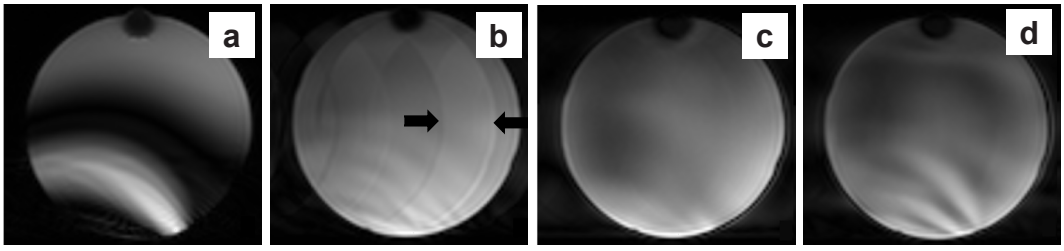

Fig. 2.6. TSE images of a phantom obtained with the surface coil transceiver, using the conventional TSE (**a**), the adiabatic TSE with linear k-space filling (**b**), the adiabatic TSE with different k-space filling (**c**) and the adiabatic TSE with twice the nominal B_1 (**d**). Note the removal of the ghost (arrow) with different k-space filling, while artifact levels increase with B_1 strength.

Adiabatic and conventional TSE images of the primary visual cortex and the left carotid artery were obtained from a healthy volunteer, demonstrating the absence of signal voids in the adiabatic sequences, when using surface coil transceivers. In addition, adiabatic and conventional TSE images were obtained in the pelvis of a patient with prostate cancer, clearly showing the seminal vesicles on the top of the prostate. Note the cancelation of the signal which the conventional TSE creates in areas close to the local RF coil (Fig. 2.7a and Fig. 2.8a,c), reflecting the zones where the intended spin excitation reaches an inversion and therefore nulls the transverse magnetization. Also the refocusing component of the refocusing pulses is spatially dependent, which worsens the cancellations. However, the excitation and refocusing pulses of the adiabatic TSE do not create these signal cancellations (Fig. 2.7b and Fig. 2.8b,d). Finally, the adiabatic TSE was also feasible in the human brain using a volume head coil (Fig. 2.9), which is operating at a maximal B_1 strength between 10 and 20 μT.

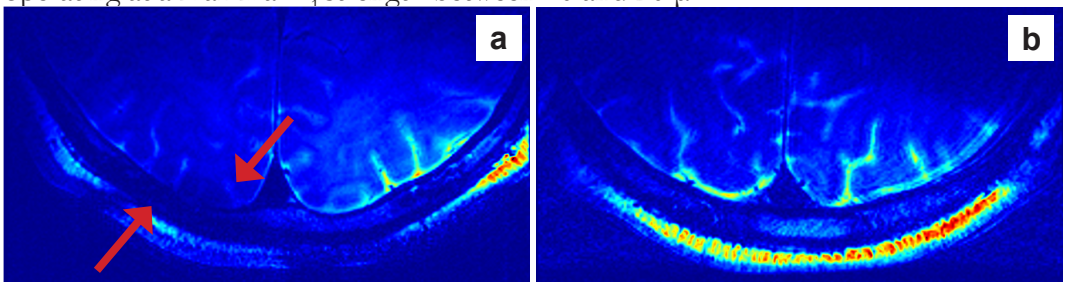

Fig. 2.7. Adiabatic TSE images of the human brain obtained with the surface coil. From a single slice of the primary visual cortex of a healthy volunteer, both a conventional (**a**) and an adiabatic (**b**) TSE were acquired using the same slice location (apart from a small movement of the head between the two scans). Note the absence of signal voids in the skull and brain structure of the images obtained with the adiabatic TSE compared to the conventional TSE (arrows). The images are shown in color to show the difference between the images in more detail.

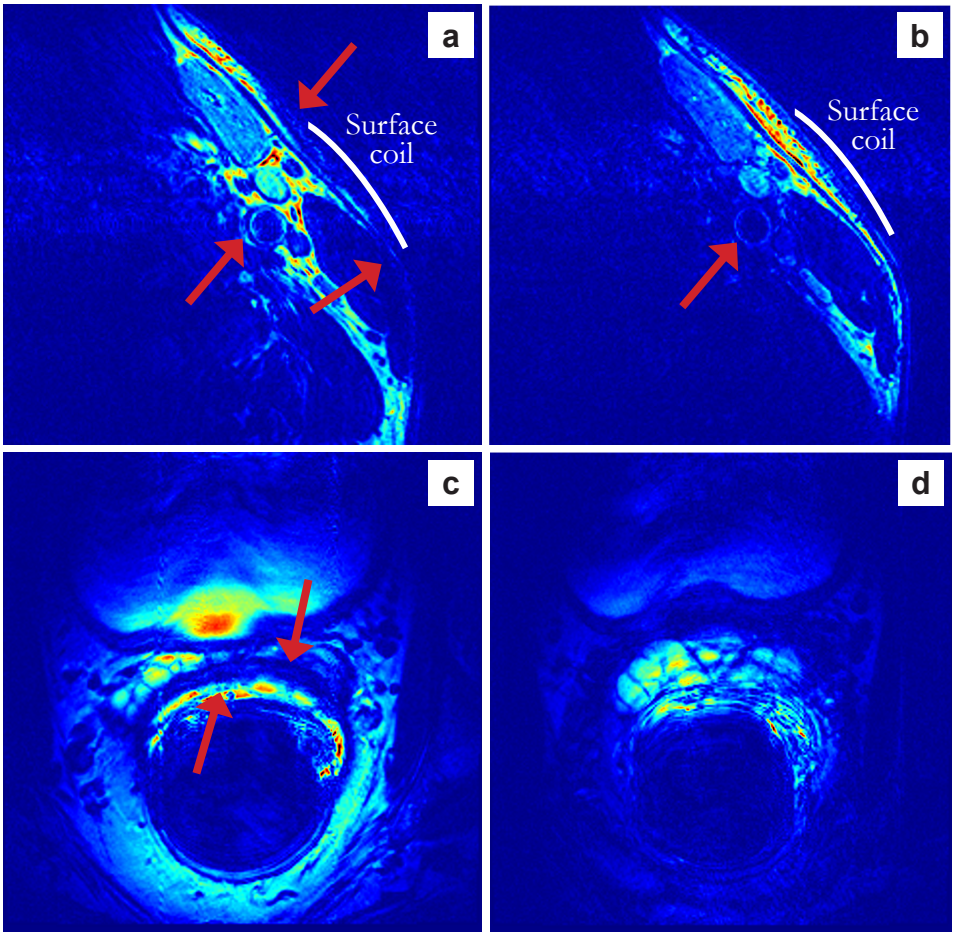

Fig. 2.8. Comparison of conventional and adiabatic TSE images of the area in the neck (**a**,**b**) and pelvis (**c**,**d**) of human volunteers. A single slice of the left carotid artery of a healthy volunteer obtained with the conventional TSE (**a**) shows low intensity of the mandible (arrows), while being uniform in the adiabatic TSE (**b**). The carotid artery (dashed arrow) is visible in both images, however, the conventional TSE shows more signal around the artery, which may be due to the limited bandwidth of the adiabatic pulses at low B_1, hence not exciting the lipid signals. A single slice in the pelvis of a patient with prostate cancer was obtained with a conventional (**c**) and an adiabatic (**d**) TSE using an endorectal transceiver. Note the black band (arrows) in the seminal vesicles on top of the prostate obtained with the conventional TSE, while being uniform when obtained with the adiabatic TSE.

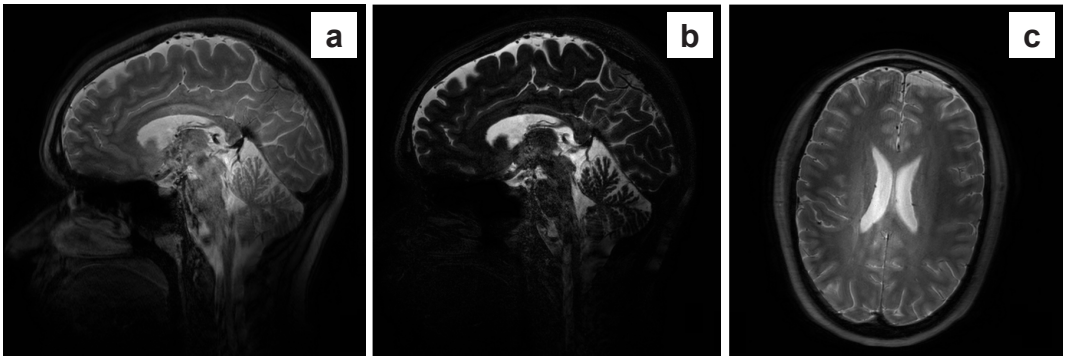

Fig. 2.9. Adiabatic TSE images of the human brain obtained with the conventional volume coil. Two sagittal images are obtained (**a,b**) with two different k-space filling methods. One with the first echoes in the center of k-space (**a**), and the other with the last echoes in the center of k-space (**b**). Also a transverse slice in the middle of the brain with the first k-space method is shown (**c**).

2.5 Discussion

We have shown that the adiabatic TSE can be applied safely in human applications, by optimizing the pulses such that they fulfill the superadiabatic condition, given the relative low B_1 strength, which is normally available in human applications at ultra-high field MRI. The superadiabatic condition is the fundamental explanation why adiabatic pulses still behave adiabatically at low B_1 strengths, though the conventional adiabaticity factors are low and predict non-adiabatic behavior. Altering the pulse duration and lowering the frequency sweep of the conventional adiabatic pulse shapes enabled the use of low B_1 values and thus resulted in a lower SAR. As a result, the bandwidth became smaller, but as most refocusing pulses do not contain slice selective gradients, this is not a problem. In fact, it may even be used to inherently suppress lipid signals.
When creating T_2-weighted images, the filling of k-space is important and therefore the desired echo for filling the center of k-space should be chosen carefully. In addition, due to the expected modulation of the signal between the even and odd echoes, careful positioning these echoes in k-space is important. In this study we have chosen to fill the upper part of k-space with the even echoes and the lower part with the odd echoes. Filling the center of k-space with either the first or the last echoes is another option to provide different T_2-weighting. Splitting the even and odd echoes in k-space will reduce the high frequency modulation over k-space by a lower frequency modulation, and thus the ghost image will only appear one pixel shifted. Another way to eliminate this ghost is to exclude half of the echoes, or to use the even echoes for one image and the odd echoes for a second image and average the two images.
As these pulse shapes are designed according to the conventional adiabatic condition, it might be possible to create other pulse shapes which reduce the SAR even

more, while still maintaining superadiabaticity. By carefully tracking the magnetization through multiple superadiabatic frames, knowledge on the phase errors between even and odd echoes can be obtained and may even be used to correct for these errors.
Although the adiabatic TSE sequence has the potential to provide better image quality, compared to the conventional TSE, it should be noted that the current adiabatic sequence can be used for single slice imaging only, therefore limits its applicability in the clinic. This is caused by the non-selective adiabatic excitation, which prevents the use of multiple slices within the T_R. So, for multi-slice scans, the sequence has to be repeated, and there is no option for exciting multiple slices in one T_R. However, spectral spatial pulses may be applied, which would allow slice selective adiabatic excitation[21]. More slices can be obtained by 3D imaging, particularly with high parallel imaging accelerations, or at a small FOV. Also conventional refocusing pulses may be considered, rather than BIR-4 pulses, particularly with the volume head coil. However, when surface coils are used, the significant non-uniformity in B_1 will still cause signal cancelations in areas where the refocusing pulse results in a 360° rather than a 180° pulse.

2.6 Conclusions

In this study, the limitations and potentials of the adiabatic TSE sequence have been demonstrated for human applications at 7 T. We have shown that, by lowering the frequency sweep, the B_1 threshold (the minimal B_1 strength for which the BIR-4 pulses behave adiabatic) will be lowered. The most important benefit of lowering the B_1 threshold is the reduction of the SAR. As a result, the superadiabatic condition, which is reached at lower B_1 values, will be violated for very high B_1 values. The violation is a result of the fact that the spins rotate around the summation vector (ω_{eff}) of the B_1 strength and the off-resonance component. When an adiabatic pulse is created for low B_1 values, the rate of change for the effective field can be minimized by reducing the FM to the same order of magnitude as the B_1. While in conventional adiabatic RF pulses the FM is significantly higher than the B_1 and therefore increased B_1 generally benefits the adiabatic performance of these pulses, in the relatively low FM values, the B_1 needs to be constrained. If not, the effective vector, where the magnetization vector is rotating around, will change too fast and therefore lose the magnetization vector. This will result in loss of the magnetization vector and the superadiabatic condition is thus violated. However, these B_1 values are much higher than the maximal B_1 strength of the surface coils (±50 μT) for human applications. For the B_1 ranges of interest, determined by these coils, the adiabatic TSE sequences provides much more homogeneous images than the conventional TSE in a non-uniform B_1 field, as demonstrated for human applications in the head, neck and pelvis at 7 T.

2.7 Acknowledgment

The authors would like to thank Robin de Graaf for the Bloch simulation program.

2.8 References

1 **Gass A, Oster M, Cohen S, Daffertshofer M, Schwarts A, Hennerici MG.** Assessment of T_2- and T_1-weighted MRI brain lesion load in patients with subcortical vascular encephalopathy. Neuroradiology 1998;40:503-506.

2 **Soyer P, Dufresne AC, Somveille E, Lenormand S, Scherrer A, Rymer R.** Differentiation between hepatic cavernous hemangioma and malignant tumor with T_2-weighted MRI: comparison of fast spin-echo and breath-hold fast spin-echo pulse sequences. Clin Imaging 1998;22:200-210.

3 **Valles F, Fiandaca MS, Eberling JL, Starr PA, Larson PS, Christine CW, Forsayeth J, Richardson RM, Su X, Aminoff MJ, Baniewicz KS.** Qualitative imaging of adeno-associated virus serotype 2-human aromatic L-amino acid decarboxylase gene therapy in a phase I study for the treatment of Parkinson disease. Neurosurgery 2010;67:1377-1385.

4 **Yen YF, Le Rouw P, Mayer D, King R, Spielman D, Tropp J, Pauly KB, Pfefferbaum A, Vasanawala S, Hurd R.** T_2 relaxation times of 13C metabolites in a rat hepatocellular carcinoma model measured in vivo using 13C-MRS of hyperpolarized [1-13C] pyruvate. NMR biomed 2010;23:414-423.

5 **Vaughan JT, Garwood M, Collins CM, Liu W, DeLaBarre L, Adriany G, Andersen P, Merkle H, Goebel R, Smith MB, Ugurbil K.** 7T vs. 4T: RF power, homogeneity, and Signal-to-Noise comparison in head images. Magn Reson Med 2001;46:24-30.

6 **Zweckstetter M, Holak TA.** An adiabatic multiple spin-echo pulse sequence: removal of systematic errors due to pulse imperfections and off-resonance effects. J Magn Reson 1998;133:134-147.

7 **De Graaf RA, Rothman DL, Behar KL.** Adiabatic RARE imaging. NMR biomed 2003;16:29-35.

8 **Garwood M, Ke Y.** Symmetric pulses to induce arbitrary flip angles with compensation for RF inhomogeneity and resonance offsets. J Magn Reson 1991;94:511-525.

9 **Garwood M, DeLaBarre L.** The return of the frequency sweep: Designing adiabatic pulses for contemporary NMR. J Magn Reson 2001;153:155-177.

10 **Tannus A, Garwood M.** Adiabatic pulses. NMR biomed 1997;10:423-434.

11 **Silver M, Joseph RI, Hoult DI.** Highly selective π/2 and π pulse generation. J Magn Reson 1984;59:347-351.

12 **De Graaf RA, Luo Y, Terpstra M, Merkle H, Garwood M.** A new localization method using an adiabatic pulse, BIR-4. J Magn Reson 1995;106:245-252.

13 **Deschamps M, Kervern G, Massiot D, Pintacuda G, Emsley L, Grandinetti PJ.** Superadiabaticity in magnetic resonance. J Chem Phys 2008;129.

14 **Hwang TL, Shaka AJ.** Water suppression that works. Excitation sculpting using arbitrary waveforms and pulsed field gradients. J Magn Reson 1995;112:275-279.

15 **Visser F, Zwanenburg JJM, Hoogduin JM, Luijten PR.** High-Resolution Magnetization-Prepared 3D-FLAIR Imaging at 7.0 Tesla. Magn Reson Med 2010;64:194-202.

16 **Klomp DWJ, Scheenen TW, Arteaga de Castro CS, Van Asten J, Boer VO, Luijten PR.** Detection of fully refocused polyamine spins in prostate cancer at 7T. NMR biomed 2011;24:299-306.

17 **Scheenen TW, Heerschap A, Klomp DWJ.** Towards ^{1}H-MRSI of the human brain at 7T with slice selective adiabatic refocusing pulses. Magma 2008;21:95-101.

18 **Matson GB.** An integrated program for amplitude-modulated RF pulse generation and re-mapping with shaped gradients. Magn Reson Imag 1994;12:1205-1225.

19 **Klomp DWJ, Bitz AK, Heerschap A, Scheenen TW.** Proton spectroscopic imaging of the human prostate at 7 T. NMR biomed 2009;22:495-501.

20 **US Food and Drug Administration.** Criteria for Significant Risk Investigations of Magnetic Resonance Diagnostic Devices. U.S. Department of Health and Human Services FaDA, Center for Devices and Radiological Health, New Hampshire, Silver Spring, MD 2003.

21 **Balchandani P, Pauly J, Spielman D.** Slice-selective tunable-flip adiabatic low peak-power excitation pulse. Magn Reson Med 2008;59:1072-1078.

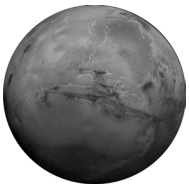

Chapter 3

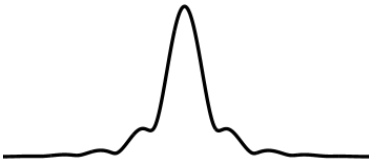

Tilt Optimized Flip Uniformity (TOFU) RF pulse for uniform image contrast at low specific absorption rate levels in combination with a surface breast coil at 7 Tesla

I.M.L. van Kalleveen[1], V.O. Boer[1], P.R. Luijten[1], D.W.J. Klomp[1]
[1]Department of Radiology, UMC Utrecht, the Netherlands

Published in 2014 in Magnetic Resonance in Medicine (74: 482-488)
DOI: 10.1002/mrm.25415

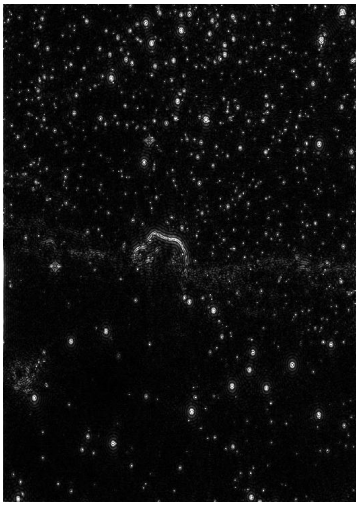

"Our virtues and our failings are inseparable, like force and matter.
When they separate, man is no more."
Nikola Tesla

Abstract

Purpose: Going to ultrahigh field MRI (e.g,.7 tesla), the non-uniformity of the B_1^+ field and the increased radiofrequency (RF) power deposition become challenging. While surface coils improve the power efficiency in B_1^+, its field remains non-uniform. In this work, an RF pulse was designed that uses the slab selection to compensate the inhomogeneous B_1^+ field of a surface coil without a substantial increase in specific absorption rate (SAR).

Theory and Methods: A breast surface coil was used with a decaying B_1^+ field in the anterior-posterior direction of the human breast. Slab selective RF pulses were designed and compared with adiabatic and spokes RF pulses. Proof of principle was demonstrated with FFE and B_1^+ maps of the human breast.

Results: *In vivo* measurements obtained with the breast surface coil show that the tilt optimized flip uniformity (TOFU) RF pulses can improve the flip angle homogeneity by 31%, while the SAR will be lower compared with BIR-4 and spokes RF pulses.

Conclusion: By applying TOFU RF pulses to the breast surface coil, we are able to compensate the inhomogeneous B_1^+ field, while keeping the SAR low. Therefore stronger T_1-weighting in FFE sequences can be obtained, while pulse durations can remain short, as shown in the human breast at
7 T.

3.1 Introduction

Dynamic contrast enhanced MRI (DCE-MRI) is widely used in clinical diagnoses of breast cancer[1]. With the current spatial and temporal resolution, sensitivity and specificity of DCE-MRI is still insufficient to obviate the need for histopathology. The spatial resolution in DCE-MRI is ultimately determined by the signal-to-noise ratio (SNR) obtainable from the contrast enhanced lesion[2].

Going to ultra-high field strength (i.e., 7 tesla) increases the SNR, however at higher field strengths the specific absorption rate (SAR) becomes even more challenging, compared with e.g., 3 T[3].

Local surface coils used for spin excitation have been suggested to overcome substantial RF power deposition[4,5], which indeed enables high resolution MRI with a strong contrast-to-noise ratio. However, local transmit coils provide an extreme non-uniform B_1^+ field, resulting in only a limited field of view where the desired flip angle is reached. In addition, image artifacts due to this non-uniformity can obscure the diagnostic performance of such scans and hence might not be clinically relevant.

Several solutions on the RF pulse part have been proposed to obtain uniform excitation with surface coils, like adiabatic RF pulses[6] and multi-dimensional RF pulses[7,8]. However, these are often SAR demanding RF pulses with a relatively long duration. Consequently, these solutions can have an impact on the repetition time (T_R) substantially, particularly in T_1-weighted MRI that uses T_R values of a few ms, resulting in increased scan times and diminished T_1 contrast.

Here we propose a different approach. Consider the so-called TONE (tilt optimized non-saturated excitation) RF pulse[9-11], which was originally created for three-dimensional (3D) magnetic resonance angiography (MRA) scans. With TONE, a slab is excited by an RF pulse which provides a decaying flip angle over the slab. With a surface RF coil combined with a conventional slab selective RF pulse we observe the same behavior: the B_1^+ field of a surface coil drops off with the distance, thus when combined with a conventional slab selective RF pulse, the flip angle decays over distance. To create a homogeneous flip angle despite of the inhomogeneous B_1^+ field, we can simply reverse the direction of the TONE pulse to the direction of field non-uniformity of the RF coil. More specifically, the spatial response function of an RF pulse can be modified to the inverse of the B_1^+ field non-uniformity in order to provide tilt optimized flip uniformity (TOFU). We compare the TOFU RF pulse with the adiabatic RF pulse and spokes pulses in simulations and show the benefits of the TOFU RF pulse in the application of contrast enhanced breast MRI.

3.2 Theory

Consider the decaying B_1^+ field of a transmit breast surface coil that decreases with increasing distance from the coil. As shown before in 7 T breast MRI, such a surface transmit coil can provide a decaying B_1^+ field in the breast, ranging from approximately 60 μT at the nipple, to approximately 20 μT at the chest wall[12] (simplified in Fig. 3.1a; black line). To determine the desired magnetization profile of the TOFU RF pulse, we invert the B_1^+ profile (Fig. 3.1b). For small flip angles we can calculate the RF pulse from its magnetization profile by applying the inverse fast fourier transform (FFT). Then, combining the B_1^+ profile of the surface coil together with the designed RF pulse results in a homogeneous flip angle distribution. To investigate the frequency spectrum of the designed RF pulse (Fig. 3.2a, solid plots), we can compare the designed RF pulse with the behavior of a conventional sinc RF pulse using 9 lobes for both RF pulses (Fig. 3.2a, dashed plots). The frequency spectra are shown in Fig. 3.2a (bottom row).

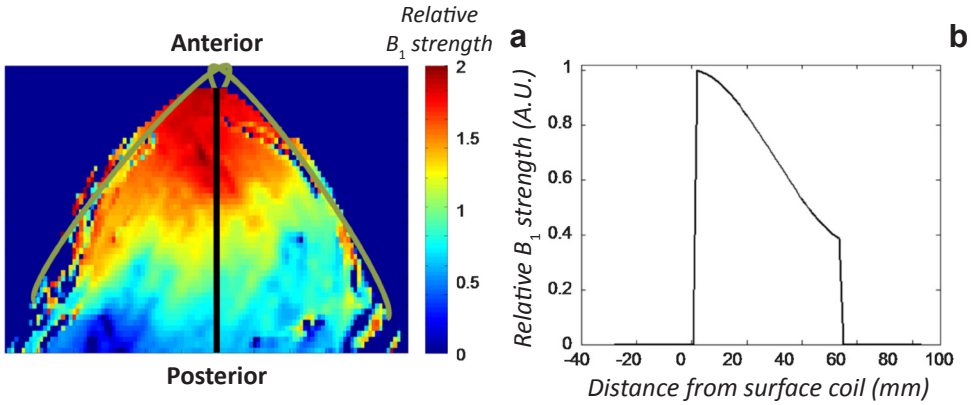

Fig. 3.1. a) The B_1^+ field map of a human breast located in a surface transmit coil (where the coil elements are visualized in gold). The color scale correspond to the relative B_1^+ intensities, where blue corresponds to the lowest B_1^+ and the red to the highest B_1^+. **b**) The B_1^+ profile from the nipple to the chest wall (represented by the black line in **a**).

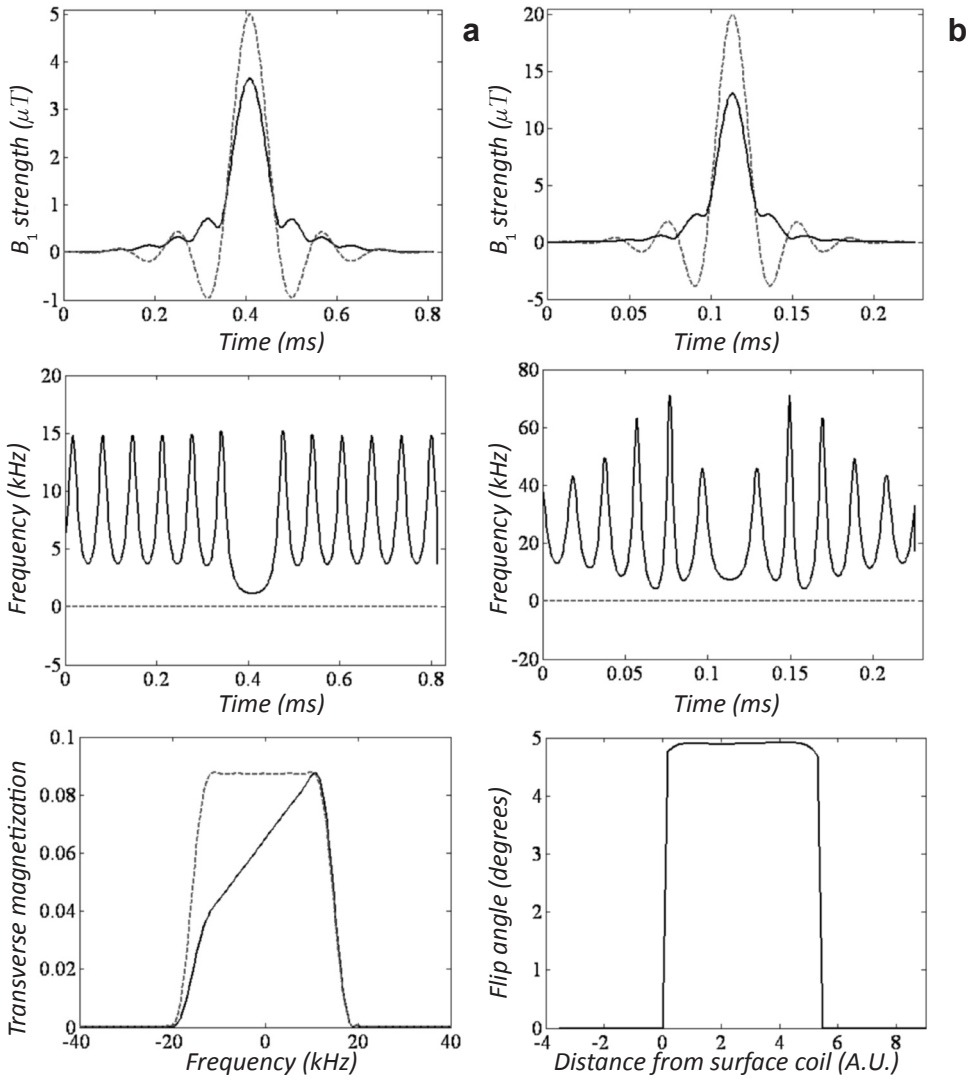

Fig. 3.2. a) Visualization of the TOFU RF pulse compared with the conventional RF pulse. The amplitude modulation of the conventional (dashed) and TOFU (solid) RF pulse normalized to the minimum B_1^+ field in the field of view (the B_1^+ field in the chest wall). Also the corresponding frequency modulations of these RF pulses are plotted and the result of the Fourier transforms of both RF pulses is visualized, which represent the magnetization profiles of these RF pulses in the low flip angle regime in a uniform B_1^+ field. The dashed line corresponds to the conventional sinc pulse and the solid line corresponds to the TOFU pulse. Both RF pulses result in the same flip angle at the end of the slab (*in vivo* in the chest wall). **b**) The simulated RF pulse which is implemented in the scanner software. Combining the amplitude and frequency modulation of the TOFU RF pulse, together with the inhomogeneous B_1^+ field of the breast surface coil, will result in the desired homogeneous flip angle over space. These simulations were performed by using the Bloch simulations at a low flip angle regime.

TOFU RF Pulse versus BIR-4 and Spokes

We compare the efficiency of the TOFU RF pulse with an adiabatic BIR-4 pulse at a low B_1 strength of 5 μT[13-15], and therefore, the pulse is against the limits of adiabaticity. Also a comparison between the TOFU and a SAR optimized spokes RF pulse is made. We are calculating and comparing the energy deposition of the RF pulses when used in the most efficient T_1-weigthed scan; i.e., shortest T_R and a relatively high flip angle of 10°.

The most power efficient spokes RF pulse will provide constructive flip angle interference between the spokes at the location of the lowest B_1^+. For the fastest spokes pulse (i.e., 2 RF pulses with one gradient blip in between), the power efficiency is calculated (assuming that only 2 spokes can provide a uniform flip angle distribution). To obtain a relatively homogeneous flip angle, the most constructive method is to add the flip angles of the two spokes at the location of the chest (where the lowest B_1^+ is present) and have them interfere destructively at the location of the nipple. To assure an identical slab profile, also 9 lobes were used for each spoke.

ProSet

Another important technique for breast imaging is the application of fat suppression. Of all techniques, the ProSet technique (principle of selective excitation technique[16]), is one of the most time efficient techniques to remove fat signal. This technique exists of binomial RF pulses[17], which uses the difference between resonance frequencies of water and fat to null the signal of fat. One of the constraints is that the time between the pulse elements in the binomial RF pulse has to be 0.5 ms (the time it takes for water and fat signals to be 180° out of phase at 7 T), which includes the gradient ramp times. Both the TOFU RF pulse, as well as the spokes RF pulse have been calculated for this fat suppression scheme, including VERSE (Variable Rate Selective Excitation) to maximize the attainable flip angle.

To apply the spokes pulse in the ProSet technique, we have to put two pulses and an additional gradient blip in the same time as normally one pulse is inserted. We set the maximum distance (i.e., slab thickness in AP direction) between the nipple and the chest wall at 120 mm. Within this region, the B_1^+ field strength varies with a factor of 3 (as also shown in Fig. 3.1b). The gradient limitations (maximal gradient strength = 40 mT/m; maximal slew rate = 200 T/m/s) were taken into account in designing the optimal RF pulse.

3.3 Methods

RF pulse design

A fixed slab selection of 12 cm was used in the anterior posterior (AP) direction (i.e.,

from the nipple (mammary papilla) to the muscle of the breast (pectoralis major)). To calculate the TOFU RF pulses, the average B_1^+ profile along the AP direction was used (Fig. 3.1). The measured B_1^+ profile was inverted and an inverse Fast Fourier Transform was applied where the center 7 lobes were used to define the RF pulse (Fig. 3.2b). The RF pulse was implemented in the scanner software as a fixed function (same as traditional pulses that are present in the scanner software).

Experimental setup

We used an RF surface coil (MR Coils BV, Drunen, the Netherlands) that is used for breast MRI at
7 T[18]. This coil setup comprises of two orthogonally aligned overlapping circular coil elements which are driven in quadrature mode. These elements are used to transmit an efficient but a non-uniform B_1^+ field, which is decaying predominantly in one dimension[12]. The integrated receive coil consists of 30 overlapping oval shaped array elements (5x3 cm^2) which are geometrically and preamp decoupled. The coil setup is interfaced to a 7 T whole body MRI system (Philips, Cleveland, OH, USA) operating on a clinical MRI console. With the available RF peak power of 4 kW, the system can provide a maximum peak B_1^+ strength of 20 μT at the chest wall or effectively 4 μT when averaged over time before local SAR exceeds 20 W/kg[19-21].

Phantom experiments were performed to demonstrate the spatial properties of the TOFU RF pulse. For this purpose, a uniform field was provided with a volume head coil (Nova Medical, Elmsfort, NY, USA) loaded with a Plexiglas sphere filled with oil (Marcol). Proton density-weighted 3D fast field echo (FFE) scans (with a nominal flip angle of 1°, a T_R of 50 ms, a field of view (FOV) of 160x160x160 mm^3 and a resolution of 1x1x1 mm^3) were obtained with a conventional and the TOFU RF pulse with the volume head coil as a transceiver to demonstrate the spatial properties of the TOFU RF pulse.

In vivo measurements were obtained with the breast surface coil in combination with a conventional and the TOFU RF pulse. B_1^+ maps (AFI[22]; FOV = 160x180x120 mm^3, resolution = 5x4.5x4 mm^3) were obtained with a conventional and the fixed TOFU RF pulse in four healthy female volunteers with different sizes of breasts (cup size A to D) to show reproducibility. The homogeneity of the flip angle was determined over the entire breast excluding the chest wall and was calculated by two means: 1. Taking the standard deviation of the flip angle divided by the mean flip angle per subject and 2. Taking the difference between the maximum and minimum flip angle value in this region divided by the mean flip angle. For the determination of the homogeneity of the fixed TOFU RF pulse, *in vivo* measured flip angle maps were used. For the calculations of the patient based TOFU RF pulse the B_1^+ map of the conventional RF pulse was used and for each subject an adjusted RF pulse was calculated. Then the

patient based TOFU RF pulse was simulated to the conventional B_1^+ map 3D turbo field echo (TFE) sequences were obtained in combination with the surface coil (FOV = 160x160x120 mm^3, nominal flip angle = 2°, T_R = 10 ms, resolution = 0.8x1x1 mm^3) with conventional and TOFU RF pulses to compare the performance.
Also a dynamic contrast enhanced sequence with ProSet fat suppression was performed on a breast cancer patient. Here, in addition to the surface transmit coil, also a high density receiver coil was inserted that facilitated high SENSE encoding[21] (ProSet flip angle = 8.5°, T_R = 9.9 ms, FOV = 160x160x160 mm^3, spatial resolution = 0.5x0.7x0.65 mm^3, SENSE = 2x4). This way, in addition to the high spatial resolution, also the high contrast can be appreciated. The study has been approved by the local ethical committee of the University Medical Centre Utrecht and written informed consents have been obtained from the volunteers.

3.4 Results

Simulations
Comparing the SAR of a BIR-4 pulse with a TOFU RF pulse to obtain a 10° flip angle, the SAR is increased at least with a factor of 21. If we compare the 2 spokes RF pulse with the TOFU RF pulse, an increase in SAR with a factor of 3.5 is obtained.
Applying the TOFU RF pulse in the ProSet technique gives an effective pulse duration of 0.4475 ms, due to sampling during the gradient ramps which are limited to 200 T/m/s. This effective pulse duration results in an effective flip angle of 10°.
Using the spokes pulse in the ProSet technique results in a triangular gradient blip with gradient surface of 0.326 mT·ms/m that takes 0.0255 ms, leaving us with a maximum pulse duration of 0.2372 ms per spoke. To play out the slice selective RF pulse, even during the ramp of the gradient the effective pulse duration will be 0.1532 ms. Consequently, the maximal flip angle available when applying spokes to the ProSet will be less than 5°.

Experimental images
With a homogeneous head coil we visualized the linear spatial profile of the TOFU RF pulse (Fig. 3.3a), demonstrating the correct implementation of the RF pulse. When applied to the human breast with the breast surface coil set as a transceiver, a more uniform image intensity can be observed (Fig. 3.3b), albeit that the non-uniform reception of the RF coil remains present.

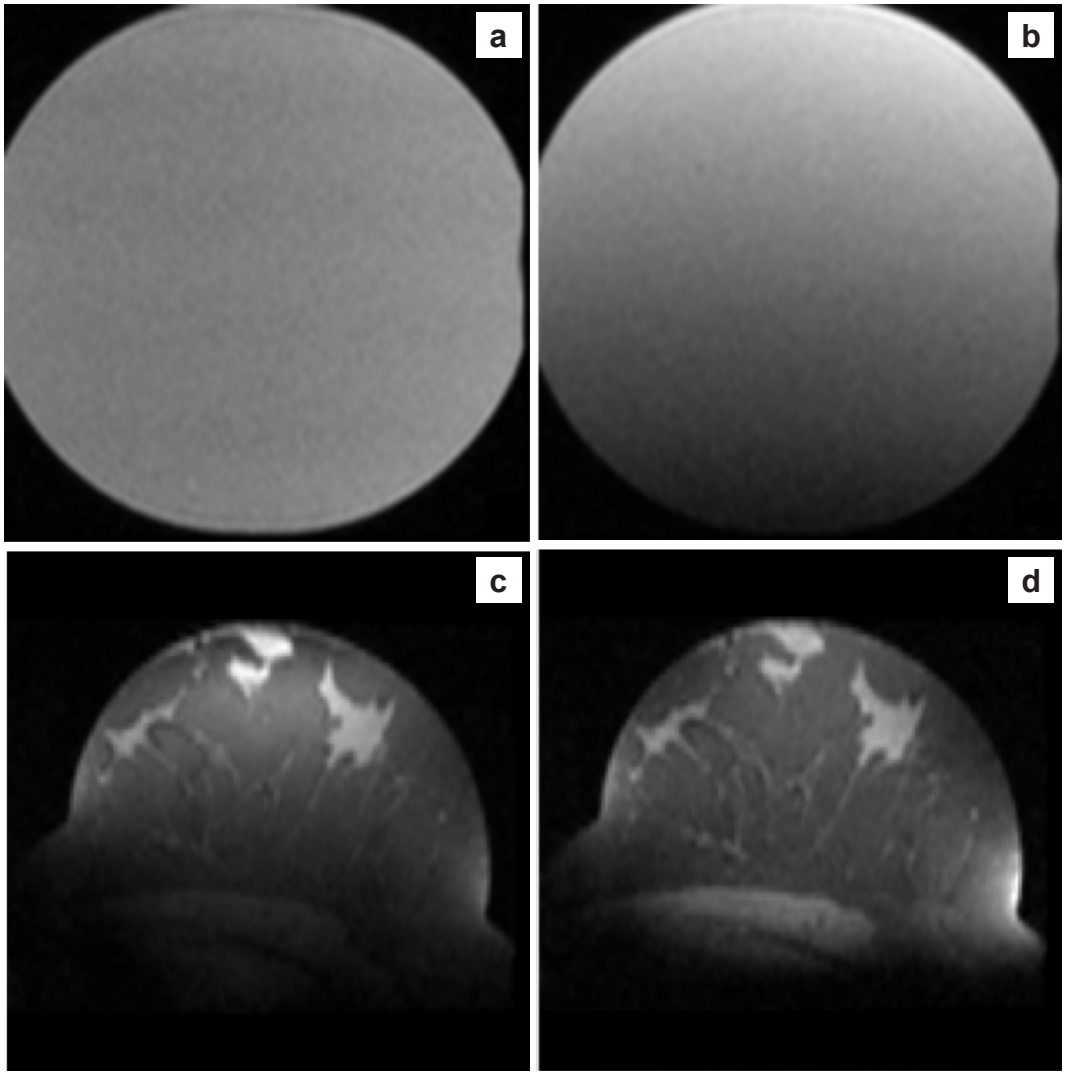

Fig. 3.3. Images obtained with a TFE sequence of an oil phantom in the homogeneous head coil with the conventional RF pulse (**a**) and the TOFU RF pulse (**b**). Note the linear signal intensity distribution over one dimension of the TOFU pulse that resembles the inverse of the flip angle distribution of the breast coil. Images from an *in vivo* TFE scan without fat suppression of a healthy volunteer, in combination with the breast surface coil. The image uniformity is substantially improved toward the chest wall, when comparing the conventional RF pulse (**c**) with the compensated RF pulse in the TFE sequence (**d**).

The flip angle (fa) maps combined with the fixed TOFU RF pulse respectively the conventional RF pulse (Fig. 3.4) gave a homogeneity improvement of 33% when considering the (famax-famin)/ famean within the breast. To remove the outliers, the maximum and minimum 5% of the data points were removed. The relative overall

standard deviation of the flip angle in the whole breast region when applying the TOFU RF pulse was 0.21. When optimizing the TOFU RF pulse per volunteer the homogeneity could be improved to 45% and the standard deviation in the flip angle can be decreased to 0.19. The optimal flip angle for conventional RF pulse was positioned in the center of the breast, whereas the same optimal flip angle for the TOFU RF pulse was positioned throughout the whole breast . This resulted in an increase in SAR of 7.5% when applying the TOFU RF pulse, instead of the conventional RF pulse.

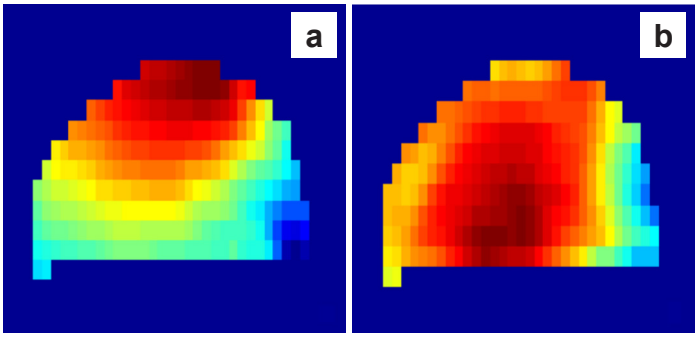

Fig. 3.4. A flip angle map measured with a conventional RF pulse (**a**) and a TOFU RF pulse (**b**). Note the strong decrease in the B_1 field the anterior-posterior position when applying a conventional RF pulse. And note the effect of the TOFU RF pulse, which creates a more homogeneous the flip angle.

With the binomial water selective excitation (ProSet), excellent fat suppression is obtained in the human breast (Fig. 3.3a). Due to its high efficiency, the compensated RF pulse could provide a flip angle of 20° within the effective time frame of 500 μs. Thereby enabling incorporation of water selective excitation at a relatively high flip angle within a short T_R to provide images with a strong T_1-weighting (Fig. 3.5: example of contrast enhanced MRI in breast cancer).

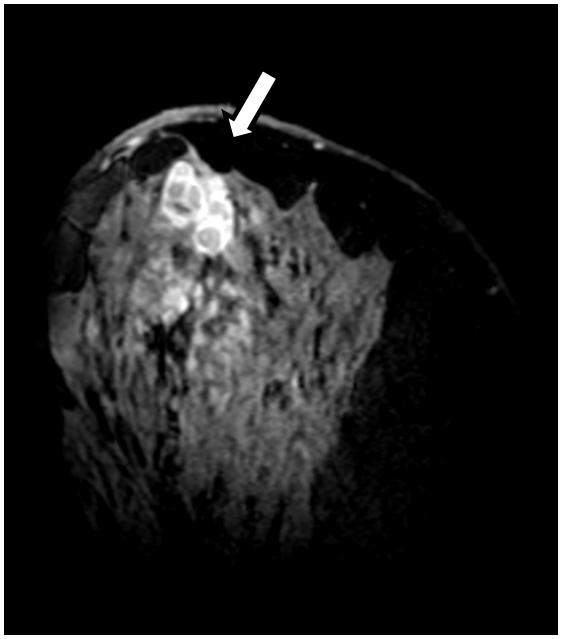

Fig. 3.5. *In vivo* contrast enhanced TFE sequence in a patient with breast cancer in combination with a binomial water selective excitation obtained at ultra-high resolution (0.5x0.65x0.7 mm^3). Note that the ultra-high resolution MRI reveals heterogeneity of contrast inside the tumor.

3.5 Discussion

In this study, we showed that slab selective RF pulses can be tuned to compensate the non-uniform B_1^+ fields of surface coil into a uniform flip angle distribution. More importantly, when combined, the high efficiency of the surface coil can be maintained to provide strong and uniform T_1-weighted contrast imaging. Consequently, even at the high field strength of 7 T, where SAR often limits strong contrast imaging, we could demonstrate the effective use of these efficient RF pulses to provide a strong T_1-weighted contrast at ultra-high resolution as demonstrated in a patient with breast cancer.

Note that we compensated the B_1^+ field to provide a uniform flip angle in only one dimension (the dominant dimension of the surface coil). The compensation works optimally if the changing B_1^+ field is perpendicular to the slab and the B_1^+ field is homogeneous throughout the slices in the slab. While it may be possible to compensate also in the other two dimensions by means of spoke pulses, this will affect the efficiency of the one dimensional TOFU RF pulse, as shown in the ProSet example.

We have shown we can improve the homogeneity in the breast, combined with the surface coil, by 33% using the TOFU pulse instead of the conventional RF pulse, with hardly increasing SAR. While in our study we used a predetermined TOFU RF pulse

based on a generalized B_1^+ field map, it is possible to calculate the TOFU RF pulse on a patient based B_1^+ map. This will require the acquisition of B_1^+ maps and online calculations. Simulations point out that this will improve the homogeneity with another 12%. If non-localized RF pulses are an option and the pulse duration is not a major restriction, spokes RF pulses consisting of more elements could be an effective option as well. However, when slab selection is a requirement anyhow, TOFU RF pulses would still be a better option. In our study, the effect of the TOFU RF pulse was shown when used in combination with the ProSet technique; where pulse duration is critical as well. Due to the short pulse duration even when a minimal number (2) of RF pulses in a spokes pulse is used, the bandwidth of the RF pulses are very high. This results in a strong selective gradient, which due to limits in gradient ramp times may not fit into the ProSet technique or leaves ample effective time for the RF pulses. In this case, comparing with the spokes RF pulses, the difference in obtainable flip angles is large. Therefore a substantially increased T_1 contrast weighting could be obtained while preserving excellent fat suppression.
In conclusion, we have shown that we are able to compensate for the inhomogeneous B_1^+ field of a surface coil, without using a high SAR demanding adiabatic RF pulse. As expected and demonstrated, particularly for low flip angles, these TOFU RF pulses can be more than 20-fold less power demanding than adiabatic RF pulses. But also compared with the least SAR demanding spokes RF pulse, the SAR will still be a factor of 3.5 lower when using TOFU RF pulses. Combining the TOFU RF pulse with a parallel transmit[23] setup, where RF shimming is used for the remaining two dimensions, may create an even more homogeneous flip angle in the spatial dimensions without effecting the RF pulse duration. Due to the combination of the TOFU RF pulse and the surface coil, we are able to obtain high flip angle duty cycles even at 7 T, which result in strong image contrast at high SNR.

3.6 References

1 **Martincich L, Montemurro F, De Rosa G, Marra V, Ponzone R, Cirillo S, Gatti M, Biglia N, Sarotto I, Sismondi P, Regge D, Aglietta M.** Monitoring response to primary chemotherapy in breat cancer using dynamic contrast-enhanced magnetic resonance imaging. Breast cancer research and treatment 2004;83:67-76.

2 **Kuhl CK, Jost P, Morakkabati N, Zivanovic O, Schild HH, Gieseke J.** Contrast-enhanced MR Imaging of the Breast at 3.0 and 1.5 T in the Same Patients: Initial Experience. Radiology 2006;239(666-676).

3 **Haacke EM, Brown RW, Thompson MR, Venkatesan R.** Magnetic resonance imaging. 1999:406-409, 858-860.

4 **Hoult DI, Busby SJW, Gadian DG, Radda GK, Richards RE, Seeley PJ.** Observation of tissue metabolites using ^{31}P nuclear magnetic resonance. Nature 1974;252:285-287.

5 **Van den Bergen B, Klomp DWJ, Raaijmakers AJE, Arteaga de Castro CS, Boer VO, Kroeze H, Luijten PR, Lagendijk JJW, Van den Berg CAT.** Uniform prostate imaging and spectroscopy at 7 T: comparison between a microstrip array and an endorectal coil. NMR Biomed 2011;24:358-365.

6 **Garwood M, DeLaBarre L.** The return of the frequency sweep: Designing adiabatic pulses for contemporary NMR. J Magn Reson 2001;153:155-177.

7 **Grissom WA, Xu D, Kerr AB, Fessler JA, Noll DC.** Fast large-tip-angle multidimensional and parallel RF pulse design in MRI. IEEE Trans Med Imaging 2009;10:1548-1559.

8 **Grissom WA, Yip C, Zhang Z, Stenger A, Fessler JA, Noll DC.** Spatial Domain Method for the Design of RF Pulses in Multicoil Parallel Excitation. Magn Reson Med 2006;56:620-629.

9 **Bernstein MA, King KF, Zhou XJ.** Handbook of MRI Pulse Sequences. 2004:138-147.

10 **Tkach JA, Masaryk TJ, Ruggieri PM, Ross JS, Dillinger J.** Use of tilted optimized nonsaturating excitation (TONE) RF pulses and MTC to improve the quality of MR angiograms of the carotid bifurcation. . SMRM Book of Abstracts 1992;Eleventh Annual Meeting of the Society of Magnetic Resonance in Medicine, Works in Progress, Berkeley, CA:3905.

11 **Purdy D, Cadena G, Laub G.** The design of variable tip angle slab selection (TONE) pulses for improved 3-D MR angiography. SMRM Book of Abstracts 1992;Eleventh Annual Meeting of the Society of Magnetic Resonance in Medicine, Works in Progress, Berkeley, CA:882.

12 **Stehouwer BL, Klomp DWJ, Korteweg MA, Verkooijen HM, Luijten PR, Mali WPTM, Van den Bosch MAAJ, Veldhuis WB.** 7 T versus 3 T contrast-enhanced breast Magnetic Resonance Imaging of invasive ductulolobular carcinoma: First clinical experience. Magn Reson Imaging 2012;31:613-617.

13 **Moore J, Jankiewicz M, Zeng H, Anderson AW, Gore JC.** Composite RF pulses for B_1^+-insensitive volume excitation at 7 Tesla. JMR 2010;205:50-62.

14 **Staewen RS, Johnson AJ, Ross BD, Parrish T, Merkle H, Garwood M.** 3-D FLASH Imaging Using a Single Surface Coil and a New Adiabatic Pulse, BIR-4. Invest Radiol 1990;25:559-567.

15 **Van Kalleveen IML, Koning W, Boer VO, Luijten PR, Zwanenburg JJM, Klomp DWJ.** Adiabatic Turbo Spin Echo in Human Applications at 7 T. Magn Reson Med 2012;68:580-587.

16 **Bernstein MA, King KF, Zhou XJ.** Handbook of MRI Pulse Sequences2004. 97-100 p.

17 **Hore PJ.** Solvent Suppression in Fourier Transform Nuclear Magnetic Resonance. JMR 1983;55:283-300.

18 **Korteweg MA, Veldhuis WB, Visser F, Luijten PR, Mali WP, Van Diest PJ, Van den Bosch MA, Klomp DWJ.** Feasibility of 7 Tesla breast magnetic resonance imaging determination of intrinsic sensitivity and high-resolution magnetic resonance imaging, diffusion-weigthed imaging, and ^{1}H-magnetic resonance spectroscopy of breast cancer patients receiving neoadjuvant therapy. Invest Radiol 2011;46:370-376.

19 **US Food and Drug Administration.** Criteria for Significant Risk Investigations of Magnetic Resonance Diagnostic Devices. U.S. Department of Health and Human Services FaDA, Center for Devices and Radiological Health, New Hampshire, Silver Spring, MD 2003.

20 **Klomp DWJ, Bitz AK, Heerschap A, Scheenen TW.** Proton spectroscopic imaging of the human prostate at 7 T. NMR biomed 2009;22:495-501.

21 **Van de Bank BL, Voogt IJ, Italiaander M, Stehouwer BL, Boer VO, Luijten PR, Klomp DWJ.** Ultra high spatial and temporal resolution breast imaging at 7T. NMR in Biomed 2012;26:367-375.

22 **Yarnykh VL.** Actual Flip-Angle Imaging in the pulsed Steady State: A method for rapid three-dimensional mapping of the transmitted radiofrequency field. Magn Reson Med 2007;57:192-200.

23 **Katscher U, Bornert P.** Parallel RF transmission in MRI. NMR Biomed 2006;19:393-400.

Chapter 4

2D Radially Compensating Excitation (RACE) pulse in combination with an internal transceiver antenna for 3D MRI of the rectum at 7 T

I.M.L. van Kalleveen[1], H. Kroeze[13], A. Sbrizzi[1], V.O. Boer[1], O. Reerink[2], M.E.P. Philippens[2], C.A.T. van de Berg[2], P.R. Luijten[1], D.W.J. Klomp[1]

[1]Department of Radiology, UMC Utrecht, the Netherlands

[2]Department of Radiotherapy, UMC Utrecht, the Netherlands

[3]Department of Medical Technology, UMC Utrecht, the Netherlands

Accepted in Medical Physics

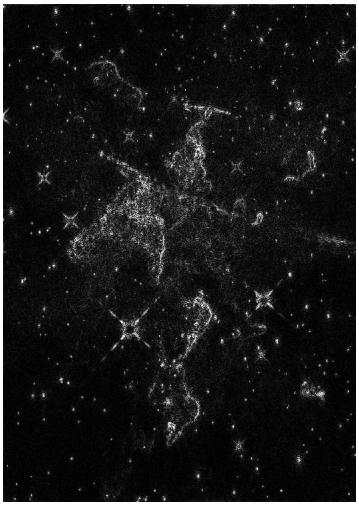

"A scientific truth does not triumph by convincing its opponents and making them see the light, but rather because its opponents eventually die and a new generation grows up that is familiar with it."

Max Planck

Abstract

Purpose: The high precession frequency in ultra-high field MRI coincides with reduced RF penetration, increased RF power deposition and consequently can lead to reduced scan efficiency. However the shorter wavelength enables the use of efficient antennas rather than loop coils. In fact, ultra-thin monopole antennas have been demonstrated at 7 T, which fit in natural cavities like the rectum in the human body. As the RF field generated by the antenna provides an extremely non-uniform B_1 field, the use of conventional RF pulses will lead to severe image distortions and highly non-uniform contrast. However, using the two predominant dimensions (orthogonal to the antenna), two-dimensional RF pulses can be designed that counteract the non-uniform B_1 into uniform flip angles. In this study we investigate the use of an ultra-thin antenna not only for reception, but also for transmission in 7 T MRI of the rectum.
Methods: The 2D radially compensating excitation (2D RACE) pulse was designed in Matlab. SAR calculations between the 2D RACE pulse and an adiabatic RF pulse (BIR-4) have been obtained, to visualize the gain in decreasing the SAR when using the 2D RACE pulse instead of an adiabatic RF pulse. We used the 7 T whole body MR system in combination with an internally placed monopole antenna used for transceive and obtained 3D gradient echo images with a conventional sinc pulse and with the 2D RACE pulse. For extra clarity, we also reconstructed an image where the receive field of the antenna was removed.
Results: Comparing the results of the SAR simulations of the 2D RACE pulse with a BIR-4 pulse shows that for low flip angles ($\theta < 41°$) the SAR can be decreased with a factor of 4.8 or even more, when using the 2D RACE pulse. Relative to a conventional sinc excitation, the 2D RACE pulse achieves more uniform flip angle distributions than a BIR-4 pulse with a smaller SAR increase (16x versus 64x).
Conclusions: We have shown that the 2D RACE pulse provides more homogeneous flip angles for gradient echo sequences when compared to a conventional sinc pulse albeit at increased SAR. However, when compared to adiabatic RF pulses, as shown by simulations, the SAR of the 2D RACE pulse can be an order of magnitude less. Phantom and *in vivo* human rectum images are obtained to demonstrate that the 2D RACE pulse can provide a uniform excitation while transmitting with a single ultra-thin endorectal antenna at 7 T. The combination of thin rectal antennas with efficient uniform transmit can open up new possibilities in high resolution imaging of rectal cancer.

4.1 Introduction

At ultra-high field MRI (e.g., 7 tesla), very high spatial resolutions can be obtained as shown in the human brain[1]. The ability to increase the signal-to-noise ratio (SNR) and thus scanning at higher resolution opened up the possibility to detect smaller lesions[2-4]. Moreover, the spectral resolution increases at higher field. This can improve the detection of altered metabolism, which may provide insight in tumor grade or treatment effects[5]. In oncology, the detection of small lesions is important in early diagnosis of tumors and in treatment monitoring of chemo-radiation, where the differentiation between treatment induced changes, such as fibrosis and residual tumor is challenging[6,7]. Applying the higher resolutions that potentially can be obtained at 7 T to the rectum may help treatment planning of patients with rectum cancer.

However, at higher field strengths, the constraint of the energy deposition applied by an RF pulse becomes stronger. This is due to the increased Larmor frequency which coincides with a higher electric field per unit of flip angle. The energy deposition (Specific Absorption Rate; SAR) scales quadratically with this electric component of the field. Therefore increasing the static magnetic field strength implies an increase in SAR for the same shaped RF pulse[8]. As a result, it remains challenging for body imaging at 7 T to obtain higher quality images compared to 3 T, as is shown in the pelvis for the prostate. Particularly when acquired with an external coil array[9], the obtainable spatial resolution of these images is still not better than the resolution reported at 3 T[10].

Fortunately, the limits of these imaging techniques at 7 T have not been reached and more efficient RF pulses or transmit coils can boost the obtainable resolution. Moreover, to overcome the global and even local SAR constraints, local surface coils, e.g., an endorectal coil, may be used as transmitters[11-13]. The higher resonance frequency also implies a shorter wavelength which is about 11 cm at 7 T in human tissue. Therefore the idea to use local antenna's as internal transmitters has been proposed[14,15]. These internal antennas open new opportunities to image internal organs, like the rectum, prostate, cervix, esophagus and arterial pathways with high sensitivity. However the B_1 field of an antenna typically decreases fast with increasing distance from the antenna. While adiabatic RF pulses[16] have been proposed to provide uniform flip angles with such non-uniform B_1 fields, these RF pulses are very SAR demanding and consequently increase the scan time. Recently, promising results in rabbits have been demonstrated, using an internal antenna with non-adiabatic (composite) RF pulses[17].

In this work, we use multi-dimensional RF pulses[18-20] which are designed to compensate the inhomogeneous B_1^+ field of an internal single channel transmit and receive antenna to obtain a homogeneous flip angle in the human rectum *in vivo*. We compare the 2D RAdially Compensating Excitation (RACE) pulse with an adiabatic BIR-4 RF pulse[21] and show that we can increase the efficiency of the pulse and substantially de-

crease the SAR, hence enabling high resolution MRI of the rectum.

4.2 Theory

Applying a conventional RF pulse to an internal antenna (Fig. 4.1) will result in an inhomogeneous flip angle distribution over the spatial dimensions (Fig. 4.2a). However, if we know the spatial behavior of the B_1 field of the antenna, we are able to calculate the desired magnetization profile of the RF pulse. Particularly in the low flip angle regime, this simply corresponds to the inverse of the B_1 map (Fig. 4.2b). By combining the desired magnetization map, excited by the RF pulse, with the B_1 map of the antenna, a homogeneous flip angle can be created (Fig. 4.2c), similar to the one dimensional B_1 compensation[22]. Electromagnetic numerical simulations of the B_1 field along the antenna were also calculated (SEMCAD, Schmid & Partner Engineering AG, Zurich, Switzerland) using an rectangular 160x160x60 mm^3 medium with a relative dielectric permittivity of 36 and conductivity of 0.4 S/m (Fig. 4.2d). The program's variable gridding facility results in a resolution of 0.075 mm close to the conductor, while maintaining a total number of voxels of 193x166x170 that resulted in a full 3D simulation within a computation time of 14 hours.

Fig. 4.1. To show the relative size, the monopole antenna is placed next to a ballpoint with a length of 14.8 cm.

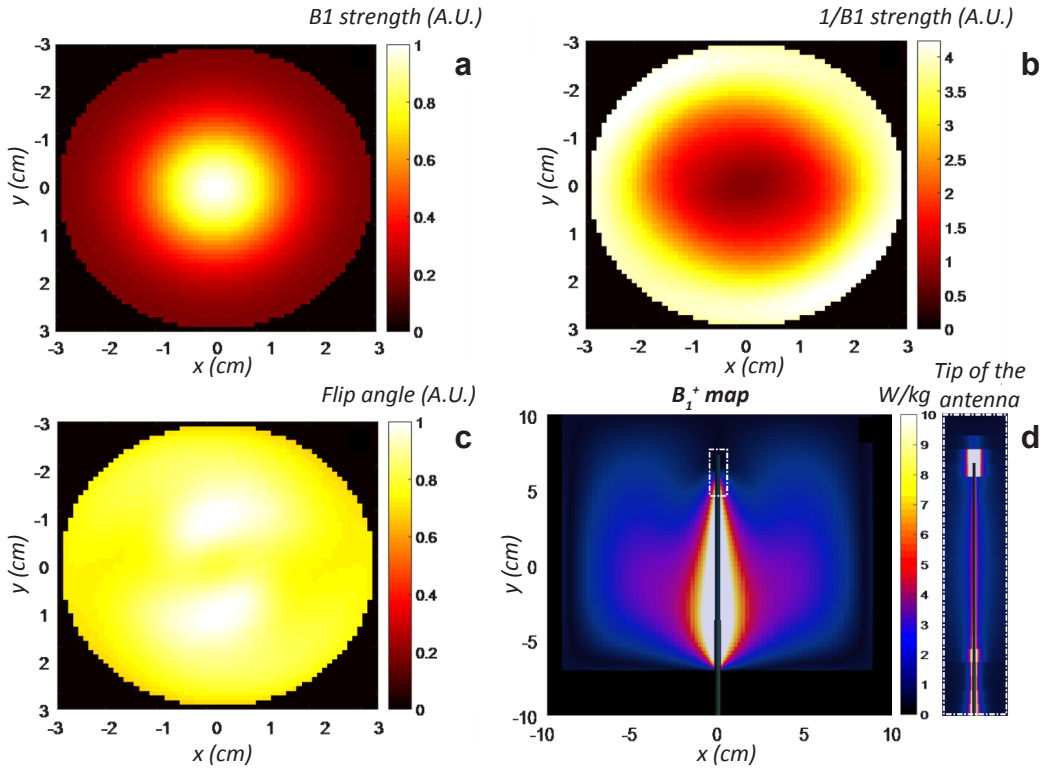

Fig. 4.2. Simulations of: **a**) the B_1 map of the transmitter antenna with a radius of 30 mm in the transverse plane shows the radially decreasing B_1^+ field. **b**) The inverted profile of the B_1 map that can be used as a target for pulse calculations in order to compensate for this and **c**) the flip angle map which is a result of the B_1 map and the optimized 2D RACE pulse simulated with the Bloch simulator. **d**) The B_1 field parallel to the antenna (gray rectangular shape) simulated in SEMCAD.

After knowing what the desired magnetization map is, the next step is to find the RF pulse which creates the desired magnetization profile. For small tip angles, the magnetization along the longitudinal axis (which is along the antenna) can be approximated to M_0 (the equilibrium magnetization). Therefore, the solution of the Bloch equation can be written as an integral over B_1, together with an expression that describes the phase accumulation which corresponds to the transmitting k-space trajectory[23] (Eq. 4.1).

$$M_{xy}(\vec{x}) = i\gamma M_0 \int_0^T B_1^+(x,y)\cdot b(t) e^{i\vec{x}\bullet\vec{k}(t)} dt \text{ , where } \vec{k}(t) = -\gamma \int_t^T G(\vec{s}) ds \qquad [4.1]$$

Where $i = \sqrt{-1}$, γ = gyromagnetic ratio, $B_1^+(x, y)$ = space dependent B_1^+ field of the RF coil, $b(t)$ = time dependent B_1 field created by the RF pulse, T = pulse duration, x

= spatial vector, k = spatial frequency vector and G = gradient vector. Eq. 4.1 shows the direct relation of the magnetization at a certain location and the RF pulse ($B_1(t)$) in combination with the gradients (G). The gradients determine the location in the transmitting k-space and the RF pulse determines the energy given to the corresponding spatial frequency.

4.3 Materials and Methods

Antenna

The antenna was created from a coaxial cable (RG223) (designed in collaboration with Machnet BV, Maarn, the Netherlands)[24]. Over a length of 300 mm, the outer isolation and shield were removed and on the last 60 mm the inner shield was also removed, which left only the insulator and central conductor at the end of the antenna. The antenna is tuned and matched, using a CLC π-network and was placed inside a balloon catheter (Rusch #18) resulting in a total diameter of 6 mm. The antenna uses a single transmit and receive channel, which can be used on any 7 T system. Finally B_1^+ and SAR simulations were obtained and a thermal test was performed in the rectum of a healthy volunteer, where a fiber optic thermometer was attached to the tip of the antenna (the hotspot based on EM simulations), while monitoring temperature over 10 min at a constant RF input power of 2 W.

RF pulse

The RF pulse was designed according to the small tip angle formula[23] adapted to include the B_1^+ inhomogeneity profile[25-27]. We made use of an in-house developed software, implemented in Matlab that efficiently solves the ill-conditioned numerical problem iteratively[20] by using a multi-shift Conjugate Gradient method for Least Squares CGLS algorithm[20,28].

For simplicity reasons and due to the substantial non-uniformity of B_1^+ field in the transverse plane, the B_1^+ inhomogeneity was modeled following the law of Biot-Savart (Fig. 4.2a). The peak RF was set not to exceed the maximum peak constraint of 50 μT and the amplitude and slew rate of the gradients were constraint by the maximum hardware values of 40 mT/m and 200 T/m/s, respectively. Consequently, a standard spiral gradient trajectory was used. Subsequently, the end of the pulse (last 10%), where the B_1^+ exceeded the 50μT, was stretched using Variable-Rate Selective Excitation (VERSE)[29]. Due to the limitations of the gradient system, a spiral k-space trajectory was used in order to design the 2D RACE pulse as short as possible, with a Field Of View (FOV) set to 6 cm. The RF pulse was optimized to obtain a uniform flip angle over a radius of 30 mm. In addition, the non-linear gradient filters that are applied in the MR system are taken into account in designing the gradient waveform.

Field cameras (Skope, Zurich, Switzerland) were used to measure the actual gradient trajectory.
Due to the severe inhomogeneity of the monopole antenna, an adiabatic RF pulse was used as a reference for the SAR comparison instead of a conventional sinc pulse. We used a BIR-4 pulse (Eq. 4.2)[16,30], which behaved adiabatically on the domain of 20 μT – 50 μT (M_{xy} > 90%).

$$b(t) = B_{1\max}\tanh(a(4t/T_p - 1)) \qquad FM(t) = \frac{A\tan(4\kappa t/T_p)}{\tan(\kappa)} \qquad \textbf{[4.2]}$$

Here the Amplitude Modulation (b) and Frequency Modulation (FM) of the BIR-4 pulse is shown, where $B_{1,max}$ = 50 μT, a = -10, T_p = pulse duration, A = 22987 Hz and $\varkappa$ = atan(10).

Bloch simulations of the BIR-4 and 2D RACE pulses were used to visualize the spatial performance of these RF pulses (both on- and off-resonance). In these simulations, the FOV of the antenna (radius of 30 mm) was taken into account. For clarifications, the mean and standard deviation of the magnetization in these simulations within the FOV of the antenna was also calculated.
For the SAR calculations, the pulse duration of the BIR-4 and the 2D RACE pulse were fixed with the same pulse length. This meant that in order to increase the flip angle for the 2D RACE pulse, the B_1 strength was increased. The SAR was calculated over a domain of flip angles (5°-90°), using Eq. 4.3[8,31] and normalized to the SAR of the BIR-4 (of the corresponding flip angle) to simplify the SAR comparison.

$$SAR\alpha\int_0^T b^2(t)\cdot dt \qquad \textbf{[4.3]}$$

Where, $b(t)$ = time dependent B_1 field played out by the RF pulse and T = pulse duration.

Sequences
A 7 tesla whole body MR system (Philips, Cleveland, USA) was used in combination with an internal monopole antenna. A phantom bottle filled with 10.1 g Agarose, 9.9 g NaCl, 0.9 g $CuSO_4$ and 500 ml H_2O was used for the comparison between a conventional RF pulse and the 2D RACE pulse using only the antenna as a transceiver. We implemented the 2D RACE pulse in a flip angle mapping method: AFI[32]. Rather than comparing to an implementation of the SAR demanding BIR-4 pulse, we obtained

3D flip angle maps with the 2D RACE pulse and with the conventional sinc RF pulse ($T_{R,1}$ = 20 ms, $T_{R,2}$ = 100 ms, T_E = 1.85 ms, FOV = 60x60x240 mm^3), which could be considered realistic RF pulses for use in human subjects.
Also 3D gradient echo images of the rectum of a healthy volunteer were obtained with the monopole antenna inserted ($T_{R,conv}$ = 15 ms, $T_{R,2D\ RACE}$ = 50 ms, FOV = 178x250x180 mm^3, resolution = 0.7x1x1 mm^3, scan time$_{conv}$ = 11:15 min, scan time$_{2D\ RACE}$ = 37:30 min).

4.4 Results

B_1^+ and SAR calculations showed a 20 W/kg 10 gram averaged peak SAR when driving the antenna at 1 W. At a distance of 20 mm from the antenna, the calculated B_1^+ efficiency was 2 μT/√W. The measured temperature increase obtained at the tip of the antenna was 0.5°C when driving the antenna with 2 W of averaged RF power (Fig. 4.3). In all remaining experiments, the maximum average RF power was set to 1 W to ensure local SAR to be less than 20 W/kg, and temperature increase less than 0.5°C.

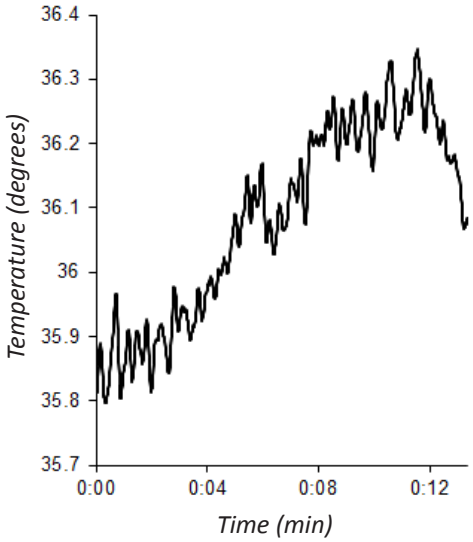

Fig. 4.3. Graph of the temperature increase of the rectum of a healthy male volunteer measured at the tip of the antenna when driving the antenna with an average RF power of 2 W for 10 min.

RF pulse and gradient design
The duration of the amplitude modulation and gradients of the 2D RACE pulse (Fig. 4.4) was 2.1 ms with a maximum B_1 strength of 50 μT, which corresponds to a flip angle of 41°. For the design of the gradients, the hardware limitations were taken into account. However due to the non-linear gradient correction filter applied by the scanner, the gradient shapes had to be adjusted to not only fulfill the hardware limits,

but also the gradient limits in the software code. This means that the implemented gradient shape for both before (in the software verifications) as well as after (output of the software: the actual gradient shape) applying the gradient correction filter has to fulfill the hardware limits. This resulted in a maximum gradient strength of 14 mT/m and a maximum slewrate of 148 T/m/s of the gradients for a FOV of 60x60 mm^2, as verified with a field probe (data not shown).

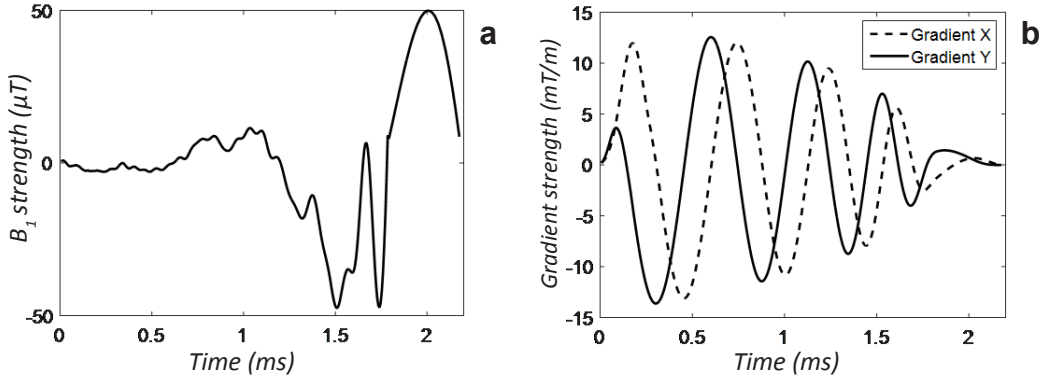

Fig. 4.4. The designed 2D RACE pulse (a) and its corresponding X (dashed) and Y (solid) gradient shapes (b).

With a maximal B_1 strength of 50 μT, the BIR-4 pulse was behaving adiabatically within a radius of 14.5 mm around the antenna, due to the radially decreasing B_1 field. Additionally, M_{xy} > 60% in the range of 12 μT – 50 μT, corresponding to a 60% percent of M_{xy} in a radius of 21.5 mm.

Bloch simulations of the BIR-4 and the 2D RACE pulse show that both RF pulses give a homogenous magnetization profile for 10° and 41° when on-resonance (Fig. 4.5a,b,d,e; Table 4.1). At higher off-resonance frequencies (i.e., 100 Hz for 2D RACE; Fig. 4.5g,h,i and 450 Hz for the BIR-4; Fig. 4.5j,k,l), the uniformity starts to degrade rapidly. As a comparison simulations of the sinc pulse are also given.

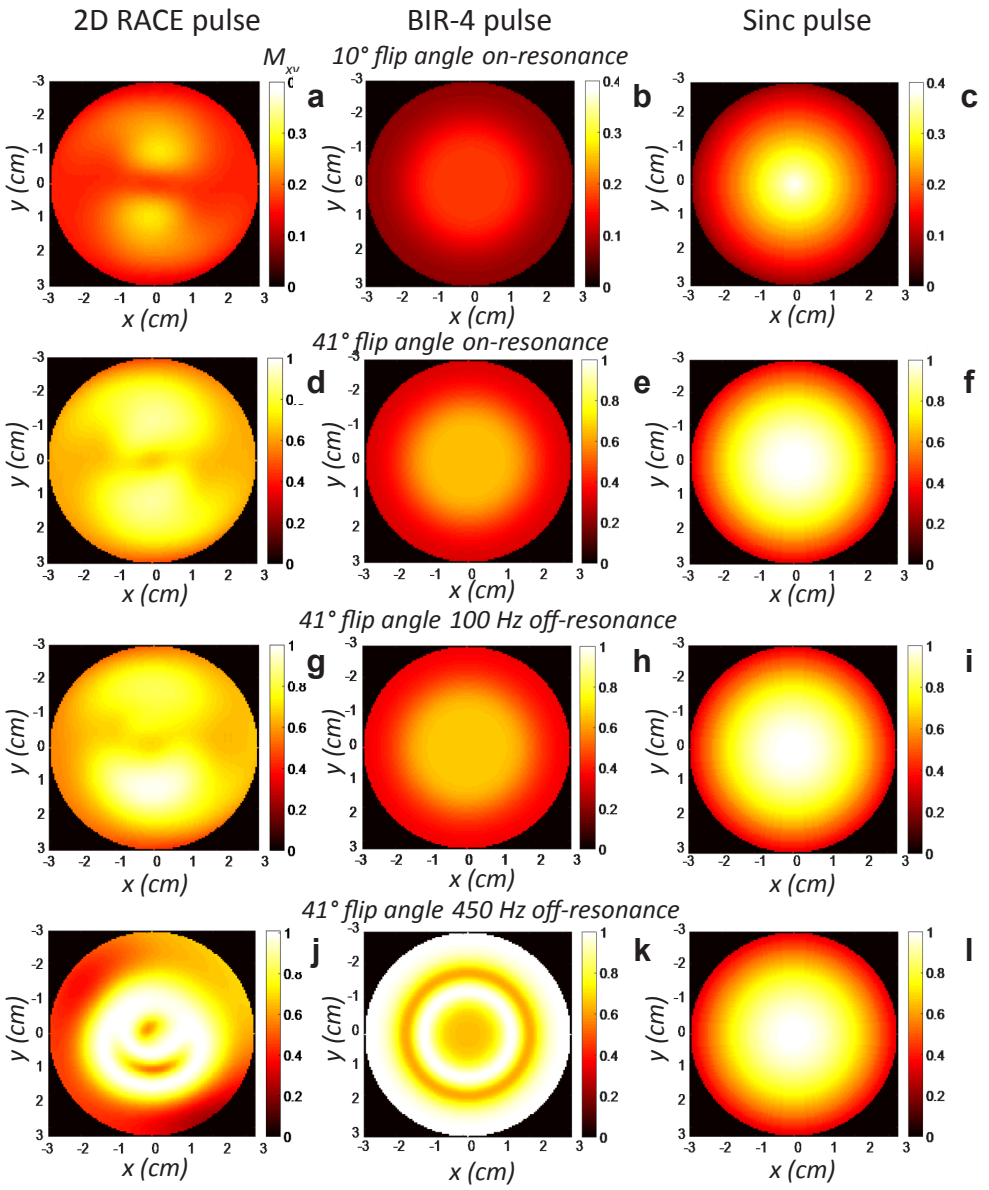

Fig. 4.5. Bloch simulations of the BIR-4 pulse, the 2D RACE pulse and the sinc pulse in combination with the non-uniform B_1 field of the internal antenna. In the left column (**a**,**d**,**g**,**j**) the simulations of the 2D RACE pulse are shown, in the middle column (**b**,**e**,**h**,**k**) represents the simulations of the BIR-4 pulse and in the right column (**c**,**f**,**i**,**l**) the simulations of the sinc pulse are shown. **a**,**b**,**c**) 10° flip angle on-resonance; **d**,**e**,**f**) 41° flip angle on-resonance; **g**, **h**, **i**) 41° flip angle off-resonance (100 Hz) and **j**,**k**,**l**) 41° flip angle off-resonance (450 Hz). The corresponding mean and standard deviation are shown in Table 1. Note that for the conventional RF pulse, the flip angle was based on the B_1 level obtained at 1.5 cm distance from the antenna.

Mxy	10° flip angle on-resonance		41° flip angle on-resonance		41° flip angle 100 Hz off-resonance		41° flip angle 450 Hz off-resonance	
	Mean	SD	Mean	SD	Mean	SD	Mean	SD
2D RACE pulse	0.188	0.0334	0.712	0.0905	0.686	0.278	0.713	0.106
BIR-4 pulse	0.116	0.0342	0.456	0.124	0.490	0.117	0.863	0.132
Conventional pulse	0.183	0.0728	0.654	0.200	0.653	0.200	0.645	0.200

Table 4.1. The mean and standard deviation in the transversal magnetization (M_{xy}) of the Bloch simulations of the 2D RACE pulse, the BIR-4 pulse and the conventional RF pulse, as shown in Fig. 4.5. The mean and standard deviation are calculated only in the FOV of the antenna, i.e., a radius of 30 mm from the antenna.

For flip angles lower than 15°, the SAR of the 2D RACE pulse is orders of magnitude lower than the BIR-4 pulse. Going to a flip angle of 41° the minimal T_R of the 2D RACE pulse would be 50 ms, while for a BIR-4 pulse this would increase to 243 ms (4.8 fold) to remain within SAR guidelines (Fig. 4.6). When compared to a conventional RF pulse with a 41° flip angle at 1.5 cm distance from the RF coil, the SAR of the 2D RACE pulse is still 16-fold higher.

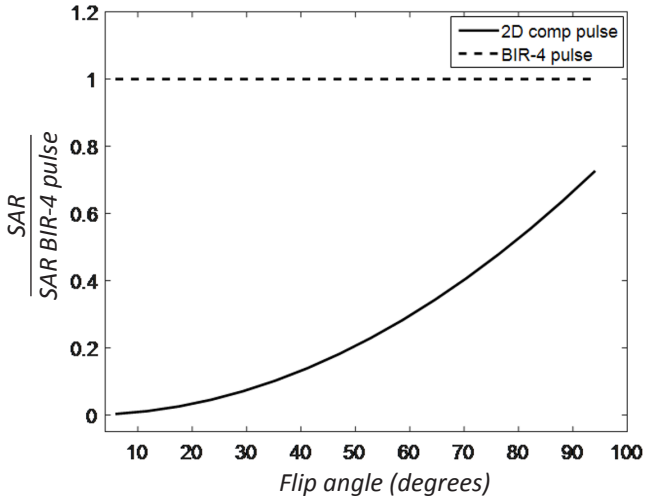

Fig. 4.6. A plot of the SAR of the 2D RACE pulse and the BIR-4 pulse (normalized to the SAR of the 90° BIR-4 pulse) against the flip angle.

Gradient echo imaging

The acquired flip angle maps of the conventional and 2D RACE pulse (Fig. 4.7) show the B_1 inhomogeneity of the antenna in combination with the conventional RF pulse and the restored flip angle homogeneity of the 2D RACE pulse.

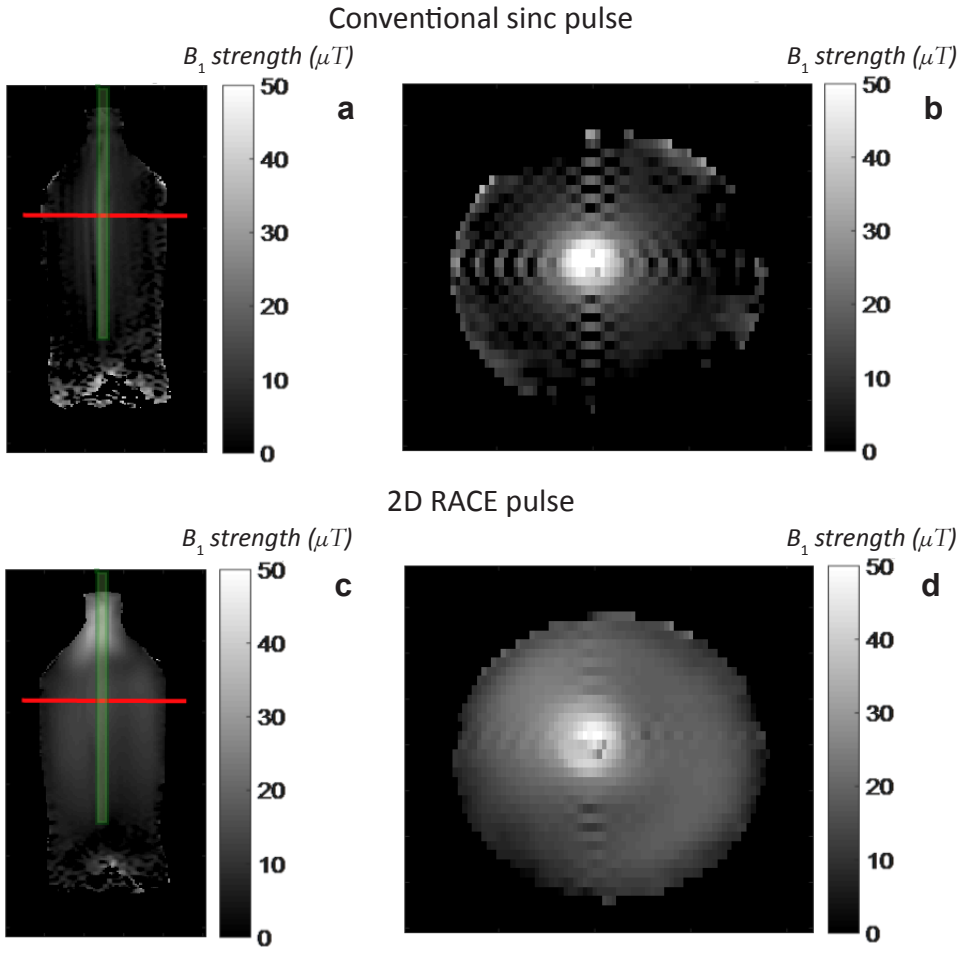

Fig. 4.7. Actual flip angle (AFI) maps of a phantom obtained with an antenna in combination with a conventional sinc pulse (**a**,**b**), and with the 2D RACE pulse (**c**,**d**). In **a**,**c**) an AFI map along the antenna is shown and in **b**,**d**) a slice perpendicular to the antenna is given. In **a**) and **c**) the vertical green bar represents the antenna and the horizontal red line indicates the location of the transverse slice of **b** and **d**. The AFI maps are obtained with the maximal B_1 strength set to 50 μT.

Finally, *in vivo* gradient echo images were obtained in the rectum of a healthy volunteer (Fig. 4.8). Comparing the conventional sinc RF pulse with the 2D RACE pulse, the 2D RACE pulse we can see an increase in signal further from the antenna, which might point to a more homogeneous flip angle. Consequently, apart from a uniform contrast weighting, also the FOV of the antenna is extended when comparing the MRI obtained with the 2D RACE to the conventional RF pulse. For clarity we also added an *in vivo* gradient echo slice where the B_1^- field has been filtered out using a profile inversely proportional of the distance to the monopole antenna (Fig. 4.8). This visualizes the difference in effect of excitation by using a sinc pulse or the 2D RACE pulse.

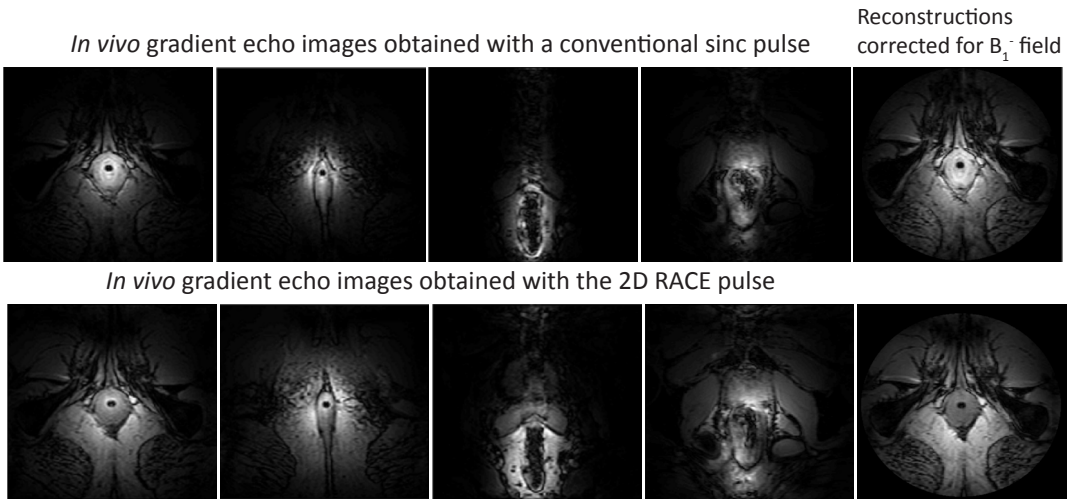

Fig. 4.8. Transversal gradient echo images obtained in the rectum of a healthy volunteer with a thin antenna (recognized by the black dot in the middle of the image). Images in the upper row show the effect of the sequence with conventional RF pulses and in the lower row the scan with the 2D RACE pulse is shown. The images with the compensating RF pulse show increased contrast homogeneity within the range of the antenna as well as an increase of FOV in the tissue. The right image is reflecting the same slice as the left image, however corrected for the calculated B_1^- field. Note the enhanced 3D field of view at high spatial resolution when applying the 2D RACE pulse (shown only for the transverse direction). Also note that in the middle image the 2D RACE pulse increases the line of sight, showing more detailed image of the rectal wall, its borders and its environmental tissue.

4.5 Discussion

The 2D RACE pulse effectively incorporated the non-uniform B_1^+ field of the internal antenna into uniform flip angle distribution. When compared to adiabatic RF pulses, the 2D RACE is an order of magnitude less SAR intensive, particularly at relatively low flip angles. This was realized by incorporating gradient trajectories into the RF pulse design, which adds additional degrees of freedom when compared to adiabatic or composite 17 RF pulses. Consequently, high resolution MRI of the rectum could be obtained with a lower SAR distribution than when using adiabatic RF pulses to create a more homogeneous flip angle distribution without the need of a multi transmit system. SAR may be even further reduced when optimizing the 2D RACE pulse for an even smaller FOV. Or visa-versa, for sequences that are not hindered by SAR (i.e., localizers), the 2D RACE may be designed to capture a larger FOV at the expense of increasing SAR.

Comparing the scan duration of the 2D RACE pulse sequence (37:30 min) with the conventional RF pulse sequence (11:15 min), the scan duration is increased with a factor 3. Consequently, providing a uniform flip angle distribution comes at a substantial cost. With the 2D RACE pulse, the SAR penalty is much less in comparison to adi-

abatic BIR-4 pulses, but still substantial. Alternative strategies that incorporate scans with conventional RF pulses obtained at multiple flip angles and calculate absolute T_1 maps[33] while correcting for B_1^+ non-uniformity may be considered as well. It is subject of further research to investigate whether the dynamic range, motion sensitivity and time penalty of these alternative strategies outweigh the simple strategy of using our proposed 2D RACE pulse."

The RF pulse design was based on a calculated B_1^+ map assuming near field approximation, which might have resulted in a small difference between the calculated B_1^+ map and the actual B_1^+ map. The reason for using the calculated B_1^+ map rather than measured map is that a high dynamic range is required due to the high B_1^+ field near the antenna, which drops off rapidly. This might not be accurately determined through measurements. For instance, look at the substantial ghosting artifacts in the B_1 map obtained in the phantom (Fig. 4.7a). Moreover, as the wavelength is much larger than the used FOV of the antenna, the B_1^+ field is expected to resemble near field dominance which simplifies calculations. The error in the design of the 2D RACE pulse, due to the difference between the B_1 field behavior (used to design the RF pulse) and the actual B_1 field, is of no issue to the BIR-4 pulse behavior. However further away from the antenna, the B_1 field strength drops and in these regions, the adiabatic condition will not be fulfilled anymore.

Another note is that the 2D RACE pulse overcompensates at some locations. In Table 4.1 and Fig. 4.5, in the on-resonance cases, the BIR-4 pulse reaches the demanded M_{xy} near the antenna and drops off because the adiabatic conditions are no longer met. The 2D RACE pulse creates the same M_{xy} near the antenna, however with increasing distance from the antenna, a small increase in M_{xy} is observed. Interestingly, the 2D RF pulse provided an even more efficient excitation than predicted. This also means that the boundaries of these 2D RF pulses concerning uniformity and SAR have not been reached and therefore the possibility of further decreasing the SAR using these pulses may very well be an option.

There were still differences between the gradient schemes we designed and the actual gradients which were played out by the scanner as measured by the field probes. However these differences were negligible when comparing the simulated flip angle maps using the calculated versus the measured gradient trajectories.

We have shown that we are able to compensate the B_1 field in two dimensions; however the B_1 field in the third dimension (along the antenna) is not compensated. Particularly at the ends of the antenna, the B_1 field is not compensated for in the RF pulse. We have therefore used 3D MRI with the readout direction along the antenna to overcome any artifacts from non-uniform tip angles outside the FOV. The proposed method can however be extended with a gradient on the third direction to compensate for B_1 variation in that direction, especially as faster and more robust B_1 mapping techniques

becomes available[34,35]. Particularly inclusion of slab selection or outer volume suppression may reduce the long scan times. Nonetheless, over a relatively large FOV in 3 dimensions, MR images could be obtained at 7 T with spatial resolutions higher than obtained at 3 T[36] with still a substantial SNR.
When applying the antenna in the rectum, there are also other challenges that may need to be addressed, such as peristaltic and breathing motion which can result in image artifacts. We have not investigated the consequence of this mismatch in this study. However, peristaltic motion can be reduced by using e.g., Buscopan or Glucagon[37].
Due to the fact that the antenna is very thin and flexible, future applications of the antenna might involve imaging from within the patient in other tissues that the rectum as well. We have already shown an application in the rectum, however imaging from within the esophagus or the arteries are also genuine applications.

4.6 Conclusion

To compensate for the two-dimensional inhomogeneous B_1 field of an internal transceiver antenna we successfully applied a 2D RACE pulse to obtain a uniform flip angle. This enables imaging (e.g., the rectum) with an internal antenna without losing image contrast within a substantial FOV of 6 cm. Moreover, the 2D RACE pulse is substantially less SAR demanding than adiabatic RF pulses. For a flip angle of 41°, the SAR is reduced by 4.8 fold when compared to a BIR-4 pulse, and can be reduced even further when smaller flip angles are used, resulting in faster imaging. Relative to the conventional sinc excitation, the 2D RACE pulse achieves more uniform flip angles distributions, while resulting in less SAR increase than a BIR-4 pulse (a factor 16 versus 64). This will allow clinical use of internal imaging at high field for e.g., rectal lesions.

4.7 References

1 **Duyn JH, Van Gelderen P, Li T, De Zwart JA, Koretsky AP, Fukunaga M.** High-field MRI of brain cortical substructure based on signal phase. PNAS 2007;104(28):11796–11801.

2 **Visser F, Zwanenburg JJM, Hoogduin JM, Luijten PR.** High-Resolution Magnetization-Prepared 3D-FLAIR Imaging at 7.0 Tesla. Magn Reson Med 2010;64:194-202.

3 **Van der Kolk AG, Hendrikse J, Zwanenburg JJM, Visser F, Luijten PR.** Clinical applications of 7 T MRI in the brain. Eur J Radiol 2013;82:708-718.

4 **Stehouwer BL, Klomp DWJ, Korteweg MA, Verkooijen HM, Luijten PR, Mali WPTM, Van den Bosch MAAJ, Veldhuis WB.** 7 T versus 3 T contrast-enhanced breast Magnetic Resonance Imaging of invasive ductulolobular carcinoma: First clinical experience. Magn Reson Imaging 2012;31:613-617.

5 **Glunde K, Jiang L, Moestue SA, Gribbestad IS.** Magnetic Resonance Spectroscopy and Imaging Guidance in Molecular Medicine: Targeting and Monitoring of Choline and Glucose Metabolism in Cancer. NMR Biomed 2011;24:673-690.

6 **O'Neill BD, Brown G, Heald RJ, Cunningham D, Tait DM.** Non-operative treatment after neoadjuvant chemoradiotherapy for rectal cancer. Lancet Oncol 2007;8:625-633.

7 **Beets-Tan RGH, Beets GL.** MRI for assessing and predicting response to neoadjuvant treatment in rectal cancer. Nat Rev Gastroenterol Hepatol 2014;11:480-488.

8 **Bernstein MA, King KF, Zhou XJ.** Handbook of MRI Pulse Sequences2004.

9 **Raaijmakers AJE, Ipek O, Klomp DWJ, Possanzini C, Harvey PR, Lagendijk JJW, Van den Berg CAT.** Design of a radiative surface coil array element at 7 T: the single-side adapted dipole antenna. Magn Reson Med 2011;66:1488-1497.

10 **Villers A, Puech P, Mouton D, Leroy X, Ballereau C, Lemaitre L.** Dynamic contrast enhanced, pelvic phased array magnetic rasonance imaging of localized prostate cancer for predicting tumor volume: correlation with radical prostatectomy findings. J Urol 2006;176:2432-2437.

11 **Van den Bergen B, Klomp DWJ, Raaijmakers AJE, Arteaga de Castro, CS, Boer VO, Kroeze H, Luijten PR, Lagendijk JJW, Van den Berg CAT.** Uniform prostate imaging and spectroscopy at 7 T: comparison between a microstrip array and an endorectal coil. NMR Biomed 2011;24:358-365.

12 **Hoult DI, Busby SJW, Gadian DG, Radda GK, Richards RE, Seeley PJ.** Observation of tissue metabolites using ^{31}P nuclear magnetic resonance. Nature 1974;252:285-287.

13 **Arteaga de Castro CS, Van den Bergen B, Luijten PR, Van der Heide, UA, Van Vulpen M, Klomp DWJ.** Improving SNR and B_1 transmit field for an endorectal coil in 7 T MRI and MRS of prostate cancer. Magn Reson Med 2012;68:311-318.

14 **El-Sharkawy AM, Qian D, Bottomley PA.** The performance of interventional loopless MRI antennae at higher magnetic field strenghts. Med Phys 2008;35:1995-2006.

15 **Erturk MA, El-Sharkawy AM, Moore J, Bottomley PA.** Interventional loopless antenna at 7 T. Magn Reson Med 2012;68:980-988.

16 **Van Kalleveen IML, Koning W, Boer VO, Luijten PR, Zwanenburg JJM, Klomp DWJ.** Adiabatic Turbo Spin Echo in Human Applications at 7 T. Magn Reson Med 2012;68:580-587.

17 **Erturk MA, El-Sharkawy AM, Moore J, Bottomley PA.** 7 tesla MRI with a transmit/receive loopless antenna and B_1-insensitive selective excitation. Magn Reson Med 2014;72:220-226.

18 **Grissom WA, Xu D, Kerr AB, Fessler JA, Noll DC.** Fast large-tip-angle multidimensional and parallel RF pulse design in MRI. IEEE Trans Med Imaging 2009;10:1548-1559.

19 **Grissom WA, McKinnon GC, Vogel MW.** Nonuniform and multidimensional Shinnar-Le Roux RF pulse design method. Magn Reson Med 2012;68:690-702.

20 **Sbrizzi A, Hoogduin H, Lagendijk JJ, Luijten PR, Sleijpen GLG, Van den Berg CAT.** Time efficient design of multi dimensional RF pulses: application of a multi shift CGLS algorithm. Magn Reson Med 2011;66:879-885.

21 **Staewen RS, Johnson AJ, Ross BD, Parrish T, Merkle H, Garwood M.** 3-D FLASH Imaging Using a Single Surface Coil and a New Adiabatic Pulse, BIR-4. Invest Radiol 1990;25:559-567.

22 **Van Kalleveen IML, Boer VO, Luijten PR, Klomp DWJ.** Tilt optimized flip uniformity (TOFU) RF pulse for uniform image contrast at low specific absorption rate levels in combination with a suface breast coil at 7 Tesla. Magn Reson Med 2014:doi: 10.1002/mrm.2541.

23 **Pauly J, Nishimura D, Macovski A.** A k-space analysis of small-tip-angle excitation. J Magn Reson 1989;81:43-56.

24 **Kroeze H, Van Kalleveen IML, Philippens MEP, Reerink O, Luijten PR, Klomp DWJ.** First results experimental thin rectal probe for high field MRI. ISMRM. Melbourne, Australia2012.

25 **Katscher U, Börnert P, Leussler C, Van den Brink JS.** Transmit SENSE. Magn Reson Med 2003;49:144-150.

26 **Zhu Y.** Parallel excitation with an array of transmit coils. Magn Reson Med 2004;51:775-784.

27 **Grissom WA, Yip C, Zhang Z, Stenger A, Fessler JA, Noll DC.** Spatial Domain Method for the Design of RF Pulses in Multicoil Parallel Excitation. Magn Reson Med 2006;56:620-629.

28 **Van den Eshof J, Sleijpen GLG.** Accurate gradient methods for families of shifted systems. Appl Numer Math 2004;49:17-37.

29 **Hargreaves BA, Cunningham CH, Nishimura DG, Conolly SM.** Variable-rate selective excitation for rapid MRI sequences. Magn Reson Med 2004;52:590-597.

30 **Garwood M, DeLaBarre L.** The return of the frequency sweep: Designing adiabatic pulses for contemporary NMR. J Magn Reson 2001;153:155-177.

31 **McRobbie DW, Moore EA, Graves MJ, Prince MR.** MRI From Picture to Proton.2003.

32 **Yarnykh VL.** Actual Flip-Angle Imaging in the pulsed Steady State: A method for rapid three-dimensional mapping of the transmitted radiofrequency field. Magn Reson Med 2007;57:192-200.

33 **Deoni SC.** High-resolution T_1 mapping of the brain at 3T with driven equilibrium single pulse observation of T_1 with high-speed incorporation of RF field inhomogeneities (DESPOT1-HIFI). J Magn Reson Imaging 2007;26:1106-1111.

34 **Nehrke K.** B, P. DREAM - a novel approach for robust, ultrafast, multislice B_1 mapping. Magn Reson Med 2012;68:1517-1526.

35 **Sacolick LI, Wiesinger F, Hancu I, Vogel MW.** B_1 mapping by Bloch-Siegert Shift. Magn Reson Med 2010;63:1315-1322.

36 **Maas M, Lambregts DM, Lahaye MJ, Beets GL, Backes W, Vliegen RF, Osinga-de Jong M, Wildberger JE, Beets-Tan RG.** T-staging of rectal cancer: accuracy of 3.0 Tesla MRI compared with 1.5 Tesla. Abdom Imaging 2012;37:475-481.

37 **Froehlich JM, Patak MA, Von Weymarn C, Juli CF, Zollikofer CL, Wentz KU.** Small bowel motility assessment with magnetic resonance imaging. J Magn Reson 2005;21:370-375.

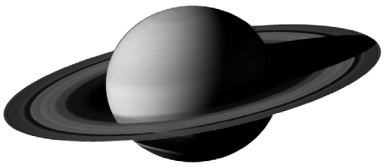

Chapter 5

High resolution T_2-weighted cervical cancer imaging: a feasibility study on ultra-high field 7 T MRI with an endorectal monopole antenna

J.P. Hoogendam[1], I.M.L. Kalleveen[2], C.S. Arteaga de Castro[2], A.J.E. Raaijmakers[2], R.H.M. Verheijen[1], M.A.A.J. van den Bosch[2], D.W.J. Klomp[2], R.P. Zweemer[1], W.B. Veldhuis[2]

[1]Department of gynaecological oncology, UMC Utrecht Cancer Center, University Medical Center Utrecht, the Netherlands

[2]Department of radiology, University Medical Center Utrecht, the Netherlands

Accepted in European Radiology

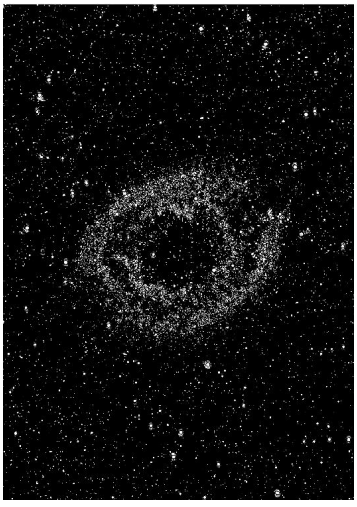

"Joy in looking and comprehending is nature's most beautiful gift."
Albert Einstein

Abstract

Objectives: We studied the feasibility of high resolution T_2-weighted cervical cancer imaging on an ultra-high field 7 T magnetic resonance imaging (MRI) system using an endorectal antenna of 4.7 mm thickness.
Methods: A feasibility study on 20 stage IB1 – IIB cervical cancer patients was conducted. All underwent pre-treatment 1.5 T MRI. At 7 T MRI, an external transmit and receive array with seven dipole antennas and a single endorectal monopole receive antenna were used. Discomfort levels were assessed. Following individualized phase-based B_1^+ shimming, T_2-weighted turbo spin echo sequences were completed.
Results: Patients had stage IB1 (n = 9), IB2 (n = 4), IIA1 (n = 1) or IIB (n = 6) cervical cancer. Discomfort (10 point scale) was minimal at placement and removal of the endorectal antenna with a median score of 1 (range: 0-5) and 0 (range: 0-2) respectively. Its use did not result in adverse events or preterm session discontinuation. To demonstrate feasibility, T_2-weighted acquisitions from 7 T MRI are presented in comparison to 1.5 T MRI. Artifacts on 7 T MRI were due to motion, locally destructive B_1 interference, excessive B_1 under the external antennas and SENSE reconstruction.
Conclusions: High resolution T_2-weighted 7 T MRI of stage IB1 – IIB cervical cancer is feasible. The addition of an endorectal antenna is well tolerated by patients.

5.1 Introduction

Accurate staging of cervical cancer is crucial for treatment planning and determines prognosis. Historically, to allow efficient and comparable staging in high incidence underdeveloped areas, the International Federation of Gynaecology and Obstetrics (FIGO) requires clinical (i.e. non-surgical) staging by physical examination[1]. This inherently introduces under- and overstaging, particularly for intermediate stages wherein estimation of (subtle) parametrial invasion by rectovaginal examination remains difficult, yet determines operability[2]. Studies comparing clinical and post-surgical histological stages in IB1, IB2, IIA1-2 and IIB have reported concordance in 82-85%, 61-77%, 35-60% and 20-59% of cases, respectively[2-4].

Following the 2009 FIGO update, and supported by (inter)national guidelines, MRI may be added to the work-up to assist clinical staging[5-7]. A meta-analysis (n = 3254, 40 studies) showed a pooled sensitivity of 84% for detection of parametrial invasion by MRI, substantially superior to the 40% achieved by clinical examination[8]. This study also identified higher B_0 field strengths and the use of fast spin echo sequences as statistically significant factors to improve the accuracy in detecting parametrial invasion[8]. Increasing the B_0 field strength to 7 T, increases the signal-to-noise ratio (SNR) and consequently allows for higher spatial or temporal resolution acquisitions[9]. While more expensive, this is potentially advantageous for the assessment of loco-regional invasion which is a predominantly anatomic, spatial resolution-dependent assessment made on T_2-weighted MR images. Moreover, at 7 T, the MRI signals are obtained at much shorter wavelengths than at lower fields, facilitating the use of ultra-thin antennas[10]. While using such an antenna in close proximity to the cervix is more laborious, SNR and thereby resolution is expected to increase even further.

We built an endorectal monopole antenna and aimed to develop dedicated T_2-weighted TSE sequences for 7 T imaging with that antenna combined with an external coil array, to image the (para)cervical anatomy in early stage cervical cancer patients. To date, no published research exists which has attempted this. We assessed patient tolerance of using an endorectal antenna. In addition, we will present the T_2-weighted images acquired at 7 T, and clinical 1.5 T MRI as a visual reference.

5.2 Materials and Methods

Design

We conducted a monocenter, prospective cohort study to develop, optimize and assess the feasibility of high resolution pelvic T_2-weighted in-vivo imaging on a 7 T MRI system using a purpose designed endorectal antenna. Inclusion criteria were: 1) a histologically proven primary malignancy of the cervix uteri,

2) FIGO stage IB1, IB2, IIA1-2 or IIB disease, and 3) a minimum age of 18 years. Patients were excluded when 1) general contra-indications for MRI existed, 2) radical surgery had already been performed or chemo- and/or radiotherapy had been initiated, or 3) uterine prolapse existed (C ≥ -6 cm, POP-Q classification[11]). When eligible, subjects were consecutively counseled between March 2014 and November 2015.
The institutional review board approved this study (clinicaltrials.gov: NCT02083848). Participants provided written informed consent. Data quality, protocol adherence and safety were independently monitored by qualified staff. At our tertiary oncologic referral center, clinical staging adheres to FIGO and national cervical cancer guidelines[1,6]. Supplemental file 1 provides details on the clinical 1.5 T MRI and treatment[12].

7 T MRI

Participants completed a safety checklist and underwent metal detector testing prior to imaging on a whole body 7 T MRI system (Achieva, Philips medical systems, Cleveland, USA) equipped with 8-channel multi-transmit functionality. Intravenous contrast agents were not administered, nor was spasmolytic medication. Adverse events were monitored in adherence to the common terminology criteria for adverse events criteria[13].
The shortened B_1 wavelength at ultra-high field MRI, which limits signal penetration and increases the risk of destructive interference, challenges cervical cancer imaging given its anatomical position deep in the female inner pelvis. To alleviate these issues, a local transmit and receive array consisting of seven 30 cm fractionated dipole antennas (MR Coils, Drunen, Netherlands) was used. This setup allows for per patient optimization of the B_1 field distribution. The technical specifications of this array, including the corresponding Specific-Absorption-Rate (SAR) implications, were recently published[14].
The internal monopole B_1 receive antenna was created in-house and specifically designed for endorectal use in 7 T MRI, and subsequently commercialized by Machnet, Maarn, Netherlands. It was positioned in a 14 Fr Foley urinary catheter with a desufflated balloon for an optimal balance between rigidity and flexibility, yielding a 4.7 mm outer diameter (Fig. 5.1). In addition to its sterilization in-between sessions, a single use, sterile cover (Ultracover 200 mm, Microtek medical, Zutphen, Netherlands) was used. Water based lubricating gel (K-Y, Johnson & Johnson, Sézanne, France) facilitated easy endorectal positioning. The region with optimal signal strength was located 6-10 cm beyond the anal verge. Patient reported levels of discomfort related to the antenna – on a Likert scale from 0 (i.e. none whatsoever) to 10 (i.e. worst imaginable) – was assessed directly after introduction and removal.

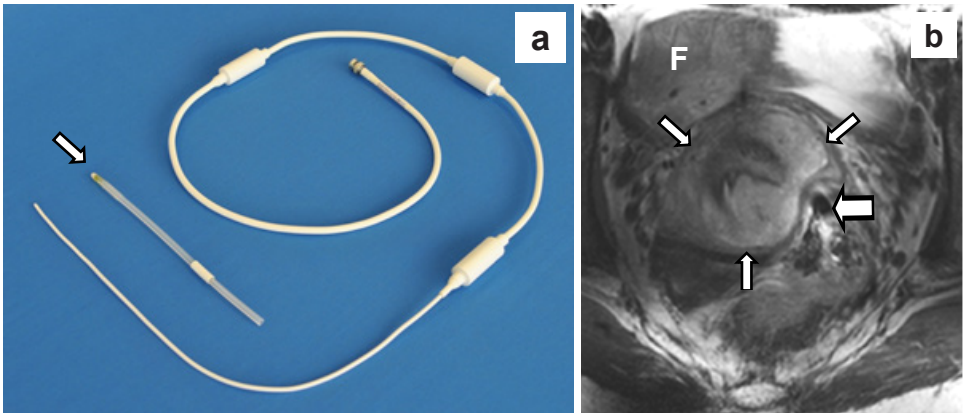

Fig. 5.1. a) Overview of the monopole antenna shown with the 14 Fr Foley urinary catheter (arrow) removed. **b**) Transverse T_2-weighted 7 T MRI of the inner female pelvis which demonstrates the close proximity of the endorectal monopole antenna (broad arrow) to this stage IB2 poorly differentiated papillary squamotransitional cell carcinoma (asterisk) of the cervix. Note the uterine fundus (**F**) and the T_2 hypointense fibrostromal ring surrounding the tumor (narrow arrows) indicative of absent parametrial invasion.

Sequence parameters were optimized for each patient in the first half of the study. From inclusion 10 and on, a standardized protocol with only minor individual adaptations was used. After a multidirectional survey was obtained for anatomical localization, phase-based B_1^+ shimming was performed per patient to maximize and homogenize the B_1^+ on the (para)cervical anatomy[15]. Herein, a single slice gradient echo sequence was repeated 7 times, each time transmitting with a different transmit antenna, while receiving with all 8 antennas. Next, following a shimmed survey, T_2-weighted TSE sequences in the transverse (repetition time (T_R) = 7000 ms, echo time (T_E) = 100 ms, radiofrequency (RF) echo train length = 16, flip angle = 90°, matrix = 640x640, field of view (FOV) = 250x400x59 mm^3, slice thickness = 3 mm, gap = 1 mm, duration = 294 s) and sagittal plane (T_R = 7000 ms, T_E = 100 ms, RF echo train length = 16, flip angle = 90°, matrix = 640x640, FOV = 250x400x73 mm^3, slice thickness = 3 mm, gap = 1 mm, duration = 294 s) were created. Also, a T_2-weighted TSE axial oblique sequence (T_R = 7000 ms, T_E = 100 ms, RF echo train length = 16, flip angle = 90°, matrix = 512x512, FOV = 350x250x39 mm^3, slice thickness = 3 mm, gap = 1 mm, duration = 322 s) angled perpendicular to the cervical canal was performed. All T_2-weighted acquisitions had a voxel size of 0.7x0.8x3.0 mm^3 and used a SENSE parallel acquisition technique (parallel reduction factor: 3). All sequences remained within the maximum local SAR limit of 10 W/kg[16].

5.3 Results

Endorectal antenna tolerance

Of the 25 women who waived participation, only 1 chose not to partake because of objections against the use of the endorectal antenna. In addition to the predetermined sample of 20 patients, 3 women provided informed consent but could not be imaged due to system unavailability. See supplemental file 2 for the corresponding flowchart. The baseline characteristics of the scanned population are outlined in table 5.1.

Tolerance of the endorectal antenna was excellent, discomfort on the 10 point scale was 'minimal' at placement with a median score of 1 (range 0-5) and reported as 'none whatsoever' for removal with a median score of 0 (range 0-2). The single outlier of 5 at placement occurred in a patient who had undergone ligation of multiple haemorrhoids 1 month earlier. In contrast, a subject with a history of excisional haemorrhoidectomy 4 years earlier had uneventful placement (score: 0) and removal (score: 1). Comparable results were found in cases with irritable bowel syndrome, chronic obstipation and deep infiltrating endometriosis.

None of the participants reported pain or a heating sensation at any time, nor did any subject request preterm termination of the MRI session. The duration in the MRI with the antenna in situ was 48.0±7.3 min. One adverse event – unrelated to the antenna – was reported, namely < 30 seconds of mild vertigo upon entering the 7 T MRI bore.

Median age (range)	39.3 (25.3 – 66.5) years
Median BMI (range)	22.3 (18.4 – 36.7) kg/m^2
	N (percentage)
Parity	
0	9 (45%)
1	3 (15%)
2	8 (40%)
WHO performance status	
0	17 (85%)
1	3 (15%)
ASA classification	
1	13 (65%)
2	7 (35%)
Stage	
IB1	9 (45%)
IB2	4 (20%)
IIA1	1 (5%)
IIB	6 (30%)
Tumor histology	
Squamous cell carcinoma	10 (50%)
Adenocarcinoma	8 (40%)
Other	2 (10%)
Tumor differentiation	
Grade 1	3 (15%)
Grade 2	8 (40%)
Grade 3	7 (35%)
Not applicable	2 (10%)
LVSI present	5 (25%)
Lymph node metastases[1]	4 (20%)
Treatment	
Robot ass. laparoscopic SLN + PLND + RVT or RH	7 (35%)
Robot ass. laparoscopic SLN + PLND + RH + adjuvant Rth[2]	1 (5%)
Robot ass. laparoscopic SLN + PLND + Chemoradiation[3]	1 (5%)
PLND + RH via laparotomy[4]	1 (5%)
Chemoradiation	10 (50%)

Table 5.1. Baseline characteristics of the 20 women who underwent 7 T MRI

[1]Determined by a composite of the SLN procedure, PLND or PET-CT as available.

[2]Adjuvant radiotherapy was indicated due to a < 5 mm resection margin.

[3]Chemoradiation substituted radical hysterectomy because of intraoperatively detected tumor-positive sentinel lymph nodes.

[4]After diagnosis and staging at our center, this patient preferred treatment at a different hospital where no laparoscopic radical surgery was performed.

BMI: body mass index, WHO: world health organization, ASA: American society of anesthesiologists, LVSI: lymphvascular space invasion, SLN: sentinel lymph node procedure, PLND: pelvic lymph node dissection, RVT: radical vaginal trachelectomy, RH: radical hysterectomy, Rth: radiotherapy.

Cervical cancer imaging

Key to our focus on T_2-weighted imaging was the visualization of parametrial invasion, which is particularly challenging when subtle and in large tumors. Here, we present three exemplary cases which represent the range of physical examination and imaging results encountered. First, Fig. 5.2 presents a woman in whom the physical examination led to a stage IB2, in agreement with 1.5 T and 7 T MRI which indicated bilaterally absent parametrial invasion. The second example was clinically staged as IB2, though right sided parametrial invasion was suspected on both MRI's (Fig. 5.3). This was motivated by unclear tumor demarcation against the parametrial fat on the right – more distinct on 7 T MRI – and a locally interrupted T_2-hypointense fibrostromal ring. The third example was a bulky IIB based on left sided parametrial invasion at rectovaginal examination. However, the 7 T MRI was considered suggestive of bilateral parametrial invasion (Fig. 5.4). All three cases received chemoradiation, hence no definitive histological proof of invasion was provided. The mean interval between the clinical 1.5 T and experimental 7 T MRI was 13.7±11.8 days. None of the 9 included women with a clinical stage IB1 tumor had an unexpected histological finding of parametrial invasion following their radical surgery.

A prior loop excision, sharp conisation or both were performed in 3, 1 and 2 women, respectively. The interval of this surgery to the clinical 1.5 T and 7 T MRI was a median 42 days (range 32-44 days) and 47 days (range 41-57 days) respectively. After radical surgery, final histology did not show residual invasive tumor in any of these cases.

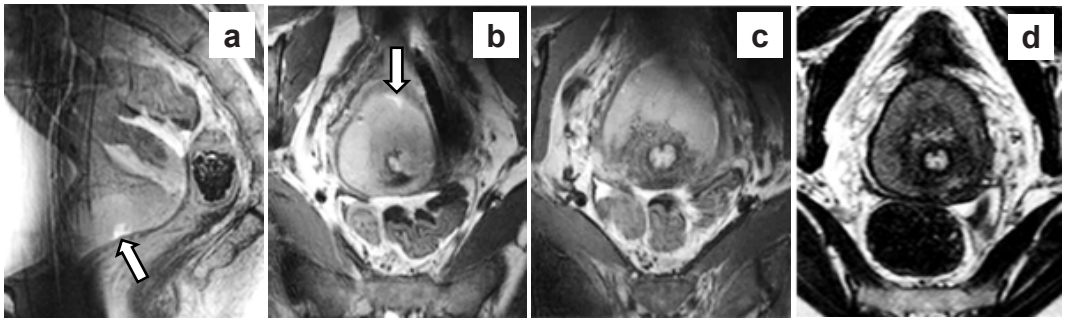

Fig. 5.2. a) Mid-sagittal and **b**) axial oblique (perpendicular to the cervical canal) T_2-weighted slice at 7 T of a 44 year old patient diagnosed with a 70 mm, stage IB2, poorly differentiated squamous cell carcinoma originating from the ventral part of the cervix. Note the visible biopsy site (arrow). **c**) Slice from the same sequence, though 12 mm cranially as Fig. 6**b**, depicting part of the healthy (T_2 hypointense) cervix invaded by tumor. **d**) axial oblique T_2-weighted slice from the clinical 1.5 T MRI, created 17 days earlier, matched to Fig. 6**c** for comparison. Note the T_2 hypointense fibrostromal ring surrounding the tumor.

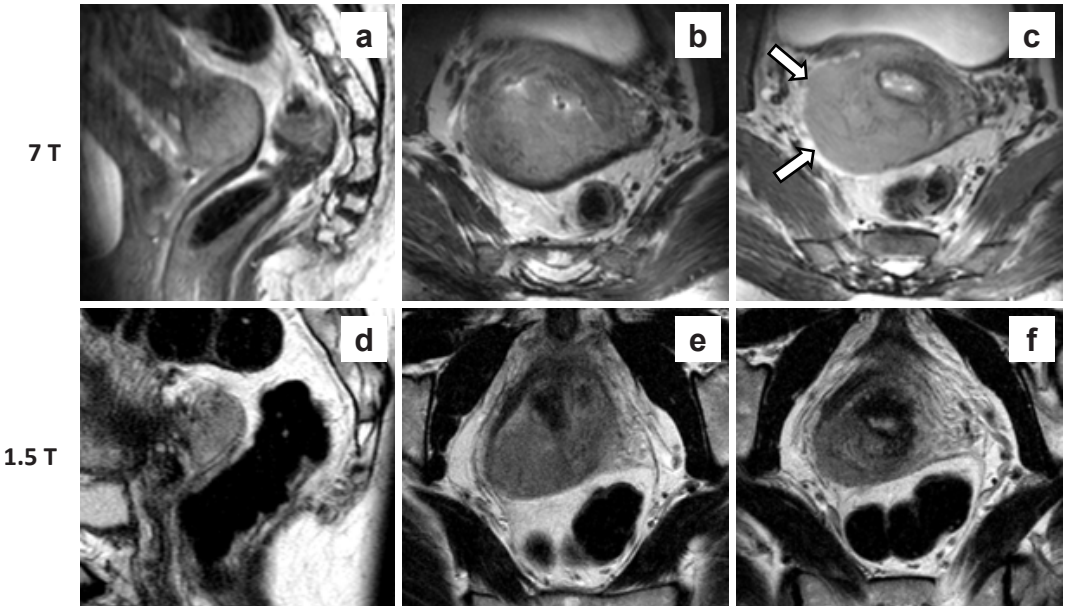

Fig. 5.3. a) Sagittal and **b**) axial oblique T_2-weighted acquisitions from the 7 T MRI of a 48 year old women diagnosed with a 80 mm poorly differentiated squamous cell carcinoma of the dorsal cervix. **c**) Slice from the same acquisition as (**b**), though positioned 12 mm cranially. Parametrial invasion was judged absent at rectovaginal palpation, leading to a clinical stage IB2. However, the unclear tumor demarcation and absent T_2 hypointense fibrostromal ring on the right (arrows) are suggestive of right sided parametrial invasion (i.e. stage IIB). **d**, **e**, **f**) The matched T_2-weighted axial oblique slices from the clinical 1.5 T MRI, created 24 days earlier, are provided for comparison.

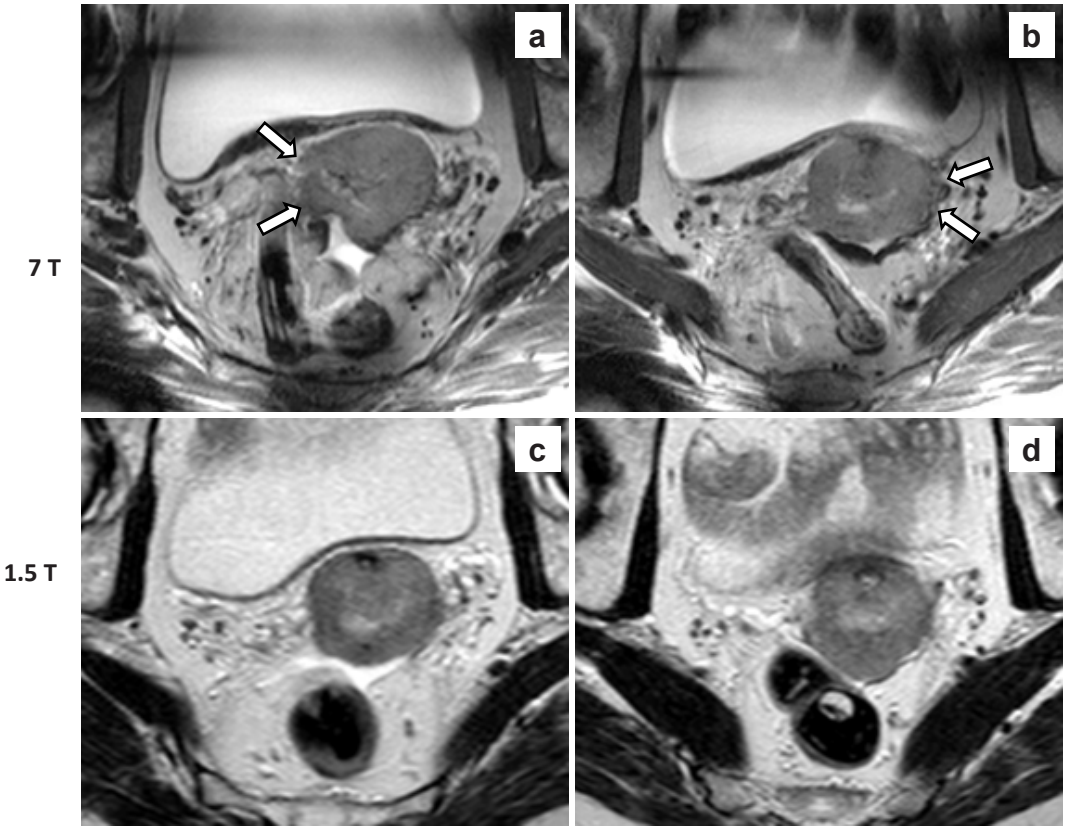

Fig. 5.4. a) Transverse T_2-weighted acquisition from the 7 T MRI of a 65 year old women diagnosed with a 50 mm moderately differentiated squamous cell carcinoma of the cervix. **b**) Slice from the same acquisition as (**a**), though positioned 8 mm cranially. Only left sided parametrial invasion was judged present at rectovaginal palpation, leading to a clinical stage IIB. However, the bilaterally unclear tumor demarcation and absent T_2 hypointense fibrostromal ring are suggestive of bilateral sided parametrial invasion (arrows). **c**, **d**) The matched transverse T_2-weighted slices from the clinical 1.5 T MRI, created 16 days earlier, are provided for comparison. Note the free fluid in the rectouterine pouch (Douglas).

Artifacts

On sagittal acquisitions motion artifacts in the phase encoding direction, caused by breathing, occurred relatively frequent (Fig. 5.5a). Secondly, non-essential anatomical regions were variably obscured by signal voids caused by destructive interference of B_1 – due to the short RF wavelength at 7 T – from the multiple independent external transmit antennas (Fig. 5.5b). Thirdly, superficial black semicircular inversion bands were present due to the inherently much higher B_1 levels directly under the elements of the external transmit and receive antenna array (Fig. 5.5c). While encountered in all participants, it posed no clinical problem as only the subcutaneous fat was obscured. Fourthly, small SENSE reconstruction artifacts were incidentally seen, and are likely

caused by destructive interference in the receive signals of the SENSE reference scan (Fig. 5.5d).

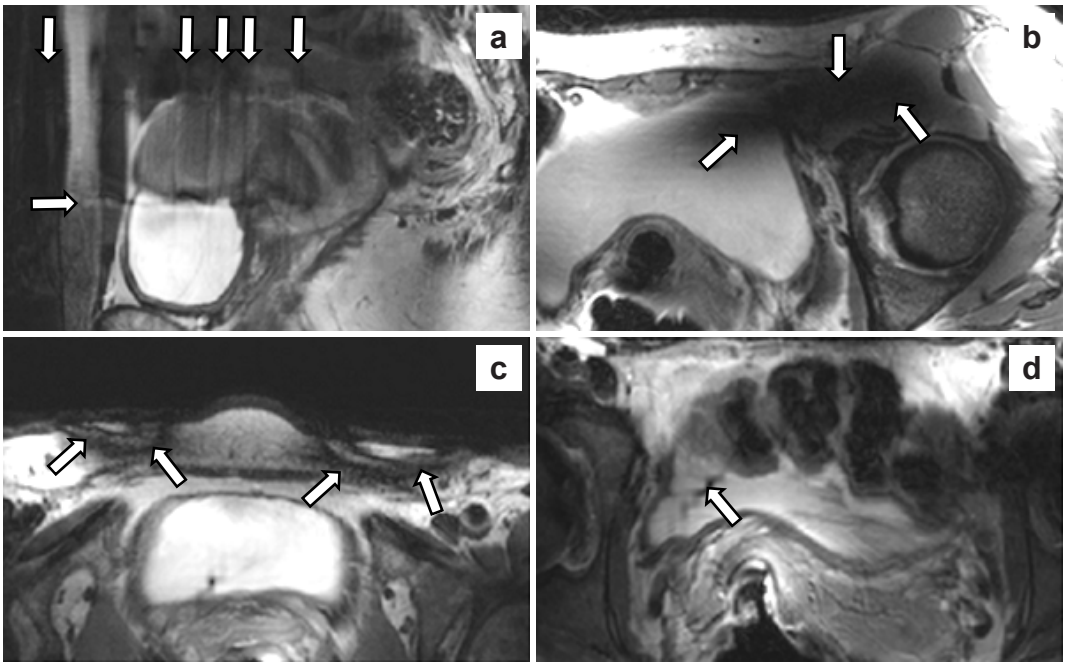

Fig. 5.5. Image artifacts that were encountered on 7 T MRI were **a**) motion artifacts, **b**) locally destructive B_1 interference, **c**) inversion bands due to too much B_1 under the external transmit and receive antennas and **d**) SENSE reconstruction artifacts. Note the unrelated vaginal tampon (asterisk) in (**c**).

5.4 Discussion

This feasibility study showed that T_2-weighted cervical cancer imaging at 7 T is achievable and that the incorporation of an endorectal antenna is well tolerated by patients. We have presented the acquired images, referenced against 1.5 T MRI, relevant for local tumor assessment. To our knowledge, no literature currently exists on 7 T MRI in cervical cancer, which in the past has been termed 'a considerable challenge'[17]. The presented study demonstrates a feasible approach to body imaging for pathology in the female pelvis.

Earlier research on 7 T MRI in the female pelvis was obtained with an external coil array only, limited to healthy volunteers and reported moderate image quality of T_2-weighted sequences[18]. Our approach incorporated an endorectal monopole antenna for optimal signal capture, improving the SNR, deep in the inner pelvis[19]. Its use was not judged as uncomfortable, nor did it prohibit study accrual. Furthermore, in our small sample, no adverse events related to the antenna were encountered.

The research group led by Nandita deSouza has published extensively on their in-house build 37 mm ring-shaped solenoid receive coil, placed endovaginally around the cervix, for 0.5-3 T MRI in stage IA, IB1 and IIA cervical cancer[20,21]. Its application appears limited to relatively small lesions, though accurate in tumor detection and volume calculation[22-24]. Unfortunately, for parametrial invasion detection on T_2-weighted imaging no conclusions have thus far been reached on the added value of this solenoid receive coil[25]. In a recent study on radical surgery (n = 25), only 1 patient had unexpected parametrial extension which was missed on MRI with the solenoid receive coil[25].
In line with the above, a limitation of our study is that none of the women clinically suspected of parametrial invasion had histological confirmation. The risk of partial verification bias is inherent to current practice guidelines which precludes radical surgery for women with tumor extension outside the cervix[6,7,26]. While definitive proof would have strengthened our case presentation, this was prohibited by the inherent design of our study which was not aimed at diagnostic accuracy.
Several technical challenges in our study on pelvic imaging at ultra-high field strength merit further explanation. The SNR advantage of the endorectal antenna is local, which limits the high resolution field of view in the feet-head direction and does not – for example – permit enhanced visualization of lymph nodes at the common iliac arteries[19]. While relevant for a clinical MRI protocol, this was not an objective of the current study which focused on the feasibility of primary tumor imaging. Secondly, at ultra-high field strengths the tissue RF power deposition is substantial and, in RF pulse intensive sequences like TSE used for T_2-weighted imaging, leads to SAR constraints. As a consequence, the repetition time has to be increased, which lengthens the scan protocol. Internal antennas may, however, alleviate this by taking advantage of its highly non-uniform spatial field distribution that can be used for zoomed imaging or high imaging accelerations[14]. In addition, the short B_1 wavelength at ultra-high field strengths causes B_1 inhomogeneity and destructive interference, yielding artifacts which may obscure relevant parts of the inner pelvic anatomy. Using multi-dimensional RF pulses, these artifacts may be removed[27]. Our individualized B_1 shimming approach, made possible by using an external body array coil with multiple elements in parallel transmission, ensured that key anatomical regions of interest (i.e. the cervix) remained visible. Finally, the SENSE reconstruction algorithm that was implemented by the manufacturer, uses at the time of the study a reference scan with a constant amplitude and phase weighting during reception. This can cause destructive interferences during reception, causing artifacts (Fig. 5.5d). These artifacts can be mitigated using interferometry techniques[28].
Future studies should focus on whether our experimental imaging technique improves clinical decision making. This includes quantifying both the diagnostic test accuracy and observer variability (i.e. reproducibility). Furthermore, we focused on T_2-weighted

imaging as it is relevant for local tumor assessment, though for clinical implementation additional sequences such as T_1-weighted MRI are desired[29]. The addition of functional imaging such as ^{1}H or ^{31}P MR spectroscopy – current experience in cervical cancer is limited to 1.5- 3 T MRI – may benefit from the increased spectral and spatial resolution at ultra-high B_0 field strengths[30,31].

In conclusion, the use of an endorectal monopole antenna to improve the SNR at the level of the cervix was well tolerated by participants and not associated with any real discomfort, nor did it lead to adverse events or hinder study accrual. We established the feasibility of T_2-weighted cervical cancer imaging with 7 T MRI. While further research is needed to reduce artifacts and substantiate its clinical impact, we demonstrated that high resolution T_2-weighted acquisitions deep in the female pelvis can be achieved with ultra-high field MRI. This combination of ultra-high field MRI and an internal antenna is promising and merits further research, including pelvic imaging for indications beyond cervical cancer.

5.5 Acknowledgements

The authors are grateful to Saskia van Amelsvoort – van de Vorst for her support with the organizational and legal aspects of this study and Fredy Visser for assisting with the first patients.

5.6 References

1 **FIGO Committee on Gynecologic Oncology.** FIGO staging for carcinoma of the vulva, cervix, and corpus uteri. Int J Gynaecol Obstet 2014;125:97-98.

2 **Quinn M, Benedet J, Odicino F.** 26th annual report of the international federation of gynaecology and obstetrics on the results of treatment in gynaecological cancer. Report of 2006 2009(26):S43-S104.

3 **Qin Y, Peng Z, Lou J, Liu H, Deng F, Zheng Y.** Discrepancies between clinical staging and pathological findings of operable cervical carcinoma with stage IB-IIB: a retrospective analysis of 818 patients. Aust NZJ Obstet Gynaecol 2009;49:542-544.

4 **LaPolla JP, Schlaerth JB, Gaddis O, Morrow CP.** The influence of surgical staging on the evaluation and treatment of patients with cervical carcinoma. Gynecol Oncol 1986;24:194-206.

5 **Odicino F, Tisi G, Rampinelli F, Miscioscia R, Sartori E, Pecorelli S.** New development of the FIGO staging system. Gynecol Oncol 2007;107(1 Suppl 1):S8-S9.

6 **Guideline cervical cancer, version 3.0**, subsection; diagnostics. Retrieved from www.oncoline.nl, a website from the Integraal kankercentrum Nederland (IKNL). Created on 22-03-2012. Retrieved on 15-01-2014.

7 **NCCN Clinical practice guidelline in Oncology.** Cervical cancer. Version 3.2013. Retrieved from www.nccn.org on 20th jan 2014.

8 **Thomeer MG, Gerestein C, Spronk S, Van Doorn HC, Van der Ham E, Hunink MG.** Clinical examination versus magnetic resonance imaging in the pretreatment staging of cervical carcinoma: systematic review and meta-analysis. Eur Radiol 2013;23:2005-2018.

9 **Kuhl CK, Träber F, Schild HH.** Whole-body high-field-strength (3.0-T) MR Imaging in Clinical Practice. Part I. Technical considerations and clinical applications. Radiology 2008;246:675-696.

10 **Erturk MA, El-Sharkawy AM, Moore J, Bottomley PA.** Interventional loopless antenna at 7 T. Magn Reson Med 2012;68:980-988.

11 **Bump RC, Mattiasson A, Bø K, Brubaker LP, DeLancey JO, Klarskov P, Shull BL, Smith AR.** The standardization of terminology of female pelvic organ prolapse and pelvic floor dysfunction. Am J Obstet Gynecol 1996;175:10-17.

12 **Hoogendam JP, Verheijen RH, Wegner I, Zweemer RP.** Oncological outcome and long-term complications in robot-assisted radical surgery for early stage cervical cancer: an observational cohort study. BJOG 2014;121:1538-1545.

13 **National Cancer Institute, US department of health and human services.** Common Terminology Criteria for Adverse Events (CTCAE), version 4.03. Published: June 14, 2010. Accessed: May 31th, 2013.

14 **Raaijmakers AJ, Italiaander M, Voogt IJ, Luijten PR, Hoogduin JM, Klomp DW, Van den Berg CA.** The fractionated dipole antenna: A new antenna for body imaging at 7 Tesla. Magn Reson Med 2016;75:1366-1374.

15 **Metzger GJ, Snyder C, Akgun C, Vaughan T, Ugurbil K, Van de Moortele PF.** Local B_1^+ shimming for prostate imaging with transceiver arrays at 7T based on subject-dependent transmit phase measurements. Magn Reson Med 2008;59:396-409.

16 **International Commission on Non-Ionizing Radiation Protection.** Medical Magnetic Resonance (MR) Procedures: Protection of patients. Health Physics 2004;87:197-216.

17 **Norris DG.** High field human imaging. J Magn Reson Imaging 2003;18:519-529.

18 **Umutlu L, Kraff O, Fischer A, Kinner S, Maderwald S, Nassenstein K, Nensa F, Grüneisen J, Orzada S, Bitz AK, Forsting M, Ladd ME, Lauenstein TC.** Seven-Tesla MRI of the female pelvis. Eur Radiol 2013;23:2364-2373.

19 **Van Kalleveen IML, Hoogendam JP, Raaijmakers AJE, Visser F, Kroeze H, Luijten PR, Veldhuis WB, Klomp DWJ.** Boosting SNR with an internal antenna and external antennas in the human cervix uteri in TSE at 7T. . Abstract no 3636, presented at the Joint Annual Meeting ISMRM-ESMRMB 2014 Available from http://wwwismrmorg/14/program_files/EP05htm Retrieved on Nov 27th 2015

20 **Charles-Edwards EM, Messiou C, Morgan VA, De Silva SS, McWhinney NA, Katesmark M, Attygalle AD, DeSouza NM.** Diffusion-weighted imaging in cervical cancer with an endovaginal technique: potential value for improving tumor detection in stage Ia and Ib1 disease. Radiology 2008;249:541-550.

21 **deSouza NM, Scoones D, Krausz T, Gilderdale DJ, Soutter WP.** High-resolution MR imaging of stage I cervical neoplasia with a dedicated transvaginal coil: MR features and correlation of imaging and pathologic findings. Am J Roentgenol 1996;166:553-559.

22 **Soutter WP, Hanoch J, D'Arcy T, Dina R, McIndoe GA, DeSouza NM.** Pretreatment tumour volume measurement on high-resolution magnetic resonance imaging as a predictor of survival in cervical cancer. BJOG 2004;111:741-747.

23 **deSouza NM, Whittle M, Williams AD, Sohail M, Krausz T, Gilderdale DJ, McIndoe GA, Soutter WP.** Magnetic resonance imaging of the primary site in stage I cervical carcinoma: A comparison of endovaginal coil with external phased array coil techniques at 0.5T. J Magn Reson Imaging 2000;12:1020-1026.

24 **deSouza NM, McIndoe GA, Soutter WP, Krausz T, Chui KM, Hughes C, Mason WP.** Value of magnetic resonance imaging with an endovaginal receiver coil in the pre-operative assessment of Stage I and IIa cervical neoplasia. BJOG 1998;105:500-507.

25 **Downey K, Attygalle AD, Morgan VA, Giles SL, MacDonald A, Davis M, Ind TE, Shepherd JH, deSouza NM.** Comparison of optimised endovaginal vs external array coil T_2-weighted and diffusion-weighted imaging techniques for detecting suspected early stage (IA/IB1) uterine cervical cancer. Eur Radiol 2015;26:941-950.

26 **Colombo N, Carinelli S, Colombo A, Marini C, Rollo D, Sessa C.** ESMO Guidelines Working Group. Cervical cancer: ESMO Clinical Practice Guidelines for diagnosis, treatment and follow-up. Ann Oncol 2012;23:Suppl 7:vii27-32.

27 **Malik SJ, Keihaninejad S, Hammers A, Hajnal JV.** Tailored excitation in 3D with spiral nonselective (SPINS) RF pulses. Magn Reson Med 2012;67:1303-1315.

28 **Brunner DO, Pruessmann KP.** $B_1(^+)$ interferometry for the calibration of RF transmitter arrays. Magn Reson Med 2009;61:1480-1488.

29 **Balleyguier C, Sala E, Da Cunha T, Bergman A, Brkljacic B, Danza F, Forstner R, Hamm B, Kubik-Huch R, Lopez C, Manfredi R, McHugo J, Oleaga L, Togashi K, Kinkel K.** Staging of uterine cervical cancer with MRI: guidelines of the European Society of Urogenital Radiology. Eur Radiol 2011;21:1102-1110.

30 **Payne GS, Schmidt M, Morgan VA, Giles S, Bridges J, Ind T, DeSouza NM.** Evaluation of magnetic resonance diffusion and spectroscopy measurements as predictive biomarkers in stage 1 cervical cancer. Gynecol Oncol 2010;116:246-252.

31 **Booth SJ, Pickles MD, Turnbull LW.** In vivo magnetic resonance spectroscopy of gynaecological tumours at 3.0 Tesla. BJOG 2009;116:300-303.

Supplemental file 1: Standard clinical care, including 1.5 T MRI sequence protocol.

At our tertiary referral centre, clinical staging adheres to FIGO and national cervical cancer guidelines. This includes a re-examination under anaesthesia when the outpatient exam is deemed or unreliable. All patients routinely undergo pelvic MRI on a 1.5 T system (Achieva/Intera, Philips Medical systems, Best, the Netherlands) with an external sensitivity encoding (SENSE) torso coil only. The protocol consists of a transversal T_2-weighted TSE sequence (repetition time (T_R) = 6667 ms, echo time (T_E) = 100 ms, flip angle = 90°, matrix = 400x280, Field of View (FOV) = 320x320 mm, slice thickness = 4 mm, gap = 0 mm), a sagittal T_2-weighted TSE sequence (T_R = 2800 ms, T_E = 100 ms, flip angle = 90°, matrix = 424x280, FOV = 300x240 mm, slice thickness = 4 mm, gap = 0 mm) and a double-oblique T_2-weighted TSE sequence angled perpendicular to the cervical canal (T_R = 3030 ms, T_E = 100 ms, flip angle = 90°, matrix = 400x280, FOV = 320x320 mm, slice thickness = 4 mm, gap = 0 mm). In addition, a transversal diffusion-weighted sequence (b-values: 0 and 800 s/mm^2), a transve rsal fat-saturated T_1-weighted sequence before and after intravenous gadolinium, and a transversal proton-density-weighted sequence of the entire abdomen were performed. In cases where a diathermic loop excision or a cold knife cone had been performed the clinical MRI was scheduled at least 30 days after such procedure to minimize tissue reaction, which may obscure residual tumour.
Stage IB1 and IIA1 patients were scheduled for a sentinel lymph node procedure with frozen section, pelvic lymph node dissection and radical hysterectomy or – in eligible patients desiring fertility preservation – a radical vaginal trachelectomy. In patients with tumour-positive (sentinel) lymph nodes, chemoradiation substituted radical uterine surgery. Stage IB2, IIA2 and IIB patients were treated primarily with chemoradiation. By design, treatment and stage decisions were uninfluenced by 7 T MRI findings, which were not reported to clinicians.

Supplemental file 2: Flowchart of patient accrual into the study.

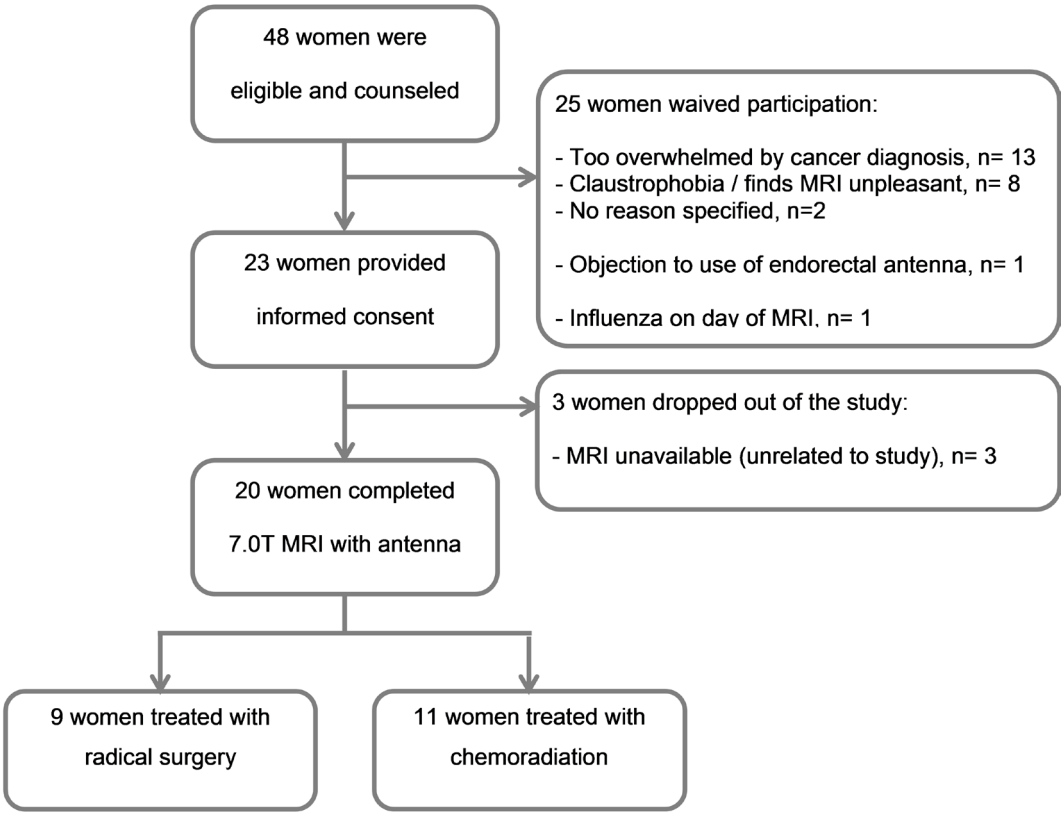

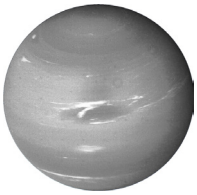

Chapter 6

Boosting the SNR by adding a receive-only endorectal monopole to an external antenna array for high-resolution T_2-weighted imaging of early stage cervical cancer with 7 T MRI

I.M.L. van Kalleveen[1], J.P. Hoogendam[2] , A.J.E. Raaijmakers[1] , F. Visser[1], C.S. Arteaga de Castro[1], R.H.M. Verheijen[2], P.R. Luijten[1], R.P. Zweemer[2], W.B. Veldhuis[1], D.W.J. Klomp[1]

[1]Department of Radiology, UMC Utrecht, the Netherlands

[2]Department of Gynaecological Oncology, UMC Utrecht Cancer Center, the Netherlands

Under revision in NMR in biomedicine

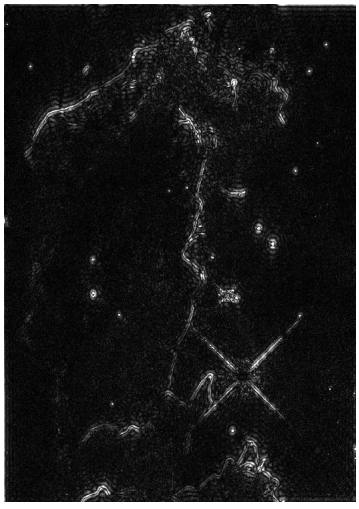

"Every great and deep difficulty bears in itself its own solution. It forces us to change our thinking in order to find it."

Niels Bohr

Abstract

We aimed to image early stage cervical cancer at ultra-high field MRI (e.g., 7 T) using a combination of multiple external and a single endorectal antenna. Here we study the Signal-to-Noise Ratio (SNR) increase and improvement of cervix MR imaging when including an endorectal monopole antenna. This should allow high resolution T_2-weighed images which facilitates the local tumor status assessment, including whether or not invasion into the surrounding connective tissue (parametria) has occurred. In a prospective feasibility study, five healthy female volunteers and six histologically proven stage IB1-IIB2 cervical cancer patients were scanned at 7 T. We used seven external fractionated dipole antennas for transmit-receive (transceive) and an endorectally placed monopole antenna for reception only. A region of interest, containing both normal cervix and tumor tissue, was selected for the SNR measurement. Separated signal and noise measurements were obtained in the region of the cervix for each element and in the near field of the monopole antenna (radius < 30 mm) to calculate the SNR gain of the endorectal antenna per patient. We obtained high resolution T_2-weighted images with a voxel size of 0.7x0.8x3.0 mm^3. A mean gain of 1.8 in SNR was obtained at the overall cervix and tumor tissue area. In four cases with optimal placement of the endorectal antenna (verified on the T_2-weighted images) the mean SNR gain was 2.2. Within a radius of 30 mm from the monopole antenna, a mean SNR gain of 2.9 was achieved; while in the 4 optimal cases near the antenna the mean SNR gain was 3.7. We have demonstrated that the use of an endorectal monopole antenna substantially increased the SNR of 7 T MRI at the (para)cervical anatomy. Combined with the intrinsic high SNR of ultra-high field MRI, this gain can be used to enhance spatial resolutions to assess tumor invasion.

6.1 Introduction

Cervical cancer is the fourth most common malignancy in women worldwide with an age standardized incidence of 14.0 cases per 100.000 women[1]. In developed regions, 1.5 T - 3 T MRI of the pelvis is the modality of choice to assist the clinical international federation of gynecology and obstetrics (FIGO) staging in the assessment of tumor size, loco-regional invasion and lymph nodal involvement[2,3]. Specifically, high spatial resolution T_2-weighted images in multiple orthogonal planes are used for the detection of parametrial invasion (i.e., into the connective tissue directly surrounding the cervix)[4]. This is clinically relevant as parametrial invasion may change stage, prognosis and treatment planning.

In analogy with the detection of capsular extension of prostate cancer[5], higher spatial resolutions are likely beneficial for the assessment of parametrial invasion. The improved detection of capsular extension in prostate cancer was demonstrated after boosting the SNR with an endorectal Radio Frequency (RF) coil at 3 T. The SNR can be further increased by the use of even a stronger B_0 magnetic field (e.g., at 7 T).

However, at ultra-high field strengths, body MRI becomes challenging. The RF transmit field (B_1^+) is severely non-uniform, and the RF power deposition (i.e., the Specific Absorption Rate, SAR) limits effective use of RF pulse intensive sequences, commonly the case in T_2-weighted MRI. With a local transceive array, driven with optimized phase settings, the B_1^+ field can be focused at a region of interest[6]. Moreover, using antenna arrays rather than conventional coil arrays, SAR can be reduced enabling efficient T_2-weighted MRI in the body at 7 T[7].

The female cervix is located centrally in the inner pelvis and is situated directly ventral to the rectum. Hence, using an endorectal coil for signal reception may boost the SNR. While loop[8] and stripline[9] designs for endorectal coils have been reported and showed successful results when applied to prostate MRI, recently also monopole antennas were demonstrated to work as an internal transceiver for 7 T MRI[10]. The advantages of the monopole over the loop or stripline designs, are its relatively thin size and potential higher SNR efficiency at depth[7]. The close anatomical distance between the cervix and the rectum allows the perpendicular B_1 field of the antenna to be used to image the cervix.

However, as the transmit field is severely non-uniform when using the monopole as a transceiver, B_1^+ compensating RF pulses are required for uniform flip angles. Erturk et al.[10] have demonstrated the use of composite pulses in rabbits. For Gradient Echo imaging (GRE), using the small tip angle (STA) approximation[11], images of the rectum[12] have been shown where 2D RF pulses are used to compensate the non-uniform B_1^+ field, when using the antenna as a transceiver. A more elegant way to benefit from the high SNR is to only use the internal antenna as a receiver, while providing a rela-

tively uniform transmit field with an external local transmit or transceive array. This way, conventional RF pulses and sequences may be used facilitating the exploration of T_2-weighted MRI at maximized SNR.
We therefore propose to use an endorectal monopole antenna for receive purposes, in addition to an external transceive coil array, to boost the SNR of T_2-weighted MRI of the human cervix, using a 7 T MR system. This study aims to quantify the gain in SNR achieved with the internal antenna versus the external antennas only in the first ever obtained high resolution T_2-weighted 7 T MR images of stage IB1-IIB2 cervical cancer patients.

6.2 Experimental

Study design and population
Following a pilot study with five healthy female volunteers to optimize logistical and technical protocols, wherein we used one volunteer for SNR calculations in the uterus and cervix to explore the SNR gain, we started a prospective feasibility study in patients. Six women diagnosed with cervical cancer were scanned between March and October 2014. Women were included if they had histologically proven stage IB1, IB2, IIA1-2 or IIB1-2 cervical cancer and were at least 18 years old. Patients were excluded when contra-indicated for MRI or if treatment with radical surgery had already been carried out or if chemo-radiation therapy had already been started. Subjects with severe uterine prolapse were also excluded. The institutional review board approved the study protocol (NL41056.041.13) and written informed consent was provided by all participants. This study was registered prospectively at clinicaltrials.gov under identifier NCT02083848.

Setup
A 7 T whole body MR system (Achieva, Philips Medical systems, Cleveland, United States of America) equipped with 8-channel multi-transmit functionality was used in combination with a local transceiver coil array of fractionated dipole antennas[7] (MR Coils B.V., Drunen, The Netherlands) and the internal monopole antenna (Machnet B.V., Maarn, The Netherlands). The seven external antennas were placed around the pelvis (Fig. 6.1a,b). We combined these elements with a single endorectally placed monopole antenna (Fig. 6.1c,d), used for receive purposes only.
The monopole antenna was encapsulated in a 14 Fr urinary catheter to enable easy insertion and for microbiological safety was placed in a single use sterile probe cover (Ultracover 200 mm, Microtek medical B.V., Zutphen, The Netherlands). Endorectal insertion, performed on the MR bed, was facilitated by sterile lubricating gel and performed by a qualified physician from the gynecological oncology department (JH).

The receive optimum of the monopole antenna was positioned 6-10 cm beyond the anal verge to obtain the optimal signal. To ensure immobilization during imaging, the external part of the antenna was fixed with tape to the medial part of the left upper leg. No spasmolytic medication was administered.

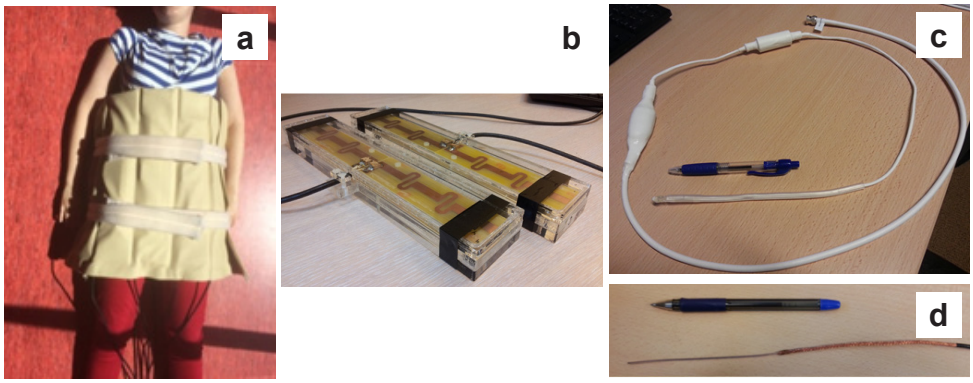

Fig. 6.1. a) The external array of fractionated dipole antennas. Elements are contained in the leather sleeve. **b**) One single fractionated dipole antenna element. **c**) The endorectal monopole antenna. The part of the antenna which is placed inside the rectum is covered by a 14 Fr urinary catheter. **d**) The endorectal antenna next to a pen to indicate its thickness.

For the volunteer low resolution sagittal SNR images (Multi-Slice (MS) GRE, T_E = 1.49 ms, T_R = 15 ms and resolution = 2x2x6 mm^3) were obtained. To support our findings, we also obtained three times the same sagittal T_2-weighted image where respectively the monopole antenna, the external antennas and both monopole and external antennas were used for receiving. B_1^+ shimming was performed with a phase-based shimming method[6] to focus on the (para)cervical anatomy. For this we used a single slice GRE sequence (T_E = 1.97 ms, T_R = 45 ms, FOV = 250x500x35 mm^3) repeated 7 times, each time driving a different transmit antenna, while receiving with all 8 elements. A low resolution T_2-weighted sagittal image (MS (Turbo Spin Echo (TSE), T_E = 272 ms, scan time = 70 s, resolution = 1.4x1.6x5 mm^3) was obtained to localize the cervix and the tumor and to determine its orientation. On the sagittal images a high resolution single-shot T_2-weighted transversal and double oblique (i.e., perpendicular to the cervical canal) sequences (MS TSE, T_E = 70 ms, T_R = 13 s, resolution = 0.7x0.8x2.5 mm^3) were planned.

Signal to noise measurements (MS GRE, T_E = 1.49 ms, T_R = 15 ms, resolution = 2x2x6 mm^3) were obtained in the same double oblique scan plane as the high resolution T_2-weighted sequence. For each patient, the scan was obtained twice; first with a nominal flip angle of 15° followed by a sequence without excitation (flip angle of 0°). The measurements were recorded with only the endorectal monopole antenna as a receiver and with only each of the external elements separate as a receiver.

The separate external elements were finally combined in a SNR optimal setting[13].

Data processing
We used MATLAB version 2014b (MathWorks, Natick, USA) to create a patient based mask (to select the region of interest) which included the cervix and the tumor. To determine the optimal gain in SNR of the monopole antenna, we also created a mask in the region around the antenna (with a radius of 30 mm). The difference in SNR was calculated using the mean signal over the area contained within the mask divided by the standard deviation of the noise scan from the same area[13]. The SNR in the selected volume was calculated per patient, when using only the monopole antenna, or when using only the external antennas. In the latter calculation we used complex weighted averaging of the signal from each element, where the weighting factor was determined from the highest SNR images[14]. For the noise scan reconstruction identical weighting factors were used as for the signal images. Finally, the SNR was calculated per patient over a region in the cervix and in the vicinity of the antenna containing around 2,000 and 9,000 voxels on average respectively.

6.3 Results

A healthy female volunteer (26 years) was scanned to visualize the gain in SNR when using only the external antennas, the internal antenna or both the external and internal antennas for receive (Fig. 6.2). Due to a lower resolution scan, the region of interest for this volunteer was chosen over the complete cervix and uterus. The SNR gain from this volunteer (white region) was a factor of 3.2.

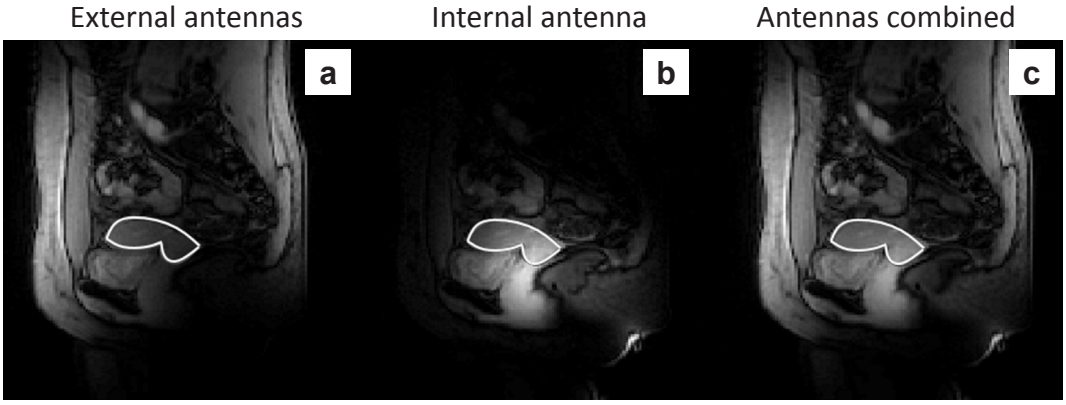

Fig. 6.2. A sagittal slice of the SNR maps (MS GRE, T_E = 1.49 ms, T_R = 15 ms and resolution = 2x2x6 mm^3) through the uterus and cervix (white region) of a healthy volunteer where for receive **a**) only the external antennas, **b**) the monopole antenna and **c**) both the external and internal antennas combined were used.

Table 6.1 provides the baseline characteristics of the six patients. The outlined coil setup enabled T_2-weighted visualization of the entire true pelvis (pelvis minor) (Fig. 6.2-6.4). Sagittal T_2-weighted images (Fig. 6.3a, 6.4a) were obtained to locate the cervix and plan the high resolution double oblique T_2-weighted scan (Fig. 6.3b, 6.4b) perpendicular to the cervical canal to image the cervix and the tumor.

Baseline characteristics of six patients

	Age (years)	BMI (kg/m2)	Prior LETTZ	Prior conisation	Largest tumor diameter (mm)	FIGO Stage	Histological type and grade	LVSI	Relevant medical history
Patient 1	40	22.4	+	+	45	IIB2	SCC, III	+	None
Patient 2	32	18.4	+	-	0*	IB1	SCC, II	-	None
Patient 3	65	26.2	-	-	50	IIB2	SCC, II	-	Excisional Haemorrhoidectomy 4 years earlier
Patient 4	30	20.2	-	+	0**	IB1	AC, I	-	None
Patient 5	33	19.2	-	-	39	IIA1	Neuro-endocrine Small cell carcinoma	+	M. Marfan
Patient 6	44	22.2	-	-	58	IB2	SCC, III	-	Laparotomy for appendicitis

Table 6.1. Clinical characteristics of the patients. BMI: Body Mass Index, LLETZ: Large Loop Excision of the Transformation Zone, FIGO: International Federation for Gynecology and Obstetrics, LVSI: LymphoVascular Space Invasion, SCC: Squamous Cell Carcinoma. +Positive. –Negative.

*Following the LETTZ, no residual tumor was visible.

**Following the conisation, no residual tumor was visible.

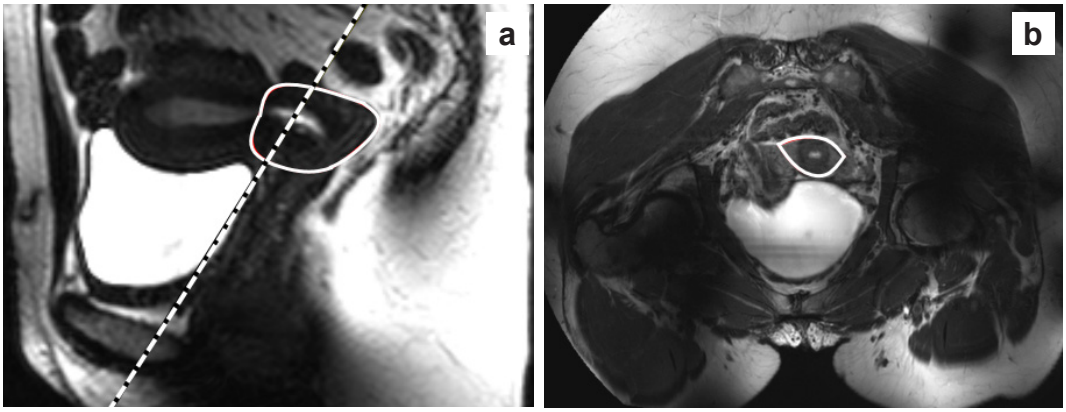

Fig. 6.3. a) Sagittal T_2-weighted image of patient 1 (MS TSE, T_E = 272 ms, T_R = 70 s, resolution = 1.4x1.6x5.0 mm^3, FOV = 246x375x105 mm^3). The white dotted line indicates the planning of the double oblique high resolution T_2-weighted scan which is placed perpendicular to the cervix. The white delineation represents the region of the cervix and the tumor in the sagittal plane on which the SNR calculations were based. **b**) The high resolution single-shot double oblique T_2-weigthed image of patient 1 (MS TSE, T_E = 70 ms, T_R = 13 s, resolution = 0.7x0.8x2.5 mm^3, FOV = 350x400x47 mm^3), where the cervix and the tumor tissue are clearly visible.

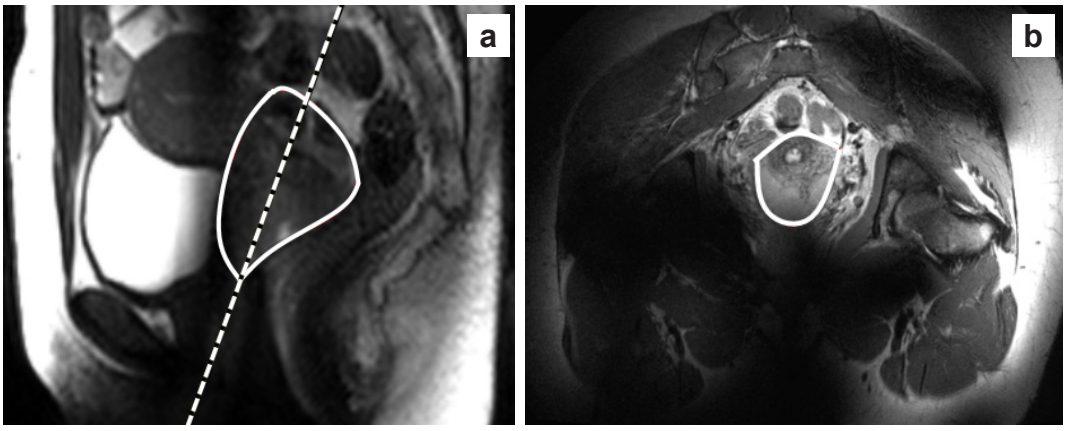

Fig. 6.4. a) Sagittal T_2-weighted image of patient 6 (MS TSE, T_E = 170 ms, T_R = 50 s, resolution = 0.9x1.6x5.0 mm^3, FOV = 375x375x85 mm^3). The white dotted line indicates the planning of the double oblique high resolution T_2-weighted scan which is placed perpendicular to the cervix. The white delineation represents the region of the cervix and the tumor in the sagittal plane on which the SNR calculations are based. b) The high resolution single-shot double oblique T_2-weighed image of patient 6 (MS TSE, T_E = 70 ms, T_R = 7 s, resolution = 0.7x0.8x3.0 mm^3, FOV = 350x400x39 mm^3), where the cervix and the tumor tissue are clearly visible. In **b**) the white delineation represents the region of interest which is used for the SNR comparison within the cervix and the cervical tumor.

We compared the SNR of the internal antenna with the optimal combination of signals from the external antennas[13]. See Table 6.2 for an overview per patient. Using the internal antenna as an extra receiver, we gained a mean factor of 1.8 in SNR in the

cervical region. In patients 5 and 6 the antenna was not fixed properly, as after the examination it had turned out to be shifted more than 5 cm out of the rectum. In these two patients, the SNR gain of the antenna is substantially reduced and therefore contributing less to the external array. However excluding these two patients, we gained a mean factor of 2.2 in SNR.

SNR ratio of monopole versus external antennas in the cervix and tumor

Cervix and tumor	SNR monopole SNR external	Number of voxels in mask
Patient 1	1.765	2229
Patient 2	2.495	1386
Patient 3	1.642	2017
Patient 4	2.978	1114
Patient 5	0.922	1911
Patient 6	0.858	3213
Mean Summary Statistics	*1.777*	*1978*

SNR ratio of monopole versus external antennas near the antenna (radius < 30 mm)

Near monopole (r < 30 mm)	SNR monopole SNR external	Number of voxels in mask
Patient 1	3.718	9253
Patient 2	3.163	15101
Patient 3	2.045	9969
Patient 4	5.834	13932
Patient 5	1.484	3178
Patient 6	1.268	2099
Mean Summary Statistics	*2.919*	*8922*

Table 6.2. SNR ratios of monopole antenna when used as a receiver only vs the external antennas only for each patient. The SNR gain was calculated in the cervix and tumor tissue and in the near field of the antenna (radius < 30 mm).

We also calculated the SNR for the internal and external antennas in the surrounding tissue of the internal antenna (in a radius of 30 mm) at the height of the cervix. In this case the overall SNR gain was a factor of 2.9, or even a factor of 3.7 in SNR gain when excluding patients 5 and 6.

6.4 Discussion

We have demonstrated a strong increase in SNR using an endorectal monopole antenna in 7 T MR imaging of early stage cervical cancer compared to using external antennas only. Furthermore, while internal antenna use has been reported in rabbits[10,15], this study is the first to report the use of internal monopole antennas in humans at ultra-high field strengths. To show the benefits of the internal monopole antenna, an SNR comparison has been made between external state of the art fractionated dipole antennas and the internal monopole antenna.

The gain in SNR depends strongly on the positioning of the monopole antenna. After the antenna has been endorectally inserted and is taped to the upper inner leg, the peristaltic motion and other patient motion might still reposition the antenna. Therefore the gain in SNR may not be optimal. To overcome this problem an external socket might keep the antenna at the right location. Examples of cases where the antenna was dislocated are shown in Table 6.2 (patient 5 and 6). Nevertheless, in these cases a more

modest SNR gain is still present.
Another option for using the monopole antenna could be to use it for transmit and receive without the external antenna array. Hereby the FOV can be reduced and as an effect we might boost the spatiotemporal resolution. The use of the monopole antenna solely as a transceiver depends strongly on its placement making the fixation of the antenna even more important. In addition, if using the internal antenna for transmit, the inhomogeneous B_1^+ field of it has to be considered. The inhomogeneous B_1^+ field results in an inhomogeneous flip angle distribution, which compromises tissue contrast. A method to overcome the inhomogeneous flip angle distribution is to use adiabatic RF pulses[16,17]. However these pulses are SAR intensive and may not be feasible to use within safety guidelines. Another method might be to use a selective excitation in the cervix that incorporates the non-uniformity in B_1^+. Other groups have already shown successfully the use of selective excitation in the brain[18,19]. The challenge with these so-called multi-dimensional RF pulses is that turbo spin echo images (T_2-weighted) require a high flip angle excitation and refocusing pulses and these 2D RF pulses are normally designed using low flip angle assumptions (Small Tip angle Approximation method[11]) and used in GRE sequences. High flip angle optimizations are more challenging[19], particularly when considering the severe non-uniformities in B_1^+ when using the endorectal antenna as a transceiver.
We used a single-shot T_2-weighted scan to overcome the peristaltic movement. By using medication (e.g., butylscopolamine or glucagon[20-22]) in combination with a multi-shot TSE or an increased number of averages, it might be possible to even gain more SNR. At 1.0 T and 1.5 T this approach has already been shown to be successful[23].
To conclude, we demonstrated that adding an endorectal monopole antenna to an external antenna array can substantially boost the SNR at the cervix. This enables higher resolution T_2-weighted image acquisitions, relevant for assessing the local tumor status in early stage cervical cancer.

6.5 References

1 **Ferlay J, Soerjomataram I, Ervik M, Dikshit R, Eser S, Mathers C, Rebelo M, Parkin DM, Forman D, Bray F.** Cancer incidence and mortality worldwide: Sources, methods and major patterns in GLOBOCAN 2012. Int J Cancer 2015;136:E359-E386.

2 **Balleyguier C, Sala E, Da Cunha T, Bergman A, Brkljacic B, Danza F, Forstner R, Hamm B, Kubik-Huch R, Lopez C, Manfredi R, McHugo J, Oleaga L, Togashi K, Kinkel K.** Staging of uterine cervical cancer with MRI: guidelines of the European Society of Urogenital Radiology. Eur Radiol 2011;21:1102-1110.

3 **Pecorelli S.** Revised FIGO staging for carcinoma of the vulva, cervix and endometrium. Int J Gynaecol Obstet 2009;105:103-104.

4 **Sala E, Wakely S, Senior E, Lomas D.** MRI of malignant neoplasms of the uterine corpus and cervix. A J R 2007;188:1577-1587.

5 **Futterer JJ, Heijmink SWTPJ, Scheenen TWJ, Jager GJ, Hulsbergen-Van de Kaa CA, Witjes JA, Barentsz JO.** Prostate Cancer: Local Staging at 3-T Endorectal MR Imaging - Early Experience. Invest Radiol 2006;238:184-191.

6 **Metzger GJ, Snyder C, Akgun C, Vaughan T, Ugurbil K, Van de Moortele PF.** Local B_1^+ shimming for prostate imaging with transceiver arrays at 7T based on subject-dependent transmit phase measurements. Magn Reson Med 2008;59:396-409.

7 **Raaijmakers AJE, Ipek O, Klomp DWJ, Possanzini C, Harvey PR, Lagendijk JJW, Van den Berg CAT.** Design of a radiative surface coil array element at 7 T: the single-side adapted dipole antenna. Magn Reson Med 2011;66:1488-1497.

8 **Klomp DWJ, Bitz AK, Heerschap A, Scheenen TW.** Proton spectroscopic imaging of the human prostate at 7 T. NMR biomed 2009;22:495-501.

9 **Arteaga de Castro CS, Van den Bergen B, Luijten PR, Van der Heide UA, Van Vulpen M, Klomp DWJ.** Improving SNR and B_1 transmit field for an endorectal coil in 7 T MRI and MRS of prostate cancer. Magn Reson Med 2012;68:311-318.

10 **Erturk MA, El-Sharkawy AM, Moore J, Bottomley PA.** 7 tesla MRI with a transmit/receive loopless antenna and B_1-insensitive selective excitation. Magn Reson Med 2014;72:220-226.

11 **Pauly J, Nishimura D, Macovski A.** A k-space analysis of small-tip-angle excitation. J Magn Reson 1989;81:43-56.

12 **Van Kalleveen IML, Kroeze H, Sbrizzi A, Boer VO, Reerink O, Phillipens, MEP, Van den Berg CAT, Luijten PR, Klomp DWJ.** 2D compensating RF pulse with uniform image contrast in combination with an internal transceiver at 7T. Proceedings of the International Society of Magnetic Resonance in Medicine conference in Salt Lake City 2013;Abstract 4245.

13 **Hayes CE, Roemer PB.** Noise correlations in data simultaneously acquired form mulitple surface coil arrays. Magn Reson Med 1990;16:181-191.

14 **Hargreaves BA, Cunningham CH, Nishimura DG, Conolly SM.** Variable-rate selective excitation for rapid MRI sequences. Magn Reson Med 2004;52:590-597.

15 **Erturk MA, El-Sharkawy AM, Moore J, Bottomley PA.** Interventional loopless antenna at 7 T. Magn Reson Med 2012;68:980-988.

16 **Garwood M, DeLaBarre L.** The return of the frequency sweep: Designing adiabatic pulses for contemporary NMR. J Magn Reson 2001;153:155-177.

17 **Van Kalleveen IML, Koning W, Boer VO, Luijten PR, Zwanenburg JJM, Klomp DWJ.** Adiabatic Turbo Spin Echo in Human Applications at 7 T. Magn Reson Med 2012;68:580-587.

18 **Moore J, Jankiewicz M, Zeng H, Anderson AW, Gore JC.** Composite RF pulses for B_1^+-insensitive volume excitation at 7 Tesla. JMR 2010;205:50-62.

19 **Grissom WA, Xu D, Kerr AB, Fessler JA, Noll DC.** Fast large-tip-angle multidimensional and parallel RF pulse design in MRI. IEEE Trans Med Imaging 2009;10:1548-1559.

20 **Froehlich JM, Patak MA, Von Weymarn C, Juli CF, Zollikofer CL, Wentz KU.** Small bowel motility assessment with magnetic resonance imaging. J Magn Reson 2005;21:370-375.

21 **Horsthuis K, Bipat S, Bennink RJ, Stoker J.** Inflammatory bowel disease diagnosed with US, MR, Scintigraphy, and CT: Meta-analysis of prospective studies. Radiology 2008;247:64-79.

22 **Florie J, Wasser MNJM, Arts-Cieslik K, Akkerman EM, Siersema PD, Stoker J.** Dynamic contrast-enhanced MRI of the bowel wall for assessment of disease activity in Crohn's disease. Am J Roentgenol 2006;186:1384-1392.

23 **Wagner M, Rief M, Busch J, Scheurig C, Taupitz M, Hamm B, Franiel T.** Effect of butylscopolamine on image quality in MRI of the prostate. Clin Radiol 2010;65:460-464.

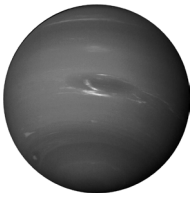

Chapter 7

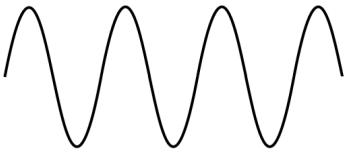

General Discussion

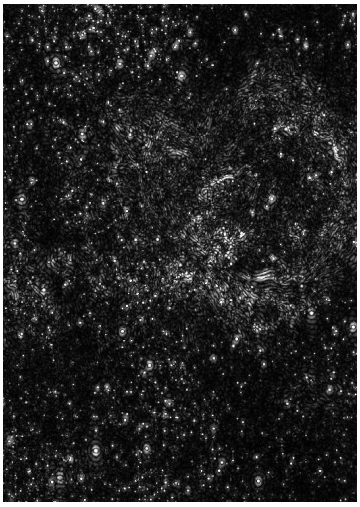

"Pick a flower on Earth and you move the farthest star."
Paul Dirac

1.41 MRI

MR imaging shows excellent soft tissue contrast in the human body. Therefore, MRI plays a prominent role in clinical diagnostics, which can become even more important when imaging resolution is increased; a property that scales with the magnetic field strength of the MRI.

1.42 Ultra-high field MRI

Compared to conventional MRI systems that operate at a magnetic field strength of 1.5 T or 3 T, the increase in the static magnetic field (B_0) to ultra-high field strength (e.g. 7 T) can provide a higher sensitivity that can be translated in increased resolution. However these ultra-high field systems coincide with a higher resonance frequency of the spins, resulting in a shorter wavelength (i.e. around 11 cm in human tissue at 7 T) of the radio frequency (RF) pulses and signals that excite and relax the spins. Due to the shorter wavelength, the excitation becomes non-uniform, resulting in images with inhomogeneous contrast weighting. Traditional RF pulses, which are designed assuming a uniform transmit field will therefore result in a spatially dependent inhomogeneous flip angle distribution. In addition, the higher frequency of the transmit pulses causes more induced eddy currents in the tissue that result in increased tissue heating, or a higher specific absorption ratio (SAR). This limits the scan duration and the RF pulse properties (i.e. duration, peak B_1 power) in the sequences itself.
To overcome these challenges intelligent pulses and setups have been designed, such as adiabatic RF pulses[1], surface coils[2] and multi-transmit systems[3]. One of the simplest approaches to overcome part of the SAR limitations is the use of surface transmit coils placed in close proximity to the tissue to be imaged. By applying a surface transmit coil, a local B_1^+ field is being applied to the neighboring tissue. However, the B_1^+ field of a surface coil is non-uniform and will result to an inhomogeneous flip angle distribution. To restore a homogeneous flip angle distribution, adiabatic RF pulses have been introduced. Unlike the traditional RF pulse, the flip angle of adiabatic RF pulses are B_1^+ independent, provided that the RF pulse is given a certain minimal B_1^+ level.
Another strategy to create a uniform flip angle is the use of multi-transmit platform systems comprised of multiple coil elements. These elements can be driven with different independent RF amplitudes and phases causing constructive and destructive interferences of RF fields such as to optimize and homogenize the flip angle for a certain region of interest. One of the biggest challenges of the multi-transmit platform might be the SAR calculations and determining the SAR hotspots. Because of safety concerns, the RF power settings of the multiple coil elements nowadays are conser-

vative, resulting in relatively long scan time. In future prospect, the knowledge of the SAR hotspots will result in a shorter scan time caused by decrease of the conservatively chosen T_R's. In this thesis, the technologies of providing a uniform excitation with efficient reception at 7 T (local transmit, adiabatic and multi-dimensional RF pulses and multi transmit solutions) are explored, and discussed in this chapter.

1.43 Local transmit

Due to the shorter wavelength, not only loop coils, but also antennas like a monopole can be used for the RF fields at 7 T. One of the most important benefits of using a monopole antenna over a loop coil, is the spatial dimension of the antenna. The antenna is ultra-thin and even fits in a bladder catheter. Therefore this coil is ideal for imaging in small cavities (e.g. the rectum), especially in case of rectum tumor patients, due to the more narrow passageway. This makes imaging in narrow cavities while applying a high B_1 field locally a perfect application for monopole antennas. In this thesis we used the monopole antenna inserted exclusively in the rectum. With this antenna as a transceiver, we imaged the rectum in a healthy volunteer (chapter 4). We also applied the monopole antenna together with seven fractionated dipole antennas[4] for 7 T MRI of the cervix in women with cervical cancer. Here we used the monopole antenna as a receiver only and showed that we can boost the SNR in the cervical region with the monopole antenna inserted in the rectum (chapter 5). A challenge is still the high signal coming from the tissue close to the monopole antenna, which can result in ghosting artifacts. These artifacts are coming e.g. from the peristaltic motion of the intestines. Using more rapid sequences (e.g. single-shot TSE) might reduce the artifacts. For further improvement, the k-space lines may be realigned in a post-processing step by implementing a pre-pulse which will register peristaltic motion by using the changes in phase.

1.44 Adiabatic RF pulses

Although adiabatic RF pulses are quite SAR intensive, these are often used in sequences that require a highly uniform spin flip (e.g. inversion recovery[5]). Still the required peak B_1 strength of an adiabatic RF pulse is sometimes quite challenging to obtain, considering the limited available RF peak power, and the robustness of the pulse is sometimes questionable, considering its operation at the non-linear boundaries of the RF amplifiers. When using a single adiabatic RF pulse in a sequence, the SAR constraints stay limited and therefore feasible at 7 T. However, when increasing the number of adiabatic RF pulses (e.g. for turbo spin echo sequences; TSE), the high RF pow-

er deposition of the pulses become a severe limitation for its applicability. Also when using sequences which require an ultra-short echo time, the relatively long duration of the adiabatic RF pulse can become a challenge to deal with.
We have designed a TSE sequence containing only adiabatic RF pulses, based on the RARE sequence[6]. However, comparing the SAR of the TSE with the traditional RF pulse versus the adiabatic RF pulses, the adiabatic TSE is much more SAR demanding and the echo time is also longer, due to the longer RF pulses. This might result in signal loss. We have used three different adiabatic RF pulses in the sequence: the adiabatic half passage (AHP), the adiabatic full passage (AFP) and the B_1 insensitive rotations using 4 segments (BIR-4). Each of these pulses have advantages and disadvantages for using them in a TSE sequence. The AHP and the BIR-4 cannot be used as slice selective RF pulses, due to the poor frequency profile these pulses create at low bandwidth. The AFP can be used as a slice selective RF pulse and in order to select a slice and the AFP is used as a refocusing pulse. In order to obtain the correct phase of all the spins, the AFP pulse has to be applied in pairs, such that the phase can be rewind. Due to the pairing of the AFP, the "pulse" becomes very long, which is not optimal. The AHP is a short pulse and works fine as an excitation pulse and due to the necessary pairing of the AFP, we used a BIR-4 pulse as a multi-echo RF pulse instead. Another note to the BIR-4 pulse is the even and odd echoes coming from these pulses. There is a phase shift between the even and odd echoes and therefore k-space reordering is required which divides the even from the odd echoes. This decreases the frequency of the artifact in k-space and result is a less prominent ghost. Another method is to remove half of the echoes[6], but this will decrease the resolution.
Looking at the article of Deschamps et al.[7], a new super-adiabatic theory has been described for adiabatic RF pulses, where multiple rotating frames can generate adiabatic RF pulses at much more relaxed RF power constraints. We have designed adiabatic RF pulses for low B_1 strengths (20 μT) which still behave adiabatic. According to the traditional adiabatic condition, these RF pulses should not behave adiabatic, however with the super-adiabatic theorem the path of the magnetization vector does not seem to be lost and therefore these pulses can still behave adiabatic for lower B_1 values. The super-adiabatic theory might even introduce new kind of pulses with even more favorable conditions for use in ultra-high field MRI.
Combining the excitation and refocusing pulses (AHP and AFP) with a multi-echo part with a hyperecho[8] may reduce the SAR even further. However, the T_1 and T_2 effects in tissues have to be taken into account for optimizing the pulse trains.

1.45 1D compensating pulses

Another type of RF transmit coil is a surface coil. Such a surface coil is used for breast

MRI at 7 T. However, surface coils have an inhomogeneous B_1 field[9], which is dominant in one dimension (anterior-posterior direction for the breast). Using the selective gradient and an RF pulse, which has a magnetization profile inversely proportional to the dominant B_1 profile of the coil, will restore the flip angle uniformity. Note that the slab selection has to be aligned with the dimension which is compensated by the RF pulse. Knowing the spatial distribution of the RF field of the coil in the dominant direction, the energy of the RF pulse that causes the excitation of the spins, can be effectively distributed. This means that the Tilt Optimized Flip Uniformity (TOFU) pulse can be less SAR demanding than a traditional RF pulse. In fact, when using the TOFU pulse in a TSE sequence, a factor of 2 reduction in SAR could be demonstrated while at the same time providing a boost in image uniformity (Fig 7.1)[10]. The RF pulse can be optimized per volunteer by using the information from the B_1 field map. While we demonstrated optimization in only one dimension, there is still a lot of potential in the way of merging spatial B_0 gradients with RF pulses. Using selective gradients or shim gradients that match the non-uniformity of RF fields might bring highly efficient RF pulses with uniform flip angles in all 3 dimensions.

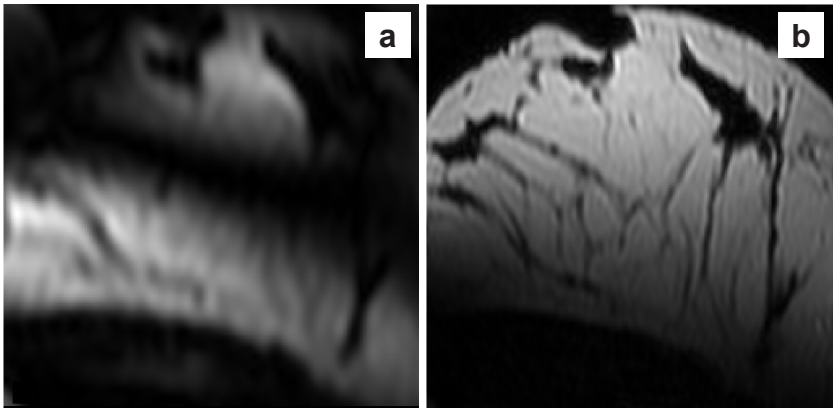

Fig. 7.1. A TSE sequence (FOV = 100x125x105 mm3, T_R = 4 s, turbo factor = 124, scan time = 6.44 minutes) with **a**) a conventional sinc pulse and **b**) the TOFU pulse in the breast of a healthy volunteer using a surface coil transceiver.

1.46 2D compensating pulses

Instead of using one B_0 gradient which stays constant, multiple variable B_0 gradients can also be useful. For a surface coil with an inhomogeneous B_1 field in predominantly two dimensions (e.g. monopole antenna), two variable gradients might restore flip angle uniformity. Combining two gradients together with an RF pulse will result in an energy distribution of the RF pulse at a certain time frame to a given location in the transmitting k-space[11], which is determined by the two gradients combined. For the

low flip angle regime the Bloch equations can be simplified to a function that describes which point in the transmitting k-space receives what kind of energy. With this formula and the desired magnetization profile of the RF pulse, a numerical optimization step can be made, which designs an RF pulse combined with two gradients that meets the requirements for uniform spin excitation[12]. However the hardware limitations of the gradient coils on the MR system can be a limiting factor, when designing the excitation pulse. Especially the slew rate (slope) of the gradient and in somewhat less prominent manner, the strength of the gradients is constraining the properties of the pulse. These components are responsible for the longer duration of the RF pulse compared to non-compensated RF pulses. We have designed an RF pulse in combination with two gradients, to provide a uniform spin flip with a monopole transceiver. Compared to adiabatic RF pulses, the 2D RACE pulse can reduce the SAR by an order of magnitude.

1.47 Multi-transmit

As an alternative to using a surface RF transceiver with adiabatic or compensating pulses for providing a uniform spin flip, an array of external antennas can be used in a multi-transmit setup. We have explored the multi-transmit setup for 7 T MRI in patients with cervical cancer. This setup consists of seven external fractionated dipole antennas[4], used for transmit and receive, and a endorectally placed monopole antenna (6-10 cm inserted), which is used for receive only. By applying RF shimming[13] with the external transmit antennas, the B_1 field can be locally optimized and made homogeneous in the cervical region. Furthermore, using an endorectal monopole antenna near the cervical region, will boost the SNR. Therefore combining the multi-transmit system with the fractionated dipole antennas for a homogeneous B_1 field in the cervix and a local monopole antenna for increased SNR results in high-resolution T_2-weighted images in the cervix.

1.48 Future perspective

Adiabatic RF pulses are used a lot and the new insights in super-adiabaticity will extend their applicability. For instance, when looking at the adiabatic TSE, which we implemented at the 7 T scanner, the SAR was drastically decreased.
By not using the first time derivative of ω_{eff}, but also glancing a little further into higher order time derivatives makes us more aware of the complexity of these RF pulses, and while the "simplistic" first order might show us that the magnetization vector is lost, this might not be the case. It is possible that with this "new" adiabaticity concept, validated with our findings at 7 T MRI, there might still be unexplored parts of

these RF pulses which might work with even more favorable conditions. Especially the minimal length and SAR of these pulses might not be obtained yet, where the design focus could lie on fulfilling the superadiabaticity theorem, instead of the conventional adiabatic theorem.

1D compensating RF pulses are easy to implement and to use. With a dominant B_1 field in one direction, which is often the case for surface coils, a 1D compensating RF pulse can reduce the B_1 inhomogeneity, while using the RF power in a more intelligent manner when compared to adiabatic RF pulses. This even results in practically no increase in scan time, when compared to a conventionally applied sinc RF pulse.

When the B_1 field is non-uniform in predominantly 1D (commonly caused by a surface loop coil), the associated flip angles can be compensated easily by using a slice selective RF pulse, where the RF pulse is designed to give the spins close to the coil a reduced effective field, and further from the coil a more effective field. This will increase the flip angle homogeneity and can even be optimized using a local B_1 map and calculating the RF pulse on the fly per subject. The energy distribution of such a standard TOFU pulse is comparable to conventional sinc pulses and much less SAR intensive than adiabatic RF pulses. These pulses can attribute e.g. in the homogeneity of the flip angle in TSE images, which are in the case of strong B_1 field drop-off, normally of bad quality without the use of adiabatic RF pulses (see Fig. 7.1). While we have demonstrated the boosted performance of the TOFU pulse in breast MRI at 7 T, it can be expanded to any other organ that can be imaged with a surface RF coil transceiver.

However when a monopole antenna is used as a transmit coil, the B_1 field radially decreases further away from the antenna and another RF pulse is needed when compensating for the inhomogeneous B_1 field. One of the methods is the design of a 2D RACE which compensates for the inhomogeneous B_1 field of the antenna transceiver. The method described by Pauly et al. only works for the low flip angle regime and therefore pulses for TSE will be more challenging. However for GE images, this method of RF pulse design can be applied as we demonstrated in MRI of the rectum. Although the 2D RACE pulse is less SAR intensive than the adiabatic RF pulses, the duration of the pulse is quite long, due to the hardware gradient limitations. Improving these limitations can speed up the 2D RACE pulse, which might be an option in the future as gradient performances can be improved. When fully understanding the behavior of these pulses, especially at higher flip angles and as refocusing pulses (for TSE), these pulses may have a lot of benefit in combination with the monopole antenna for e.g. 7 T MRI in rectal cancer.

Combining the endorectally inserted monopole antenna with the dipole antennas at the multi-transmit platform, is beneficial for both uniformity and maximization of the SNR maximized. Care must be taken to deal with the very high signal obtained close to the coil, which is challenging when using multi-echo sequences. However, particularly

for MRI of the cervix, the 2D TOFU pulse may be adapted to exclude spin excitation close to the antenna. Or combining the external transmit antennas for uniform transmit with an outer volume suppression pulse generated with the monopole antenna. In fact, combining multiple transmit configurations with a patient study, could even facilitate uniform MRI with localized MR spectroscopy, where high bandwidth adiabatic RF pulses can be used with the monopole antenna and conventional RF pulses with the external antennas. For instance, in spectroscopy methods of the cervix and the surrounding tissue (i.e. parametria), where the focus lies on the parametria and tumor extend, the locally high SNR of the antenna is most definitely beneficial. In future perspective the spectroscopy might give more detailed information about parametrial invasion and therefore combined with the high resolution anatomical MRI at 7 T may change the treatment planning.

1.49 References

1 **Garwood M, DeLaBarre L.** The return of the frequency sweep: Designing adiabatic pulses for contemporary NMR. J Magn Reson 2001;153:155-177.

2 **Van den Bergen B, Klomp DWJ, Raaijmakers AJE, Arteaga de Castro, CS, Boer VO, Kroeze H, Luijten PR, Lagendijk JJW, Van den Berg CAT.** Uniform prostate imaging and spectroscopy at 7 T: comparison between a microstrip array and an endorectal coil. NMR Biomed 2011;24:358-365.

3 **Katscher U, Bornert P.** Parallel RF transmission in MRI. NMR Biomed 2006;19:393-400.

4 **Raaijmakers AJE, Ipek O, Klomp DWJ, Possanzini C, Harvey PR, Lagendijk JJW, Van den Berg CAT.** Design of a radiative surface coil array element at 7 T: the single-side adapted dipole antenna. Magn Reson Med 2011;66:1488-1497.

5 **Visser F, Zwanenburg JJM, Hoogduin JM, Luijten PR.** High-Resolution Magnetization-Prepared 3D-FLAIR Imaging at 7.0 Tesla. Magn Reson Med 2010;64:194-202.

6 **De Graaf RA, Rothman DL, Behar KL.** Adiabatic RARE imaging. NMR biomed 2003;16:29-35.

7 **Deschamps M, Kervern G, Massiot D, Pintacuda G, Emsley L, Grandinetti PJ.** Superadiabaticity in magnetic resonance. J Chem Phys 2008;129.

8 **Hennig J, Scheffler K.** Hyperechoes. Magn Reson Med 2001;46:6-12.

9 **Van de Bank BL, Voogt IJ, Italiaander M, Stehouwer BL, Boer VO, Luijten PR, Klomp DWJ.** Ultra high spatial and temporal resolution breast imaging at 7T. NMR in Biomed 2012;26:367-375.

10 **Van Kalleveen IML, Boer VO, Luijten PR, Klomp DWJ.** High B_1 efficiency with uniform image contrast in 3D FFE and TSE at 7T. ISMRM. Melbourne, Australia2012.

11 **Pauly J, Nishimura D, Macovski A.** A k-space analysis of small-tip-angle excitation. J Magn Reson 1989;81:43-56.

12 **Sbrizzi A, Hoogduin H, Lagendijk JJ, Luijten PR, Sleijpen GLG, Van den Berg CAT.** Time efficient design of multi dimensional RF pulses: application of a multi shift CGLS algorithm. Magn Reson Med 2011;66:879-885.

13 **Metzger GJ, Snyder C, Akgun C, Vaughan T, Ugurbil K, Van de Moortele PF.** Local B_1^+ shimming for prostate imaging with transceiver arrays at 7T based on subject-dependent transmit phase measurements. Magn Reson Med 2008;59:396-409.

SUMMARY

Adiabatic RF pulses are useful pulses for inhomogeneous B_1 fields caused by surface RF coils, however the increase in SAR will lengthen the T_R, and possibly also the T_E if the adiabatic pulses become too long. Using the superadiabaticity theorem the increase in SAR can already be reduced, making it possible to use an adiabatic TSE in humans at 7 T (chapter 2). However the length of the T_R might still be too long to make the full adiabatic TSE clinically acceptable.

On the other side, it is possible to design a 1D or 2D RF pulse which compensates the inhomogeneous B_1 field and create a uniform flip angle distribution. Using a TOFU pulse in combination with a breast surface coil (chapter 3), the simplicity lies in the already present gradient and due to the more efficient spin energy distribution, the RF pulse will become less SAR intensive and making it compete with the conventional sinc pulses. The TOFU pulse does require a slab selective 3D sequence. Also, the direction of placing the slab selection has to align with the dominant inhomogeneous B_1 field.

If the B_1 field of a coil is not dominantly inhomogeneous in one dimension, but in two dimensions, the TOFU pulse does not work anymore and other options should be considered. For compensating the radial inhomogeneous B_1 field of a monopole antenna, a 2D RACE pulse is designed (chapter 4). The RF pulse works in the low flip angle regime and contains less SAR than adiabatic RF pulses. Therefore the 2D RACE pulse might be the best choice for the extreme inhomogeneous B_1 field of the antenna. A comparison with conventional pulses have been shown in vivo in the human rectum. The duration of the 2D RACE pulse is determined by the hardware limitations of the gradients. The slew-rate and the maximal strength are limited in the sense that the RF pulse itself had to be stretched in order to suffice the hardware limitations, which makes the 2D RACE pulse relatively long.

The endorectally inserted monopole antenna can boost the SNR substantially, not only for imaging the rectum, but also for MRI of the cervix (chapter 6). In this method the monopole is used as a receive-only coil. Combining the endorectal receiver with seven external dipole antennas on a multi-transmit platform, makes the setup capable of providing uniform excitations with high SNR. The local B_1 shimming by setting the amplitude and phase of the external elements independently, is a mechanism to obtain a homogeneous B_1 field in the cervix and its close surroundings. Using the monopole antenna to boost the SNR locally will give even more detailed information about the cervical structures. This setup makes it possible to image cervical cancer patients, which may, or may not, have parametrial invasion (cervical tumor growth in its surrounding connective tissue) in earlier stages. Detection of parametrial invasion may be used for further treatment planning (chapter 5).

SAMENVATTING

Adiabatische RF pulsen zijn nuttige pulsen wanneer een oppervlakte RF spoel een inhomogeen B_1 veld veroorzaakt, maar deze pulsen vragen meer SAR en maken de T_R hierdoor langer. Ook kan de T_E langer worden wanneer de adiabatische puls te lang duurt. Kijkende naar de theorie over superadiabaticiteit, de adiabatische pulsen kunnen met minder SAR ontworpen worden, waardoor een adiabatisch TSE op 7 T in mensen haalbaar is (hoofdstuk 2). De duur van de T_R kan alleen nog steeds te lang zijn, waardoor een complete adiabatische TSE misschien niet klinisch relevant is.
Een andere mogelijkheid om het inhomogene B_1 veld tegen te gaan, is het ontwerpen van 1D of 2D RF pulsen, die dit B_1 veld compenseren. Wanneer de ontwikkelde TOFU puls (hoofdstuk 3) in combinatie met een oppervlakte borstspoel wordt ingezet, kan samen met de al bestaande gradiënt een homogene excitatie gecreëerd worden. Bovendien wordt door de efficiëntere manier van de energie verdeling van de RF puls, de TOFU puls qua SAR vergelijkbaar met een conventionele sinc RF puls. Een 3D plak selectieve is nodig wanneer de TOFU puls wordt toegepast. De richting van de plak moet hierbij gelijk zijn aan de richting van de niet-uniformiteit van het B_1 veld.
Als het B_1 veld van een spoel niet sterk inhomogeen is in één richting, maar in twee richtingen, dan werkt de TOFU puls niet en moet er gekeken worden naar andere oplossingen. Voor het compenseren van het inhomogene B_1 veld van een monopool antenne, welke zich radiaal gedraagt, is er een 2D RACE puls ontworpen (hoofdstuk 4). Deze RF puls werkt voornamelijk goed in lage flip hoek regimes en bevat minder SAR dan adiabatische RF pulsen. Hierdoor lijkt de 2D RACE puls de beste keuze om het extreem inhomogene B_1 veld van de antenne te compenseren. In in vivo resultaten in het menselijk rectum zijn vergelijkingen met de conventionele pulsen gemaakt. De hardware limieten van de gradiënten waren de beperkende factoren voor de lengte van de 2D RACE puls. De helling en maximale sterkte van de gradiënten waren behaald voordat de RF puls zelf aan de limieten zat. Hierdoor is de ontworpen RF puls zelfs nog wat verlengd, zodat de bijbehorende gradiënten konden worden gebruikt.
Als we de monopool antenne intern in het rectum in de buurt van de cervix plaatsen, kunnen we de antenne ook alleen als ontvangst spoel gebruiken en hierbij nog steeds een sterke toename van SNR observeren (hoofdstuk 6). Het combineren van de monopool antenne met zeven verdeelde externe dipool antennes op het multi-transmit platform levert bovendien een uniforme flip hoek op. Door de amplitude en fase van de externe elementen afzonderlijk te instellen, kunnen we lokaal in de cervix en omliggende weefsel het B_1 veld homogeen maken. Gedetailleerde informatie rondom de cervix kan worden verbeterd door middel van de monopool antenne, welke de SNR lokaal verhoogd. Deze setup zou gebruikt kunnen worden voor onderzoek naar de mogelijkheid om het verschil van wel of geen parametria invasie (tumorweefsel in om-

liggende bindweefsel) in eerdere stadia in cervicale tumor patiënten te diagnosticeren. Deze informatie is zeer belangrijk voor de verdere behandeling van deze patiënten (hoofdstuk 5).

List of Publications

Journal articles

Boosting the SNR by adding a receive-only endorectal monopole to an external antenna array for high-resolution T_2-weighted imaging of early stage cervical cancer with 7T MRI.
Van Kalleveen, I.M.L., Hoogendam, J.P., Raaijmakers, A.J.E., Visser, F., Arteaga de Castro, C.S., Verheijen, R.H.M., Luijten, P.R., Zweemer, R.P., Veldhuis, W.B., Klomp, D.W.J. Under review at NMR in biomed.

High resolution T_2-weighted cervical cancer imaging: a feasibility study on ultra-high field 7 T MRI with an endorectal monopole antenna.
Hoogendam, J.P., **Van Kalleveen, I.M.L.**, Arteaga de Castro, C.S., Raaijmakers, A.J.E., Verheijen, R.H.M., van den Bosch, M.A.A.J., Klomp, D.W.J., Zweemer, R.P., Veldhuis, W.B. Accepted in European Radiology 2016.

2D radially compensating excitation pulse in combination with an internal transceiver antenna for 3D MRI of the rectum at 7 T.
Van Kalleveen, I.M., Kroeze, H., Sbrizzi, A., Boer, V.O., Reerink, O., Philippens, M.E., van der Berg, C.A., Luijten, P.R., Klomp, D.W.J. Accepted in Med Phys 2016.

Proton observed phosphorus editing (POPE) for in vivo detection of phospholipid metabolites.
Wijnen, J.P., Klomp, D.W.J., Nabuurs, C.I.H.C., de Graaf, R.A., **van Kalleveen, I.M.L.**, van der Kemp, W.J.M., Luijten, P.R., Kruit, M.C., Webb, A., Kan, H.E., Boer, V.O. Accepted in NMR in biomed 2015.

Tilt optimized flip uniformity (TOFU) RF pulse for uniform image contrast at low specific absorption rate levels in combination with a surface breast coil at 7 Tesla.
Van Kalleveen, I.M.L., Boer, V.O., Luijten, P.R., Klomp, D.W.J. Magn Res Med 2014; 74:482-488.

Adiabatic turbo spin echo in human applications at 7 T.
Van Kalleveen, I.M.L., Koning, W., Luijten, P.R., Boer, V.O., Luijten, P.R., Zwanenburg, J.J.M. Klomp, D.W.J. Magn Res Med 2012;68:580-587.

Conference procedures

Choline detection in human cervical cancer using an internal antenna and external antennas at 7T.
Van Kalleveen, I.M.L., Hoogendam, J.P., Raaijmakers, A.J.E., et al.
Oral presentation, 23th ISMRM Annual Meeting & Exhibition 2012, Toronto, Canada.

Boosting SNR with an internal antenna and external antennas in the human cervix uteri in TSE at 7T.
Van Kalleveen, I.M.L., Hoogendam, J.P., Raaijmakers, A.J.E., et al.
Poster presentation, 22th ISMRM Benelux Meeting 2014, Maastricht, The Netherlands.
Poster presentation, 22th ISMRM Annual Meeting & Exhibition 2014, Milan, Italy.

2D Compensating RF Pulse with Uniform Image Contrast in Combination with an Internal Transceiver at 7T.
Van Kalleveen, I.M.L., Kroeze, H., Sbrizzi, A., et al.
Oral presentation, ISMRM Benelux Meeting 2013, Rotterdam, The Netherlands.
Poster presentation, ISMRM scientific workshop: Ultra-high field MRI 2013, Noordwijk aan zee, The Netherlands.
Poster presentation, 21th ISMRM Annual Meeting & Exhibition 2013, Salt Lake City, UT, USA. Magna cum laude merit award

High B_1 efficiency with uniform image contrast in 3D FFE and TSE at 7T.
Van Kalleveen, I.M.L., Boer, V.O., Luijten, P.R., et al.
Oral presentation, 20th ISMRM Benelux Meeting 2012, Leuven, Belgium.
Oral presentation, 20th ISMRM Annual Meeting & Exhibition 2012, Melbourne, Australia. Magna cum laude merit award

Adiabatic turbo spin echo for human applications at 7T.
Van Kalleveen, I.M.L., Boer, V.O., Luijten, P.R., et al.
Oral presentation, 19th ISMRM Annual Meeting & Exhibition 2011, Montreal, Canada.

Curriculum Vitae

Irene van Kalleveen werd geboren op 24 januari 1984 te Amersfoort. Na haar HAVO diploma in 2001 te hebben behaald, heeft ze via de ROC avondschool haar VWO in 2004 weten te bemachtigen. Hierna heeft ze de universitaire opleiding Natuurkunde en Sterrenkunde te Utrecht gevolgd en in heeft in 2010 haar bachelortitel behaald. Het bachelor onderzoek was een literatuur onderzoek getiteld: "Supermassive blackholes". Hierbij werd naar de supermassieve zwarte gaten in sterrenstelsels gekeken. Hierna is ze de master opleiding "Biomedical Image Science" ingegaan waarbij ze in aanraking kwam met de schitterende wereld van de MR fysica. Hier was het mogelijk om zowel mensen te kunnen helpen in de medische sector, als wel in de complexe natuurkunde van de MRI scanner te kunnen duiken, welk zelfs tot op spin niveau kan worden bestudeerd. Tijdens een hoorcollege van Dr. Dennis Klomp over de 7 tesla MRI scanner, waarbij alle uitdagingen werden opgesomd, ging haar hart sneller kloppen. Ze liet haar kans dan ook niet lopen en sprak Dennis Klomp na het hoorcollege gelijk aan voor zowel een literatuuronderzoek als wel een afstudeeronderzoek. Met een grote glimlach is ze die dag het hoorcollege uitgelopen. Het onderwerp van het literatuuronderzoek was "^{1}H water suppression" waarbij gekeken werd naar de verschillende water suppressie technieken gebruikt worden bij spectroscopie en welke voor- en nadelen er aan de verschillende methoden kleven. Hierbij werd ze tevens begeleid door Vincent Boer. Tijdens het research project was het onderzoek doen naar de mogelijkheid om een turbo spin echo sequentie te ontwikkelen welke puur bestaat uit adiabatische RF pulsen, welke succesvol is ontwikkeld en gepubliceerd. Tijdens haar PhD heeft ze onder leiding van Prof. Dr. Peter Luijten en Dr. Dennis Klomp onderzoek gedaan naar de B_1 inhomogeniteit van RF pulsen in combinatie met verscheidene oppervlakte spoelen en een monopool antenne op de 7 tesla MRI scanner in het UMC Utrecht. Zowel RF puls design en simulaties als Philips puls (en andere zaken) programmeren waren de leidraad gedurende dit onderzoek. Op dit moment is Irene werkzaam op de 7 Tesla MRI scanner in het Academisch Medisch Centrum en Spinoza Centrum te Amsterdam.

Dankwoord

Peter, dank je wel voor alle input en leuke ideeën tijdens en buiten de groupmeetings. Ik heb diep respect voor hoe je alles op de rails houdt, maar ik vraag me wel af: mis je het scannen niet zo af en toe?

Dennis, tja voor jou zijn er te weinig woorden. Je was mijn werkvader en sparpartner. Ik heb zo enorm veel van je geleerd. Om een paar dingen te noemen: ik heb geleerd om me niet aangevallen te voelen wanneer iemand vragen stelt, om niet negatief naar nieuwe ideeën te kijken, om buiten het boekje om te denken. Ik heb ontzettend genoten van alle sparmomenten (hieraan denk ik nog vaak terug). Dank je wel voor alles!

Jaap, je bent echt een gouden vent! De positiviteit die je uitstraalde was zelfs voelbaar bij de soms ietwat knorrige Fredy. Ik kan onze scansessies nog goed herinneren. De frustratie dat er weer iets fout gaat bij de scanner en de euforie over de mooie cervix plaatjes. Ik heb enorm met je gelachen en genoten van de soms ietwat gestreste scanmomenten. Dank je wel voor je inzet bij zowel het scannen, als de bijdrage aan dit proefschrift.

Anja, ook voor jou schieten woorden eigenlijk te kort. Je inspireert me op meerdere vlakken en ik heb diep respect voor jouw vechtlust. Ik vind het geweldig dat je naar het grotere geheel kijkt en je beslissingen maakt op basis waarvan je gelukkig wordt. Je bent mijn ISMRM maatje en ik heb zoveel mooie dingen met je mogen meemaken. Ik hoop dat ik jou voor de rest van mijn leven mijn vriendin mag noemen. Ow ja, en dank je dat je mijn paranimf bent!

Mariska, jij was mijn allereerste roomie. Je hebt me veel geleerd, vooral Matlab gewijs. Elke keer als je langskomt en ik bak taart, zal ik altijd rekening houden met je allergieën. Je wilt niet weten hoe mijn keuken er op zo'n moment uitzag :') Elke moeite om maar geen chocola of noten per ongeluk in jouw taart te krijgen werd uitgevoerd. Helaas moest je afhaken als paranimf (wie gaat er dan ook zo'n studie doen :P).

Vincent, ik heb ontzettend veel van je geleerd. Zowel op inhoudelijk als sociaal vlak. De manier hoe jij luchtig kan doen over hoeveel kennis je hebt, siert je. Ik zit nu sinds kort fulltime in de spectroscopie en heb nog meer respect voor je gekregen!

Daniel, jij was toch wel een beetje mijn tweede werkvader. Je wijze raad, interessante weetjes en gezelligheid. Ik hoop in de toekomst nog een keer met je te kunnen samenwerken.

Catalina, toen ik de allereerste keer in het vliegtuig zat, zat ik naast je. Ik weet nog hoe jou rust over het vliegen mij kalmeerde. Het feit dat ik op de terugweg paniekaanvallen in het vliegtuig heb gehad, komt natuurlijk doordat je toen niet naast me zat ;) Je bent zowel slim als gezellig en ik ben blij dat ik daarvan heb mogen genieten :). Ik heb enorm genoten van je optredens ("Miauw") en je flamenco oefeningen. Helaas zie ik je te weinig, maar weet dat je in mijn hart zit.

Wouter, "Hoe is de sfeer?", "wat vind je van …" Deze zinnen blijf ik de rest van mijn leven meedragen :') Ik heb genoten van onze sparmomenten en filosofische gesprekken.

Alessandro, Jij blijft mijn stiekeme link met de wiskunde kant in mij waarbij ik me wel eens afvroeg of ik die bachelor niet had moeten afmaken. Dank je wel voor al je enthousiasme, humor en input. Voor mij ben je een maestro ;)

Fredy, de scansessies met de cervix patiënten en de discussies op Q4/Q2 zullen me bijblijven, heerlijk hoe jij soms met een knipoog de knorrepot kan uithangen. Ik kan het heel erg waarderen. Dank je wel voor alle mooie sparmomenten en lessen over hoe Philips bepaalde sequenties en pulsen nou weer heeft gedefinieerd. Heerlijk hoe jij over sport (en dan vooral wielrennen) kan praten. Bedankt voor alle leuke en leerzame momenten en bedankt voor alle hulp bij de cervix patiënten.

Sylvia, ik denk nog steeds terug aan onze gesprekken. Jij was een beetje mijn werkmoeder. Geweldig hoe je ondanks het natuurkundige zooitje van Q2/Q4/Q2, de dingen zo goed kon regelen. Je bent een fantastische vrouw.

Alexander, Jij was toch wel een beetje mijn link met Amersfoort, maar helaas ben je verhuisd toen ik juist naar Amersfoort verhuisde (toeval? ;)). Je verhalen over de groentetuin (zelfs met TV debuut) en je geniale antenne ontwikkeling zullen me bijblijven. Daarnaast moeten we de gezellige momenten op de ISMRM zeker niet vergeten.

Hanneke, dank je wel voor onze fijne gesprekken. Helaas zien we elkaar te weinig, maar bij mij geldt zeker niet uit het hoofd, uit het hart :). Je bent een geweldige positieve vrouw en ik hoop daar nog vaak van te mogen genieten.

Bertine, ik heb vrij veel met je meegemaakt. Dank je wel voor alle mooie tripjes en je luchtigheid over dingen, dat relativeerde mij ook :). Bedankt voor je luisterend oor tijdens onze gesprekken.

Wybe, dubbele doctor, jij blijft voor mijn gevoel een beetje mijn adiabaat maatje. Heerlijk hoe je soms een beetje pessimistisch kan overkomen, omdat je feitelijk een reele kijk hebt op bepaalde dingen, terwijl iedereen om je heen overstroomt van positiviteit. Ik blijf me erover verbazen hoeveel kennis je elke keer weer uit je mouw tovert. "Dit molecuul heeft een binding met dat molecuul en dan kan je dit verwachten". Ik heb diep respect voor je.

Hugo, dank je wel voor alle hulp en feedback. Je hebt me mooie en wijze lessen geleerd :).

Jill, het tripje naar Brussel was supergezellig. Het is altijd mooi om naar je Belgische accent te luisteren en te horen dat je iets serieus bedoelt ("serieus").

Christine, ik heb genoten van onze spartijd met Chiel en het gevogel in de code om de POCE sequentie erin te krijgen. Ik heb je daar echt zien groeien qua PPE ervaring. Dank je wel voor je doorzettingsvermogen.

Debra, thank you for the great cooperation, your positive feedback and great ideas. I love our brainstorm sessions :) You are awesome!

Jeroen, surfdude. Jouw relaxte (coole) manier van aanpak bracht een bepaalde rust. Thanks daarvoor en voor de vele Matlab tips.

Arjan, Ik heb veel genoten van die droge humor van je :) en ik zal het dansen op het ISMRM eindfeest nooit vergeten. Geweldig!

7T groep, **Hans**, **Nikki**, **Anita**, **Alexandra**, **Janot**, **Jannie**, **Ronald**, **Joep**, **Jolanda**, **Alex**, **Bart**, **Anouk**, **Martijn**, **Anna**, **Astrid**, **Arjen**.

en om met de beroemde woorden van W. Koning te spreken: "Namen noemen is namen vergeten" ;)

Bedankt allemaal voor de heerlijke baksels, gesprekken, ideeën, borrels (en etentjes erna omdat we te lang borrelden). Er zijn enorm veel goede herinneringen, hier zou ik een apart boek over kunnen schrijven :)

Ik voel me een meisje dat het nest heeft verlaten. Dank jullie wel voor het thuisgevoel.

Lieve **AMC** en **Spinoza collega's** dank jullie wel voor jullie steun tijdens het afmaken van het proefschrift.

Anneloes, dank je wel dat je mijn paranimf bent. Ik waardeer je eerlijkheid en geniet erg van je soms wat flauwe grapjes (vandaar dat je Klaas waarschijnlijk mag). Ondanks dat ik je nog niet erg lang ken, weet ik wel dat jij een vriendin voor het leven bent! xxx

Mam, ik schiet bijna vol nu… (dat begint lekker). Ik ben je zo dankbaar voor alle momenten dat we samen met wiskunde bezig waren. In de beginfase legde je mij dingen uit. Toen ik wat verder in de wiskunde kwam, zaten we er beiden soms met vraagtekens naar te kijken en kwamen we uiteindelijk samen tot een eureka moment. En tenslotte, toen ik op de universiteit zat en de wiskunde boven je pet ging. Je liet nadenken en het uitleggen, waardoor ikzelf de vraagstukken kon oplossen. Dit is nog maar één van de vele dingen waar ik je dankbaar voor ben.

Pap, dank je wel voor alle inspiratie. Wat ik ook doe, ik weet dat je trots op me bent. Dank je wel dat je dit elke keer weer laat weten.

Klaas, dank je wel voor je geduld en je relaxte mode. Die heb ik de afgelopen tijd erg goed kunnen gebruiken. Ik ben gelukkig met jou :) xxx